



**HAL**  
open science

## Some selected functionalized catenanes, rotaxanes and the DNA for nonlinear optical applications

Robert Czaplicki

► **To cite this version:**

Robert Czaplicki. Some selected functionalized catenanes, rotaxanes and the DNA for nonlinear optical applications. Physics [physics]. Université d'Angers, 2008. English. NNT : . tel-00447183

**HAL Id: tel-00447183**

**<https://theses.hal.science/tel-00447183>**

Submitted on 14 Jan 2010

**HAL** is a multi-disciplinary open access archive for the deposit and dissemination of scientific research documents, whether they are published or not. The documents may come from teaching and research institutions in France or abroad, or from public or private research centers.

L'archive ouverte pluridisciplinaire **HAL**, est destinée au dépôt et à la diffusion de documents scientifiques de niveau recherche, publiés ou non, émanant des établissements d'enseignement et de recherche français ou étrangers, des laboratoires publics ou privés.

# Some selected functionalized catenanes, rotaxanes and the DNA for nonlinear optical applications

THESE DE DOCTORAT

Spécialité : Physique

ECOLE DOCTORALE 3MPL

présentée et soutenue publiquement

le : **26 Novembre 2008**

à : l'Université d'Angers

par: **Robert CZAPLICKI**

Devant le jury ci-dessous :

Marc SALLE, *Président*, Professeur, Université d'Angers, France

Jean EBOTHE, *Rapporteur*, Professeur, Université de Reims, France

Stelios COURIS, *Rapporteur*, Professeur, Université de Patras, Grèce

François KAJZAR, *Examineur*, Directeur de Recherche, Université d'Angers, France

Céline FIORINI-DEBUISSCHERT, *Examineur*, Directeur de Recherche, CEA de Saclay,  
France

Aurelia MEGHEA, *Examineur*, Professeur, Politehnica de Bucarest, Roumanie

Mihai POPESCU, *Examineur*, Directeur de Recherche, National Institute of Materials  
Physics, Roumanie

Bouchta SAHRAOUI, *Directeur de thèse*, Professeur, Université d'Angers, France

*Laboratoire des Propriétés Optiques des Matériaux et Applications, FRE CNRS 2988  
Université d'Angers, 2 boulevard Lavoisier, 49045 ANGERS Cédex 01*



## Acknowledgments

I would like to express my gratitude to my supervisor, Professor Bouchta SAHRAOUI, who gave me the chance to carry out a PhD in Angers and opened doors to a fascinating research for me. Prof. Bouchta SAHRAOUI is a really nice person. His expertise and kindness make me realize how lucky I am to have him as my advisor. He constantly helped and encouraged me in difficult times. His suggestions and guidance were always right

I am very grateful to all the members of the POMA Laboratory, to all of them who already left and to the ones that are always close. Special thanks to my colleagues Zacaria ESSAIDI, Dr Zouhair SOFIANI, Dr Jérôme LUC, Dr Karim BOUCHOUIT and Dr Adil HABOUCHA.

I also want to thank Dr Beata DERKOWSKA, Dr Oksana KRUPKA, and Dr Abdelkrim EL-GHAYOURY for their help, kindness and scientific discussion.

I would like to thank Dr Ileana RAU, Dr François KAJZAR, Prof. Waclaw BALA, Prof. Andrzej MINIEWICZ and Prof. Antoni MITUS for scientific discussion and their help in scientific problems.

I also would like to thank the group of Dr David LEIGH (especially Dr Jose BERNA) from School of Chemistry at the University of Edinburgh for synthesis of canenanes and rotaxanes molecules.

My gratitude I send to Dr Georges BOUDEBS for performing the Z-scan experiments.

I am very grateful to Dr Anna MIGALSKA-ZALAS for performing the theoretical calculations.

I am very grateful to group of prof. George A. STANCIU from Center for Microscopy-Microanalysis and Information Processing at the University “Politehnica” of Bucharest in Romania for give me the possibility of measurments in their laboratory.

I am indebted to Alain MAHOT and Christophe CASSAGNE for their technical support, solving problems with lasers and instantaneous help during experiments.

I would like to acknowledge the European community for financial supporting under contract NMP4-CT-2004-013525 (Hy3M, Hydrogen - bond geared Mechanically Interlocked Molecular Motors).

I also would like to thank the *L'Association Inter-Universitaire des Pays de la Loire pour la Valorisation de la Recherche et le Développement des Relations Economiques* (UNIVALOIRE) for financial support.

I am indebted to my family for their continual supports and cheering through the years.

Finally, I would like to give my special thanks and all my love to my fiancée, Ania. Without her love, support, understanding and caring I would not have survived.

*Je dédie cette thèse  
à ma chérie Ania*



# Table of contents

<b>List of Figures</b>	<b>xi</b>
<b>List of Tables</b>	<b>xv</b>
<b>General Introduction</b>	<b>1</b>
<b>Chapter 1 Molecules</b>	<b>5</b>
1.1 Introduction to the chapter . . . . .	5
1.2 Interlocked molecules . . . . .	5
1.3 Catenanes and rotaxanes . . . . .	6
1.3.1 Synthesis of catenanes and rotaxanes . . . . .	7
1.3.2 Functionalization of rotaxanes . . . . .	12
1.4 Deoxyribonucleic acid . . . . .	14
1.4.1 DNA Properties . . . . .	16
1.4.2 Functionalization of DNA . . . . .	17
<b>Chapter 2 Basis of linear and nonlinear optics and quantum chemistry</b>	<b>19</b>
2.1 Introduction to the chapter . . . . .	19
2.2 Interaction of light with matter . . . . .	20
2.2.1 Maxwell equations . . . . .	20
2.2.2 Transmission, absorption, and reflection . . . . .	22
2.2.3 Macroscopic polarization . . . . .	24
2.2.4 Phase matching . . . . .	24
2.2.5 Second order susceptibility . . . . .	25
2.2.6 Third order susceptibility . . . . .	26
2.2.7 Microscopic polarization . . . . .	27
2.3 Quantum chemistry . . . . .	28

---

2.3.1	Hartree-Fock method . . . . .	29
2.3.2	Configuration interaction method . . . . .	29
<b>Chapter 3 Experimental Techniques</b>		<b>31</b>
3.1	Introduction to the chapter . . . . .	31
3.2	Degenerate four-wave mixing . . . . .	32
3.3	Z-scan . . . . .	33
3.4	Harmonic generation . . . . .	35
3.4.1	Second harmonic generation . . . . .	35
3.4.2	Third harmonic generation . . . . .	36
3.5	Photoinduced diffraction gratings . . . . .	37
3.5.1	Photoisomerization of azobenzene . . . . .	38
3.5.2	Degenerate two-wave mixing technique . . . . .	39
3.6	Other techniques . . . . .	40
3.6.1	Spin coating . . . . .	40
3.6.2	Atomic force microscope . . . . .	41
<b>Chapter 4 Results - catenanes and rotaxanes</b>		<b>43</b>
4.1	Introduction to the chapter . . . . .	43
4.2	Spectral characterization . . . . .	44
4.3	Degenerate four-wave mixing . . . . .	45
4.3.1	Nonlinear transmission . . . . .	45
4.3.2	Phase conjugation measurements . . . . .	46
4.3.3	Time resolved measurements . . . . .	52
4.4	Z-scan . . . . .	54
4.5	Second harmonic generation . . . . .	56
4.6	Third harmonic generation . . . . .	58
4.7	Quantum chemical calculations . . . . .	59
4.7.1	Dipole moment and HOMO-LUMO bandgap . . . . .	60
4.7.2	First and second order hyperpolarizability . . . . .	61
<b>Chapter 5 Results - DNA</b>		<b>67</b>
5.1	Introduction to the chapter . . . . .	67
5.2	Spectral characterization . . . . .	67
5.3	Second harmonic generation . . . . .	71

---

5.4	Third harmonic generation . . . . .	72
5.5	Degenerate two-wave mixing . . . . .	74
<b>Chapter 6 Conclusions and perspectives</b>		<b>81</b>
6.1	Conclusions . . . . .	81
6.2	Perspectives . . . . .	83
6.2.1	New family of rotaxanes . . . . .	83
6.2.2	DNA holography . . . . .	83
<b>Bibliography</b>		<b>85</b>
<b>Appendix A Systems of units</b>		<b>99</b>
<b>Appendix B Notations, symbol and abbreviations</b>		<b>101</b>
<b>Appendix C Publications and communications</b>		<b>105</b>
C.1	Publications . . . . .	105
C.2	Communications . . . . .	107



# List of Figures

1.1	Schematic representation of [2] catenane (left) and [2] rotaxane (right) molecules. . . . .	6
1.2	Schematic representation of three types of movements in rotaxanes: (a) pirouetting, (b) shuttling, and (c) clipping (transformation of [2] rotaxane into [2] catenane). . . . .	7
1.3	Schematic representation of synthesis route for catenane: (a) - clipping, and three types of synthesis routes for rotaxane: (b) - capping, (c) - clipping, and (d) - slipping. . . . .	8
1.4	Synthesis of <i>catenane</i> molecule proposed by A.G. Johnston et al. [46, 47].	9
1.5	Synthesis of <i>fumrot</i> molecule proposed by A.G. Johnston et al. [48, 49].	10
1.6	Chemical structure of <i>macrocycle</i> molecule. . . . .	10
1.7	Chemical structure of <i>catenane</i> molecule. . . . .	11
1.8	Chemical structure of <i>thread</i> molecule: C <sub>36</sub> H <sub>70</sub> N <sub>2</sub> O <sub>2</sub> ; Exact mass: 562.54373; Mol. Wt.: 562.9532; C, 76.81; H, 12.53; N, 4.98; O, 5.68 . . . .	11
1.9	Chemical structure of <i>rotaxane</i> molecule. . . . .	12
1.10	Chemical structure of <i>fumrot</i> molecule. . . . .	12
1.11	Chemical structure of pure (a), mono- (b), and di- (c) substituted <i>fumrot</i> [50]. . . . .	13
1.12	Absorption spectra of pure, mono-, and di- substituted <i>fumrot</i> [50]. . . .	13
1.13	Refractive index dispersion in evaporated thin films of pure (triangles), mono-nitro (circles) and di-nitro <i>fumrot</i> (squares). Full figures show ordinary whereas the open the extraordinary index of refraction, respectively. Solid lines are Sellmeier fits [50]. . . . .	14
1.14	Chemical structure of DNA segment and surfactant CTMA. . . . .	16
1.15	Chemical structure of Disperse Red 1. . . . .	16

2.1	Geometry of second harmonic generation process (left) and energy-level diagram describing this process (right). . . . .	26
2.2	Third harmonic generation process (left) and energy level diagram (right). . . . .	27
3.1	DFWM experimental setup: <b>RO</b> - delay line, <b>P</b> - polarizer, <b>Phs</b> , <b>Phc</b> - synchronization and control photodiodes, <b>BS</b> - beam splitter, <b>D</b> - diaphragm, <b>M</b> - mirror, <b>L</b> - lens, $\lambda/2$ - half wavelength plate, <b>PMT</b> - photomultiplier tube, $\langle 1 \rangle$ , $\langle 2 \rangle$ - pump beams, $\langle 3 \rangle$ - probe beam, $\langle 4 \rangle$ - fourth beam. . . . .	33
3.2	Z-scan experimental setup: <b>S</b> - sample, <b>BS</b> - beam splitter, <b>L</b> - lens, <b>M</b> - mirror. . . . .	34
3.3	Schematic representation of the experimental setup for SHG (and THG) measurements: <b>BS</b> - beam splitter, $\lambda/2$ - half wave plate, <b>P</b> - polarizer, <b>L</b> - convergent lens (250 mm), <b>F</b> - selective filter, <b>Phs</b> - synchronization photodiode, <b>Phc</b> - control photodiode and <b>PMT</b> - photomultiplier tube. . . . .	36
3.4	Schematic setup for diffracting grating formation experiment, <b>M</b> - mirror, <b>BS</b> - beam splitter, <b>P</b> - polarizer, $\lambda/2$ - half wave plate, <b>S</b> - sample, <b>Ph</b> - photodiode. . . . .	39
4.1	Theoretical (black) and experimental (blue) absorption spectra for <i>rotaxane</i> dissolved in chloroform (0.05 g/L). . . . .	44
4.2	Theoretically calculated absorption spectra for <i>rotaxane</i> , <i>macrocycle</i> , <i>thread</i> and <i>catenane</i> (peaks counted from the left side) molecules. . . . .	46
4.3	DFWM results for CS <sub>2</sub> , <i>rotaxane</i> (5 g/L and 10 g/L), CHCl <sub>3</sub> , <i>thread</i> and DMSO. . . . .	47
4.4	DFWM results for <i>fumrot</i> and <i>catenane</i> . . . . .	48
4.5	Comparison of DFWM results for investigated molecules and their solvents. . . . .	49
4.6	Time resolved measurements for CS <sub>2</sub> , <i>thread</i> , CHCl <sub>3</sub> , <i>catenane</i> , <i>rotaxane</i> , <i>fumrot</i> and DMSO. . . . .	53
4.7	Z-scan pattern for chloroform (1064 nm). . . . .	54
4.8	Z-scan pattern for a solution of 10 g/L of <i>rotaxane</i> in chloroform (1064 nm). . . . .	55
4.9	Third harmonic generation maker fringes for the glass substrate and 150 nm thick <i>fumrot</i> thin film deposited on glass substrate. . . . .	59
4.10	Electrostatic potential distributions HOMO (left) and LUMO (right) for (a) <i>macrocycle</i> , (b) <i>catenane</i> , (c) <i>thread</i> and (d) <i>rotaxane</i> . . . . .	62

---

4.11	Dispersion of the molecular first order hyperpolarizabilities $\beta_{xxx}^h$ for investigated molecules. . . . .	63
5.1	The absorbance spectra of DNA-CTMA (curve 1), DNA-CTMA-DR1 (5%) (curve 2) and DR1 (curve 3) in solutions. . . . .	68
5.2	The absorbance spectra of DNA-CTMA (curve 1) and DNA-CTMA-DR1 (5%) (curve 2), DNA-CTMA-DR1 (10%) (curve 3), DNA-CTMA-DR1 (15%) (curve 4) thin films. . . . .	69
5.3	Chemical structures of PMMA (a) and PVK (b) matrices. . . . .	70
5.4	The absorbance spectra of thin films of DNA-CTMA-DR1 (1), PMMA-DR1 (2), PVK-DR1 (3) and PVK alone (4). . . . .	70
5.5	Transmission image that reveals second harmonic generation (white area). The DNA-CTMA-DR1 thin film deposited on the glass substrate were investigated. . . . .	71
5.6	Measured (shapes) and calculated (solid lines) THG intensities for glass substrate, DNA-CTMA and DNA-CTMA-DR1 thin films. . . . .	72
5.7	Example of the dynamics of the gratings inscribed in the PMMA-DR1, PVK-DR1 and DMA-CTMA-DR1 materials using 16 ps pulses of 532 nm laser light with a 10 Hz repetition rate. Monitoring was done using a He-Ne laser light scattering. . . . .	75
5.8	The dynamics of diffracting grating formation with two times started and two times stopped of writing process. The “532 on” means switching on the inscription laser light, while the “532 off” - the cutting off it during the permanent presence of the probe cw He-Ne laser beam. . . . .	76
5.9	Dynamics of the build up and decay of the grating process in DNA-CTMA-DR1 for two polarizations of writing beams: <i>ss</i> - upper curve, <i>pp</i> - lower curve and details after each pulse of writing beams - inset. . . . .	77
5.10	AFM two-dimensional views of surface topography (left) and cross-section plots (right) for PMMA-DR1 (a), PVK-DR1 (b) and DNA-CTMA-DR1 (c) after degenerate two-wave mixing experiment. . . . .	78
5.11	Image of DNA-CTMA-DR1 sample measured by confocal scanning laser microscope. Picture was taken during cross section sample’s scanning. . . .	79



# List of Tables

4.1	Third order susceptibility values for studied molecules. . . . .	50
4.2	Z-scan results. . . . .	56
4.3	SHG results for <i>catenane</i> molecules. $\chi_{zzz}^{(2)}$ - diagonal, $\chi_{xxz}^{(2)}$ - off diagonal components of quadratic nonlinear susceptibility [50]. . . . .	57
4.4	The third order nonlinear optical susceptibility results, for catenanes and rotaxanes, determined by THG technique. . . . .	58
4.5	Principal parameters of the investigated molecules. . . . .	63
4.6	Calculated and measured values of first and second order hyperpolarizabilities. . . . .	64
5.1	The third harmonic generation results for studied samples. . . . .	73



# General Introduction

Nanotechnology and nanoscience are attracting and promising disciplines of applied science that integrate a broad range of topics related to physics, chemistry, biology and medicine. It involves the study and use of materials or devices extremely tiny (100 nanometers and smaller). The manipulation of single atoms and molecules for the construction of nanoscale devices is a promising direction in science. The wide and unlimited imagination of people opens each day new doors for fascinating world of nanoscience. What was impossible few years ago today is common and used. In the nearest future a lot of applications will be in nanoelectronics, nanobiotechnology, material science and information storage. However to reach this level a basic research is needed. The new, efficient materials are needed to create new, efficient applications.

Nonlinear optics has been the subject of intensive research, because of its wide applications in the field of photonics, nanophotonics and optoelectronics such as optical signal processing, integrated optics, optical sensing, optical limiting, optical computing etc. Optical materials are of prime importance in nonlinear optical applications [1, 2, 3].

The experimental nonlinear optics was “born” in 1961 with the observation of second harmonic generation by Franken *et al.* where coherent, high-intensity laser light with a wavelength of 694 nm, impinging on a quartz crystal produced radiation at twice frequency (or half the wavelength, i.e., 347 nm) of the incident radiation [4]. While early theoretical work concerning nonlinear optical processes, like two photon absorption [5] or saturation of an atomic transition (observed experimentally), had been done, it was the advent of the laser (or “optical maser” as it was originally called). Numerous nonlinear optical phenomena have been discovered since then. As laser technology progressed, nonlinear optics has become increasingly more mature and several comprehensive text books have been written on this subject [6, 7, 8, 9, 10]. First observations of nonlinear optical phenomena evoke changes of refractive index were achieved by Faraday, Kerr, Cotton, Mouton and others. In the 70s and 80s Kerr discovered and reported Kerr effect (magnetic and quadratic electric effect). Bruhl observed larger molecular refraction

in molecules with double bond. Sutton reported that  $\pi$  conjugated molecules had much larger linear polarizabilities than saturated organic molecules. Two photon absorption was observed (for organic molecules) in 1963 (33 years after theoretical prediction by Goeppert-Mayer [5]). At the same time second harmonic generation in a single crystal was observed. Russian scientists concluded that charge transfer in molecules amplified second harmonic generation [11, 12]. Important element in the field of nonlinear optics was the observation by Maker of fringes of second harmonic light when a thin film was rotated in respect to the fundamental beam. These are now called "Maker fringes".

Catenanes and rotaxanes are a class of functional organic molecules composed of mobile parts and designed for use in various types of practical applications. Their architectures are very attractive because the components of molecule are held together by a dynamic mechanical bond which can be controlled at the molecular level using light [13, 14, 15], electric [16] or chemical stimulation [16]. They can exhibit interesting properties and can be used as molecular transistors [17], shuttles [16, 18, 19, 20, 21], brakes [22], ratchets [23, 24] turnstiles [25], for modification of surface [26, 27], for macroscopic transport [28], and as molecular muscles [29]. The idea of the rotaxane molecule comes from 60s when the molecules were first proposed [30] and shown to exist [31, 32]. Since then, many different types of such molecules have been proposed, synthesised and described in the literature [33, 34, 35, 36].

We are focusing on nonlinear optical properties which are very interesting but still deserves for investigations. In this work we will present and discuss experimental results of third order nonlinearity and photoinduced grating formation. The experimental investigations include different techniques (absorption spectroscopy, harmonics generation, z-scan, degenerate four-wave mixing and two-wave mixing). Determination of third order susceptibility using degenerate four-wave mixing technique give us information about electronic and rotational contribution of third order susceptibility at the same time, however using third harmonic generation only the electronic part of third order susceptibility can be determined. Some theoretical calculations of the third order nonlinear optical coefficient base on geometry optimization and corresponding quantum chemical calculations founded on semi-empirical method within a framework of the restricted Hartree-Fock approach. These calculations are supplementary to experimental work.

The structure of this thesis contains 6 chapters.

The first chapter is devoted to the presentation the molecules investigated in this work. The introduction to the catenanes and rotaxanes family is presented as well as detailed information concerning investigated molecules. The very important case is their functionalization. Some examples of modification were also presented. The natural catenanes are presented in DNA chains. Due to this fact the second part of this chapter is devoted to this molecule. In this case the functionalization is more important as will change drastically the properties making DNA useful for physical applications.

The second chapter is an introduction to the linear and nonlinear optics, nonlinear optical phenomena and basis of quantum chemistry.

The third chapter describes the experimental techniques used in this work. Experiments allowing to know the nonlinearities of material as degenerate four-wave mixing, second and third harmonic generation and z-scan are described in details. Close to them is degenerate two-wave mixing technique which is a bridge between the basic research and useful applications (optical holography). Other used techniques are mentioned at the end of this chapter.

The fourth and fifth chapters contain the experimental results for catenanes and rotaxanes (chapter four) and modified DNA (chapter five).

In the sixth chapter the discussion of presented results is made as well as prediction and proposition to future continuation. Some of experiments and phenomena are only checked and still need to be verified and developed.



# Chapter 1

## Molecules

### Contents

---

<b>1.1</b>	<b>Introduction to the chapter</b>	<b>5</b>
<b>1.2</b>	<b>Interlocked molecules</b>	<b>5</b>
<b>1.3</b>	<b>Catenanes and rotaxanes</b>	<b>6</b>
1.3.1	Synthesis of catenanes and rotaxanes	7
1.3.2	Functionalization of rotaxanes	12
<b>1.4</b>	<b>Deoxyribonucleic acid</b>	<b>14</b>
1.4.1	DNA Properties	16
1.4.2	Functionalization of DNA	17

---

### 1.1 Introduction to the chapter

In this chapter the description of molecules will be presented. The chapter is divided for two parts due to two different molecules involved. Nevertheless these two different types of molecules are connected each other on some levels.

### 1.2 Interlocked molecules

The concept of interlocked molecules is known from sixties when H.L. Frisch and E. Wasserman [30] proposed first two-ring catenane. Up to now supramolecules of up to 4 components were synthesized and still the number of components increases. Nevertheless

these are relatively small molecules (molecular weight:  $M_w = 10^3$ ) while in nature large ( $M_w = 10^5$ ) catenanes are present in deoxyribonucleic acid (DNA) molecules.

### 1.3 Catenanes and rotaxanes

Generally speaking catenanes and rotaxanes (cf. Fig. 1.1) are mechanically interlocked molecules composed of parts (smaller molecules), held together as a consequence of mechanical linking rather than by covalent bonds, where one (or more of them) can move and/or positioning with respect to the other. This special architecture makes them very interesting as possible candidates for molecular machine-type applications in the field of photonics, optoelectronics, optical data storage and nonlinear optics.

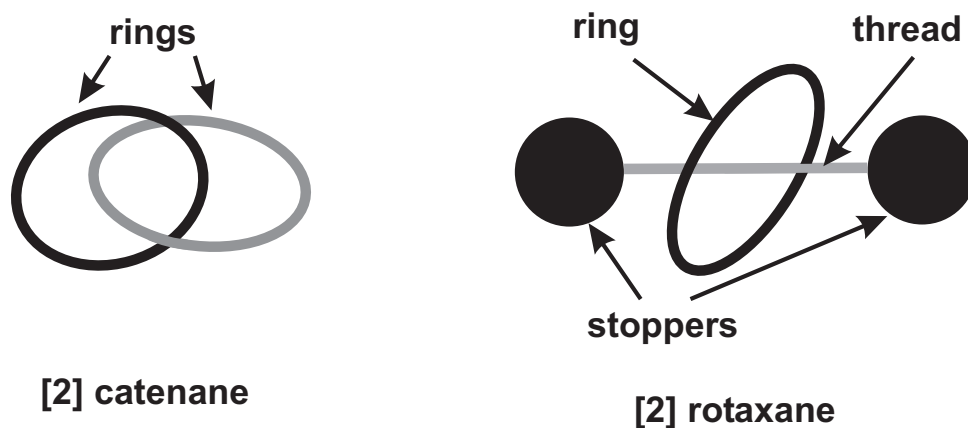


Figure 1.1: Schematic representation of [2] catenane (left) and [2] rotaxane (right) molecules.

In 2000 International Union of Pure and Applied Chemistry started the project namely “Nomenclature for Rotaxanes and Catenanes” (today: “Macromolecular Nomenclature Note No. 24”) which collected and ordered the nomenclature for these molecules. The names of catenanes and rotaxanes originate from Latin: *catena* means “chain”, *rota* and *axis* mean “wheel” and “axle”, respectively. The number appearing in the notation at the beginning of the name (in square brackets) denotes the total number of linear and macrocyclic components.

The catenane molecule is made from interlocked macrocycles which are able to move independently (with respect to another one(s)). This movement is called *pirouetting*.

The same movement appears in the case of rotaxanes (cf. Fig. 1.2(a)). However in the case of rotaxanes the macrocycle (one or more) is located on the linear part called thread. Such molecule is named pseudorotaxane. By completing the ends of thread by two bulky stoppers the pseudorotaxane starts to be the rotaxane. The unique architecture of rotaxane molecule leads to increasing degrees of freedom. In the case of rotaxane the macrocycle can not only rotate around the thread but can also move along it. This movement, called shuttling, is limited by stoppers.

During last years many significant progress have been made in the aim to control and to exploit molecular level mechanical motion [37, 38, 39, 40, 41, 42, 43].

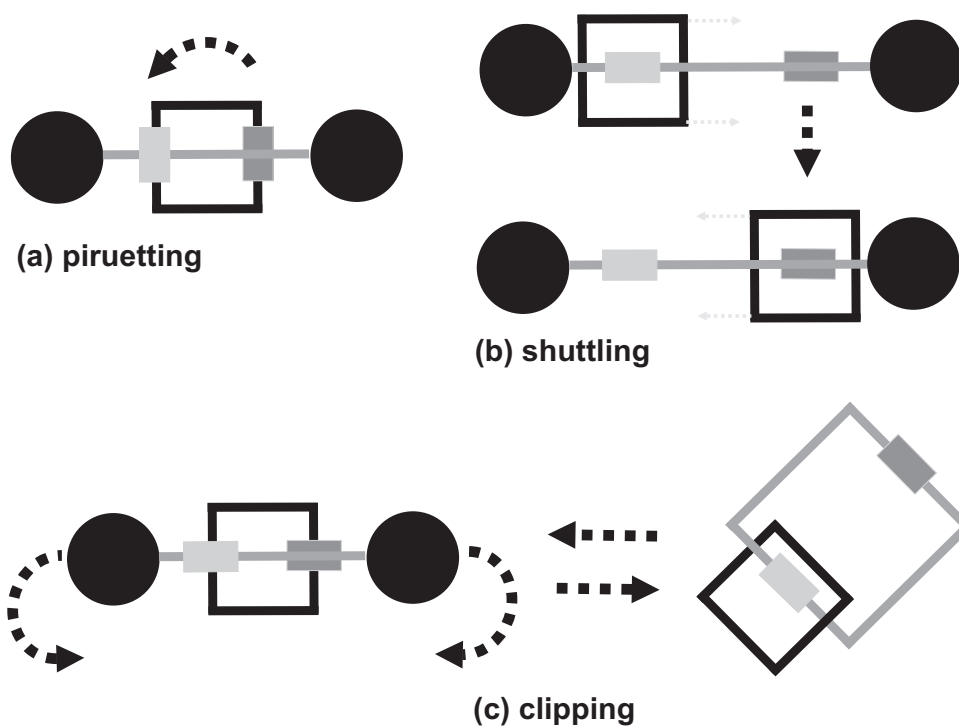


Figure 1.2: Schematic representation of three types of movements in rotaxanes: (a) pirouetting, (b) shuttling, and (c) clipping (transformation of [2] rotaxane into [2] catenane).

### 1.3.1 Synthesis of catenanes and rotaxanes

First syntheses of catenanes and rotaxanes were based on statistical threading approaches or on chemical conversion [44]. To obtain the catenane molecule one ring must be clipped on the second one (cf. Fig. 1.3(a)).

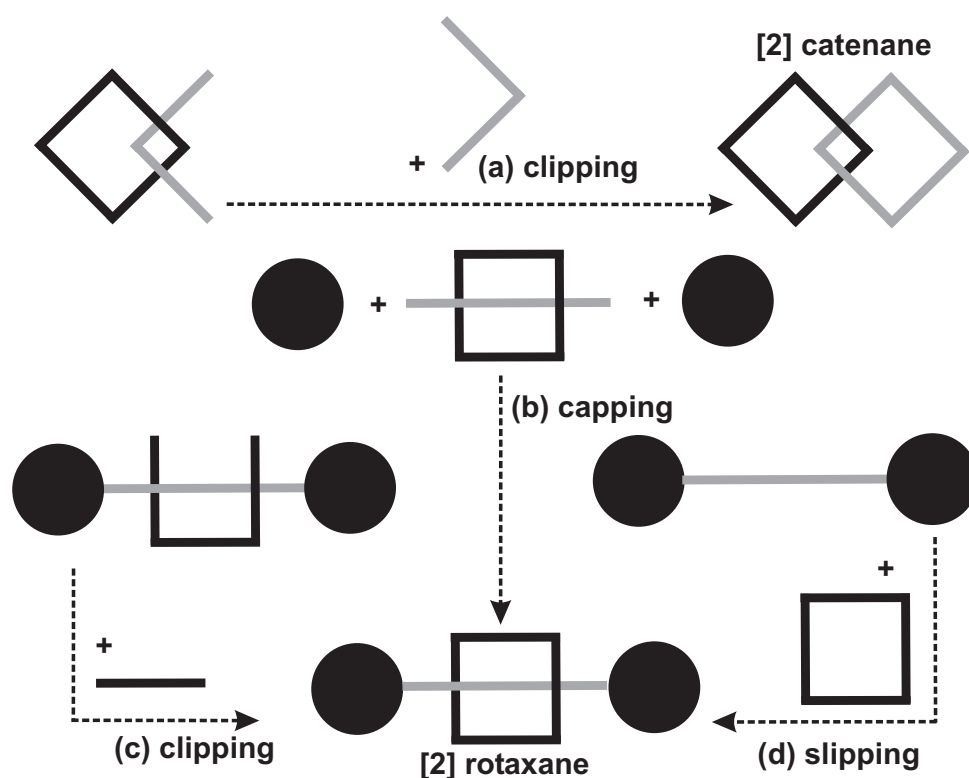


Figure 1.3: Schematic representation of synthesis route for catenane: (a) - clipping, and three types of synthesis routes for rotaxane: (b) - capping, (c) - clipping, and (d) - slipping.

In the case of rotaxanes, there are three possible approaches to their formation: synthesis of macrocycle and then of linear component (thread) followed by its end-capping (cf. Fig. 1.3(b); process often referred to as “stopping”); clipping of performed dumbbell with a suitable  $u$ -type component that is subsequently cyclized around the thread (cf. Fig. 1.3(c)), and slipping of a preformed ring over the stoppers of a preformed dumbbell-stopped component into a thermodynamically favourable site on the rod part of the dumbbell (cf. Fig. 1.3(d)) [45].

To obtain the catenane molecule the simple 2 + 2 condensation technique of para-xylylene diamine and isophthaloyl chloride was used. The procedure was done in the presence of a base and in a suitable solvent [46, 47]. This method for synthesis the benzylic amide [2] catenane (1,7,14,20-tetraaza-2,6,15,19-tetraoxo-3,5,9,12,16,18,22,25-tetrabenzocyclohexosane)-(1',7',14',20'-tetraaza-2',6',15',19'-tetraoxo-3',5',9',12',16',18',22',25'-tetrabenzocyclohexosane); further called *catenane*)

molecule was proposed by A.G. Johnston et al [46, 47] and gave a high yield (cf. Fig. 1.4). The same group (D.A. Leigh's group from University of Edinburgh) proposed the synthesis route for benzylic amide [2] rotaxane (fumaramide [2] rotaxane, further called *fumrot*) preparation [48, 49] (cf. Fig. 1.5).

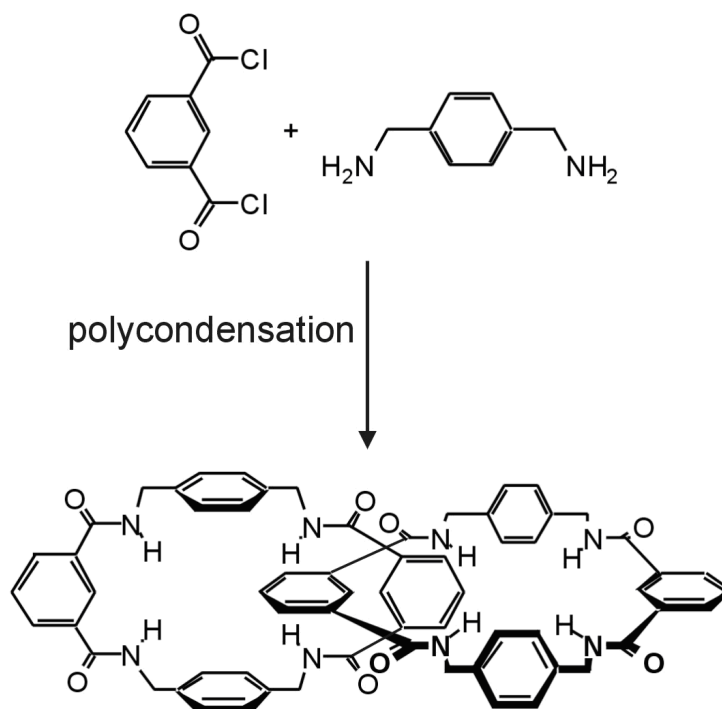


Figure 1.4: Synthesis of *catenane* molecule proposed by A.G. Johnston et al. [46, 47].

Additional for the mentioned molecules: *catenane* (cf. Fig. 1.10) and *fumrot* (cf. Fig. 1.8) in our work the molecules of benzylic amide macrocycle (1,7,14,20-tetraaza-2,6,15,19-tetraoxo-3,5,9,12,16,18,22,25-tetrabenzocyclohexosane, further called *macrocycle* (only for theoretical calculations, cf. Fig. 1.6, [41, 48]), thread with aliphatic chains (further called *thread*, cf. Fig. 1.8) and fumaramide [2] rotaxane with aliphatic chains (further called *rotaxane*, cf. Fig. 1.9) were used.

The molecule of thread *thread*:  $N^1, N^1, N^4, N^4$ -tetraisoctylfumaramide,  $R_2NCOCH=CHCONR_2$  where  $R$  is  $CH_2CH(CH_2CH_3)CH_2CH_2CH_2CH_3$  was synthesised as follows:

To an ice-cooled solution of diisooctylamine (7.2 mL, 23.9 mmol) and triethylamine (4.6 mL, 32.6 mmol) in 20 mL of anhydrous benzene a solution of fumaryl chloride (1.3 mL,

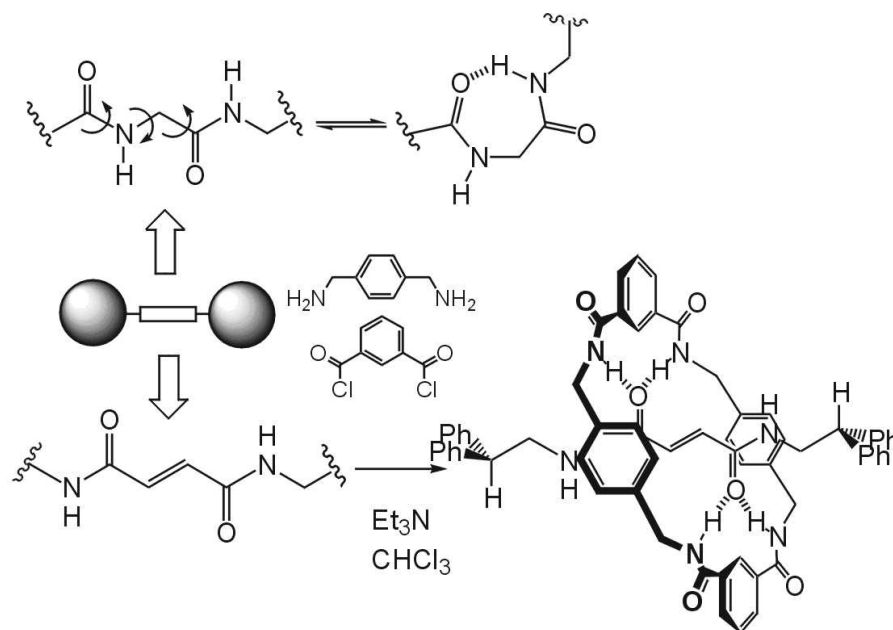


Figure 1.5: Synthesis of *fumrot* molecule proposed by A.G. Johnston et al. [48, 49].

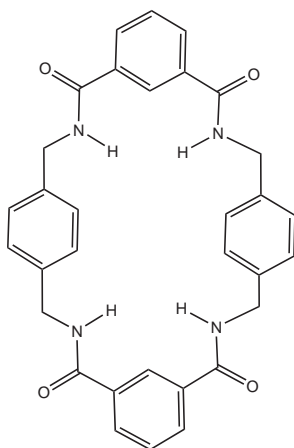


Figure 1.6: Chemical structure of *macrocycle* molecule.

10.9 mmol) in 5 mL of benzene was added. The reaction mixture was stirred for 12 hours after which, 50 mL of ethyl acetate was added. The organic phase was washed with 1 M aqueous HCl ( $2 \times 50$  mL), saturated aqueous  $\text{NaHCO}_3$  ( $3 \times 50$  mL), brine (50 mL), dried over anhydrous  $\text{MgSO}_4$ , filtered and concentrated under reduced pressure. The resulting

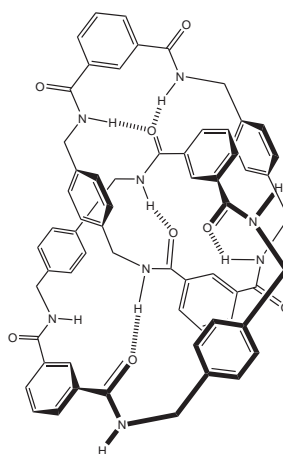


Figure 1.7: Chemical structure of *catenane* molecule.

red oil was purified using short-path flash column chromatography on silica gel (eluent:  $\text{CHCl}_3/\text{MeOH}$  97.5 : 2.5) to give the titled product (**thread**, 4.36 g, 71%).

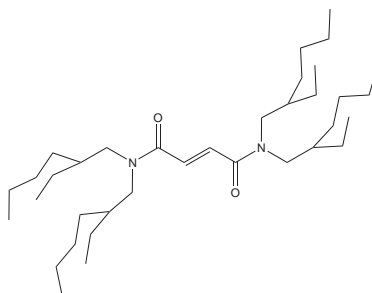


Figure 1.8: Chemical structure of *thread* molecule:  $\text{C}_{36}\text{H}_{70}\text{N}_2\text{O}_2$ ; Exact mass: 562.54373; Mol. Wt.: 562.9532; C, 76.81; H, 12.53; N, 4.98; O, 5.68

In the case of *rotaxane*: [2]-(1,7,14,20-tetraaza-2,6,15,19-tetraoxo-3,5,9,12,16,18,22,25-tetrabenzocyclohexacosane)-[(E)-*N,N,N',N'*-tetrαιοctylbutendiamide]-rotaxane the following synthesis were used: Solutions of isophthaloyl dichloride (2.31 g, 11.37 mmol) in 40 mL of  $\text{CHCl}_3$  and of p-xylylenediamine (1.55 g, 11.37 mmol) in 40 mL of  $\text{CHCl}_3$  were added simultaneously to a solution of *N*<sup>1</sup>,*N*<sup>1</sup>,*N*<sup>4</sup>,*N*<sup>4</sup>-tetrαιοctylfumaramide (0.40 g, 0.71 mmol) in 200 mL of  $\text{CHCl}_3$  and  $\text{Et}_3\text{N}$  (3.2 mL) over a period of 3 hours using motor-driven syringe pumps.

After further 3 hours the resulting mixture was filtered and the filtrate was concentrated under reduced pressure. The residue was subjected to column chromatography on silica gel using a solvent gradient of  $\text{CH}_2\text{Cl}_2$  to  $\text{CH}_2\text{Cl}_2/\text{AcOEt}$  (from 96/4 to 80/20) to obtain the titled product as a colourless solid (*rotaxane*, 101 mg, 13%).

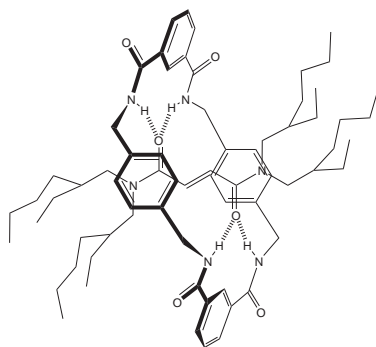


Figure 1.9: Chemical structure of *rotaxane* molecule.

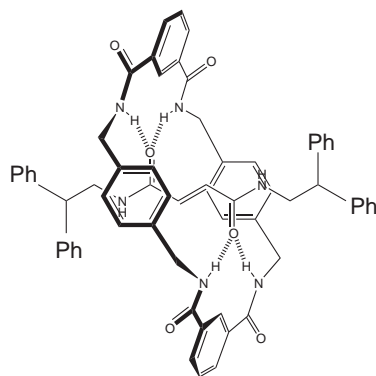


Figure 1.10: Chemical structure of *fumrot* molecule.

All molecules (catenanes, rotaxanes and their parts) were synthesised by group of Dr David Leigh from School of Chemistry at the University of Edinburgh.

### 1.3.2 Functionalization of rotaxanes

The rotaxane molecule can be functionalized either by modifying the tread (i.e. modification of *fumrot*'s *thread* to get *rotaxane* as a result), either by modifying the macrocycle

through attaching functionalized group. An example of modifying the macrocycle is pre-

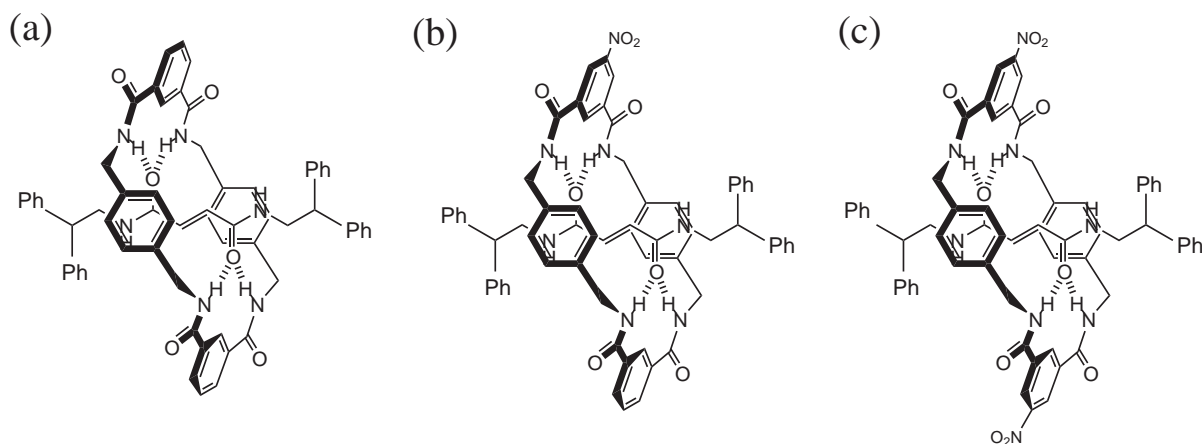


Figure 1.11: Chemical structure of pure (a), mono- (b), and di- (c) substituted *fumrot* [50].

sented in Fig. 1.11, where one nitro group ( $\text{NO}_2$ ) was added (mono-nitro *fumrot*, cf. Fig. 1.11(b)), or two nitro groups were added (di-nitro *fumrot*, cf. Fig. 1.11(c)). The

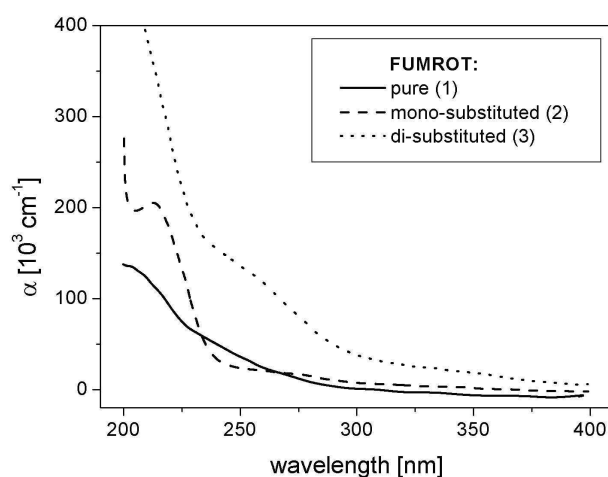


Figure 1.12: Absorption spectra of pure, mono-, and di- substituted *fumrot* [50].

absorption spectra of modified in this way *fumrot* with mono and di-substitution are shown in Fig. 1.12 [50]. Such modification, which does not alter significantly the absorp-

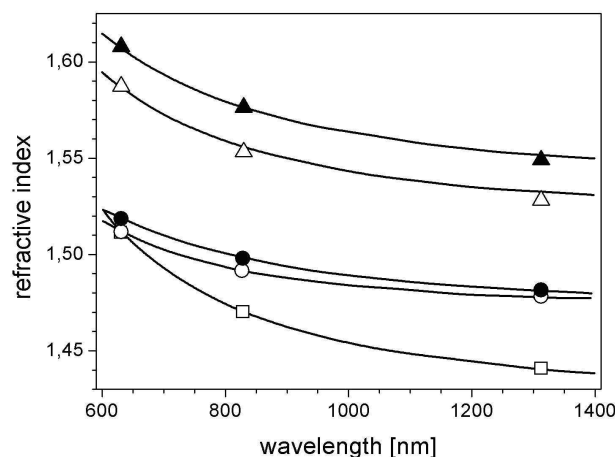


Figure 1.13: Refractive index dispersion in evaporated thin films of pure (triangles), mono-nitro (circles) and di-nitro *fumrot* (squares). Full figures show ordinary whereas the open the extraordinary index of refraction, respectively. Solid lines are Sellmeier fits [50].

tion band, influence significantly the structural order and the value of refractive index through the influence of the substitution on the molecular packing in solid state. For the films of functionalized rotaxane, it was observed that the nitro group reduces the birefringence, the film becoming isotropic when two nitro groups were added (cf. Fig. 1.13). Also it was observed that the indices of refraction decrease with substitution due to less perfect packing [50].

## 1.4 Deoxyribonucleic acid

As it was mentioned previously the large catenanes are present in deoxyribonucleic acid (DNA) molecules which are the center of interest for scientist since 50s, when J. Watson and F. Crik discovered their double helices structures [51]. Firstly only the biologists and biochemists start to interest with this supermolecule and its role in biological life and living species. Since few years DNA attracts also an interest as material for potential applications in optics, photonics and electronics [52, 53, 54, 55, 56, 57, 58, 59].

DNA is a nucleic acid that contains the genetic instruction on the sequence of the aminoacids in proteins. DNA is composed of a sequence of four phosphate group, sugar

and bases: purines - adenine (A), guanine (G) and pyrimidines - cytosine (C) and thymine (T). These four bases form hydrogen bonds which stabilize double helix of DNA as well as forces generated by the hydrophobic effect and  $\pi$ -stacking. Therefore the double helix of nucleobase pair of DNA, with  $\pi$ - $\pi$  stacking structure, form a tunnel ready to the electron transfer [60].

DNA itself is an optically passive material. In order to render it active, one has to functionalize it with photoresponsive molecules. These molecules can be blended with the DNA matrix by intercalation in stacked layers of nucleic acid bases of the helix, by inserting into the major and minor grooves of DNA helix or by electrostatically stacking on the surface of DNA helix [61, 62].

The DNA-CTMA system was obtained in the following way. A 6 g/L solution of DNA in 18 M $\Omega$  cm deionized water at 20° C, was obtained using a magnetic stirrer during the night. The CTMA surfactant, with a slightly higher concentration (6.2 g/L), was dissolved under the same conditions in 18 M $\Omega$  cm deionized water. One litre of the aqueous DNA-Na<sup>+</sup> solution was added dropwise to 1 L of aqueous solution of cationic amphiphiles and mixed at room temperature during 6 hours. The precipitated DNA-CTMA surfactant complex was collected by vacuum filtration through a 0.4  $\mu$ m nylon filter, washed with 18 M $\Omega$  cm deionized water and then dried in vacuum at 35° C.

The obtained in this way DNA-CTMA complex is insoluble in water, but soluble in such organic solvents as chloroform, benzene and a large number of alcohols including isopropanol, methanol, ethanol and butanol. These solvents are more convenient in thin film processing and device fabrication than water.

The DNA molecule is highly transparent with limited  $\pi$  electron conjugation (phenyl rings), that is why not large  $\chi^{(3)}$  susceptibility is expected. Therefore to increase its nonlinear optical (NLO) response we have doped DNA-CTMA with N-Ethyl-N-(2-hydroxyethyl)-4-(4-nitrophenylazo)aniline (Disperse Red 1, DR1) dopant, known for the  $\pi$  electron delocalization.

The Disperse Red 1 chromophore, purchased from Aldrich, was purified by a double recrystallization from an absolute methanol solution. Its chemical structure is shown on Fig. 1.15

Chemical preparation (purification, functionalization...) of materials was made by Dr Oksana Krupka from University of Angers.

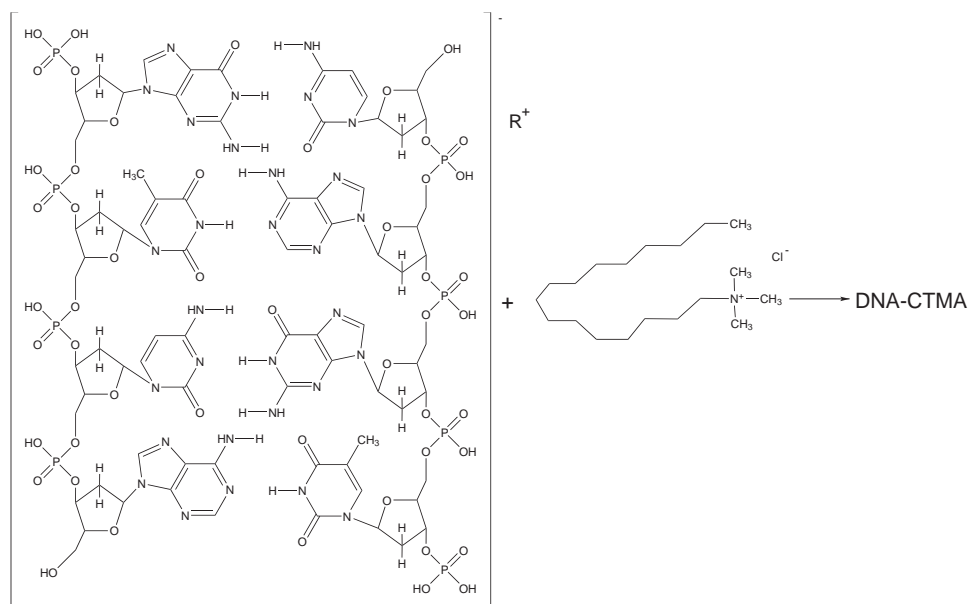


Figure 1.14: Chemical structure of DNA segment and surfactant CTMA.

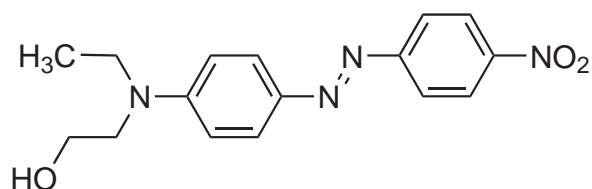


Figure 1.15: Chemical structure of Disperse Red 1.

### 1.4.1 DNA Properties

Unusual properties of the double helix are not easily replicated in conventional organic and inorganic materials like  $\pi$ - $\pi$  stacking structure of the base pairs of DNA which forms a tunnel ready for electron transfer and gives the film materials of high transparency or easy intercalation or insertion fluorescent dyes in the helices whose resulting in greatly enhanced fluorescence intensity. Moreover this interaction are relatively non-specific that involves insertion of all part of the ligand between adjacent base pairs and insertion of all or part of the ligand in a minor grooves [60]. Succeeding an interesting property is

exceptional chiral secondary structure makes DNA able to turn the plane of the linearly polarized light [63].

DNA is the most famous biomaterial, renewable resource and inherently biodegradable. Moreover, as the most of the organic materials it is abundant and expensive wasting product of the industry.

Although a lot of the properties about “the molecule of life” are known, it is still a mystery, which attracts the interest of the wide scientific community. [64, 65, 66, 67, 53, 54, 55, 56, 57, 58, 59].

The invaluable source of DNA for scientific investigations is salmon and scallop milt and roe. Green deoxyribonucleic acid is first isolated from frozen salmon milt through a homonization process, then make subject to an enzymatic and a carbon treatment to degrade the proteins and for decolorization, respectively. After this processes, DNA solution is filtered and precipitated by adding acetone, again filtered and dried. Obtained in that way purified DNA possesses high molecular weight (about  $M_w = 8000$  kDa) which can be reduced to  $< 200$  kDa by sonication process [54, 68].

Purified DNA strands possess attractive physical properties for its applications in photonics and molecular electronics, but they are sensitive for the fabrication methods and environment conditions. Also, the dissolubility only in water and inefficient mechanical strength for the fabrication make the application of this biomaterial as a part of the optic or electro optic devices unprofitable.

### 1.4.2 Functionalization of DNA

The most common cationic surfactant complex which is intercalate to DNA structure is cetyltrimethyloammonium chloride (CTMA), but adding to DNA such compounds as cetylbenzylidimethylammonium (BDMA) or cetylpyridinium chloride (CP) results in similar properties like DNA-CTMA complex [60].

The cationic surfactant alkyl chains are from the one side sufficiently long to improve poor mechanical property of the DNA and on the other hand enough short to not damage the double helix structure of DNA. This length causes that compounds are still water-soluble what facilitate DNA-cationic surfactant complex preparation process.

DNA and compounds described above are separately dissolved in the water. Two solutions mix and precipitate. During preparation cationic surfactant complex replaced the sodium cation of the DNA. Resulting DNA-surfactant complex is water-insoluble but dissolved in organic solvent such as ethanol, methanol, butanol, chloroform solvents or

chloroform/alcohol blend. This complex possesses efficient mechanical strength and high thermal stability limit which makes it suitable for device fabrication. Thin films made from DNA- cationic surfactant complex solutions are characterized by low optical loss and high optical quality [54].

# Chapter 2

## Basis of linear and nonlinear optics and quantum chemistry

### Contents

---

<b>2.1</b>	<b>Introduction to the chapter</b>	<b>19</b>
<b>2.2</b>	<b>Interaction of light with matter</b>	<b>20</b>
2.2.1	Maxwell equations	20
2.2.2	Transmission, absorption, and reflection	22
2.2.3	Macroscopic polarization	24
2.2.4	Phase matching	24
2.2.5	Second order susceptibility	25
2.2.6	Third order susceptibility	26
2.2.7	Microscopic polarization	27
<b>2.3</b>	<b>Quantum chemistry</b>	<b>28</b>
2.3.1	Hartree-Fock method	29
2.3.2	Configuration interaction method	29

---

### 2.1 Introduction to the chapter

In this chapter the introduction to nonlinear optics is done. Some physical basis will be presented as well as models describing nonlinear phenomena. The basis of quantum chemistry will be presented in order to introduce some methods of chemical calculations.

## 2.2 Interaction of light with matter

The real start of interest and investigation for nonlinear optics dates back to the early sixties when first laser became available to all scientists.

Beam of light, which strike material, causes oscillation of atoms charges. In a linear material the amount of charge displacement is proportional to the instantaneous magnitude of the electric field. The frequency of oscillating charges and the frequency of incident light are the same. The oscillating charges either emit light at that frequency or the energy is transferred into non-radiative modes that result in material heating or other energy transfer mechanisms. It is easy to show that for an isotropic and homogeneous material, the radiated light travels in the same direction as the incident light beam. The linear refractive index of a material ( $n$ ), is defined as the ratio of light speed in vacuum ( $c$ ), to the speed of light in the material ( $v$ ). If the motion of some of the charges within the material decays without producing light, some of the light intensity is lost from the incident beam by scattering, and absorbance. The absorbance is defined as a ratio of light intensity absorbed by material to the light intensity incident into the material divided by the material thickness. The absorbance and refractive index, are linear optical properties of a material for low intensity incident light [12, 69, 70, 71].

### 2.2.1 Maxwell equations

The purpose of nonlinear optics is to understand the nonlinear behaviour in the induced polarization and to analyse and control its influence on the propagation of light in the matter. The NLO phenomena can be represented by the Maxwell's equations (2.1-2.4) in C.G.S. unit system:

$$\nabla \cdot \vec{D} = 4\pi\rho, \quad (2.1)$$

$$\nabla \cdot \vec{B} = 0, \quad (2.2)$$

$$\nabla \times \vec{E} = -\frac{1}{c} \frac{\partial \vec{B}}{\partial t}, \quad (2.3)$$

$$\nabla \times \vec{H} = \frac{4\pi}{c} \vec{j} + \frac{\partial \vec{D}}{\partial t}, \quad (2.4)$$

where:  $\vec{E}$  is the electric field vector,  $\vec{H}$  is a magnetic field vector,  $\vec{B}$  is the magnetic induction vector,  $\vec{D}$  is the electric displacement vector,  $\vec{j}$  is the current density vector,  $\rho$

is the charge density, and  $c$  is the speed of light in vacuum. For nonconducting medium (electromagnetic field is considered in a vacuum) the Eqs (2.1-2.4) reduce to

$$\nabla \cdot \vec{D} = 0, \quad (2.5)$$

$$\nabla \cdot \vec{B} = 0, \quad (2.6)$$

$$\nabla \times \vec{E} = -\frac{1}{c} \frac{\partial \vec{B}}{\partial t}, \quad (2.7)$$

$$\nabla \times \vec{H} = \frac{1}{c} \frac{\partial \vec{D}}{\partial t}. \quad (2.8)$$

The four field vectors ( $\vec{D}$ ,  $\vec{B}$ ,  $\vec{E}$ ,  $\vec{H}$ ) are linked by the following material equations (2.9-2.10):

$$\vec{D} = \vec{E} + 4\pi\vec{P}, \quad (2.9)$$

$$\vec{B} = \vec{H} + 4\pi\vec{M}, \quad (2.10)$$

where  $\vec{P}$  is the electric polarization and  $\vec{M}$  is the magnetic polarization. When we consider pure dielectric material (without current density and without magnetic field), the following relationships are satisfied:

$$\rho = 0, \quad \vec{j} = 0 \quad \text{and} \quad \vec{M} = 0. \quad (2.11)$$

Substituting Eqs. (2.9-2.10) into Eqs. (2.5-2.8), and taking into account that material is isotropic and nonmagnetic (2.11), the equation for electric field of the light wave in terms of electric polarization will be given:

$$\nabla \times \nabla \times \vec{E} - \frac{1}{c^2} \frac{\partial^2 \vec{E}}{\partial t^2} = \frac{4\pi}{c} \frac{\partial \vec{P}}{\partial t}. \quad (2.12)$$

In the linear regime when the electric field is small relatively to the intra-atomic field, the electric polarization vector is proportional to the electric field vector:

$$\vec{P} = \chi^{(1)} \vec{E}, \quad (2.13)$$

where the  $\chi^{(1)}$  is linear electric susceptibility which characterize the linear properties of matter.

Substituting Eq. (2.13) into Eq. (2.12) the equation describing the wave propagation can be written as follows:

$$\nabla^2 \times \vec{E} - \frac{1}{c^2}(1 + 4\pi\chi^{(1)})\frac{\partial^2 \vec{E}}{\partial t^2} = 0, \quad (2.14)$$

where  $1 + 4\pi\chi^{(1)} = \epsilon$ . The solution of Eq. (2.14) is a wave:

$$\vec{E} = \vec{E}_0 \exp(i(\vec{k}\vec{r} - \omega t)), \quad (2.15)$$

where  $\vec{k}$  is the wave vector which is defined as follows:

$$\vec{k} = \frac{\omega}{v}\vec{u}, \quad (2.16)$$

where  $\vec{u}$  is the unit vector in the direction of wave propagation.

Equation (2.16) can be also presented in following way:

$$k^2 = \epsilon \frac{\omega^2}{c^2} \quad (2.17)$$

and then the real part of the refractive index is given by:

$$n = \frac{c}{v} = \sqrt{\epsilon}, \quad (2.18)$$

where  $v$  is the velocity of propagation of the electromagnetic disturbance. Taking square of Eq. (2.18) and remembering that  $1 + 4\pi\chi^{(1)} = \epsilon$  we receive:

$$n^2 = \epsilon = 1 + 4\pi\chi^{(1)} \quad (2.19)$$

In transparent media, refraction index depends only on properties of medium and on wavelength of incident beam, and does not depend on intensity of incident beam [12, 69, 72].

### 2.2.2 Transmission, absorption, and reflection

The beam of light which travel through the medium is connected with light's energy absorption.

We consider monochromatic beam incident on the medium. When the beam (with intensity  $I$ ) travels thickness  $l$ , intensity of light will decrease. This dependence is given by Lambert's Beer law:

$$I = I_0 \exp(-\alpha l), \quad (2.20)$$

where  $\alpha = 4\pi\kappa/\lambda$  is absorption coefficient,  $\kappa$  is the extinction coefficient,  $\lambda$  is the wavelength,  $I_0$  is the light intensity of incident beam and  $I$  is the intensity of transmitted beam.

Reflection and transmission of light waves occur because the frequencies of the light waves do not match the natural frequencies of vibration of the medium. When light of these frequencies strike a medium, the electrons in the atoms of the object begin to vibrate. But instead of vibrating in resonance at large amplitude, the electrons vibrate for brief periods of time with small amplitudes of vibration; then the energy is reemitted as a light wave. If the medium is transparent, then the vibrations of electrons are passed on to neighbouring atoms through the bulk of the material and reemitted on the opposite side of the medium. Such frequencies of light waves are said to be transmitted. If the object is opaque, then the vibrations of the electrons are not passed from atom to atom through the bulk of the material; rather the electrons vibrate for short periods of time and then reemit the energy as a reflected light wave. Such frequencies of light are said to be reflected.

The relation between intensity of transmitted light and intensity of incident light is called transmission ( $T$ ) and is given by:

$$\frac{I}{I_0} = T = \exp(-\alpha l). \quad (2.21)$$

However the relation between intensity of reflected light ( $I_R$ ) and intensity of incident light is called reflection ( $R$ ) and is given by:

$$\frac{I_R}{I_0} = R. \quad (2.22)$$

If the medium thickness is equal  $l$ , then through the first border of the medium pass only the part of radiation equal  $(1 - R)I_0$ , second border is reached by  $(1 - R)I_0 \exp(-\alpha l)$  and external goes out  $(1 - R)^2 I_0 \exp(-\alpha l)$ . The radiation reflected in the medium can also go out but then it is widely weakened. Coefficient of transmission, in the case of multi-reflection we can write as follows:

$$T = \frac{(1 - R)^2 \exp(-\alpha l)}{1 - R^2 \exp(-2\alpha l)}. \quad (2.23)$$

We can neglect the second part in denominator and then Eq. (2.23) is written as follows [69]:

$$T \approx (1 - R)^2 \exp(-\alpha l). \quad (2.24)$$

From Eq. (2.24) we can determine coefficient of linear absorption which is given by:

$$\alpha = -\frac{1}{l} \ln \left[ \frac{T}{(1-R)^2} \right]. \quad (2.25)$$

### 2.2.3 Macroscopic polarization

When the intensity of light is sufficiently high (e.g., from laser) a small additional polarization will appear, so that the total polarization can be written as

$$\vec{P} = \vec{P}_L + \vec{P}_{NL}, \quad (2.26)$$

where  $\vec{P}_{NL}$  is a nonlinear function of the applied field.

This polarization  $\vec{P}$  can be developed into a power series of the electric field:

$$\vec{P} = \vec{P}_i(\vec{r}, t) = \chi_{ij}^{(1)} \vec{E}_j + \chi_{ijk}^{(2)} \vec{E}_{jk}^2 + \chi_{ijkl}^{(3)} \vec{E}_{jkl}^3 + \dots, \quad (2.27)$$

where

- $\chi^{(1)}$  is the first-order susceptibility which is responsible for linear phenomena such as refraction and absorption,
- $\chi^{(2)}$  is the second-order optical susceptibility includes second harmonic generation (SHG), linear electro-optic effect (Pockels effect) and frequency mixing,
- $\chi^{(3)}$  is the third-order optical susceptibility includes third harmonic generation (THG), degenerate four-wave mixing (DFWM) and optical Kerr effect (OKE), phase conjugation Degenerate, saturation absorption, photoinduced absorption and electrooptic Kerr effect.

### 2.2.4 Phase matching

Many phase-sensitive nonlinear processes, in particular parametric processes such as frequency doubling, sum- and difference frequency generation, parametric amplification, and four-wave mixing, require phase matching to be efficient. Essentially this means to ensure that a proper phase relationship between the interacting waves is maintained along the propagation direction. More precisely, one ensures that the phase mismatch is close to zero; for example, for frequency doubling with collinear beams the phase mismatch is given by:

$$\Delta k = k_2 - 2k_1, \quad (2.28)$$

where  $k_1$  and  $k_2$  are the wavenumbers of the fundamental and second harmonic beam, respectively. Without chromatic dispersion, we would have  $k_2 = 2k_1$ , so that the phase mismatch vanishes, but dispersion generally causes a non-zero phase mismatch if no special measurement techniques are taken to avoid this.

Phase matching for frequency doubling can be achieved by using two different polarization directions for pump and second-harmonic wave (birefringent phase matching). One may use propagation along some crystal axes and adjust the crystal temperature so that phase velocities of both waves are equal. This is called noncritical phase matching, because the alignment of the propagation direction is not critical. Alternatively, one may control the crystal orientation or the angle between the propagation directions of interacting beams to achieve phase matching. Due to the more critical angular alignment, this is called critical phase matching.

When phase matching is achieved, the group velocities of the interacting waves are in general still not matched; there is a certain group velocity mismatch, which limits the interaction length for pulses and the spectral range (called phase matching bandwidth) in which phase matching is achieved. Also, there is only a finite range of beam angles where phase matching works - particularly for critical phase matching. This range of angles is usually called the angular phase-matching bandwidth.

### 2.2.5 Second order susceptibility

Frequency doubling is a phase-sensitive process which usually requires phase matching to be efficient. High conversion efficiencies can be achieved even with moderate or low average pump powers when the pump light is delivered in the form of pulses, generated with a mode-locked or Q-switched laser. This is simply because for a given average power a pulsed laser exhibits higher peak powers. For frequency conversion of ultra short pulses, the effective interaction length and thus the conversion efficiency can be limited by group velocity mismatch.

In mathematical description of SHG we assume that the medium is lossless at both fundamental frequency ( $\omega_1$ ) and second harmonic frequency ( $\omega_2 = 2\omega_1$ ), so that the nonlinear susceptibility obeys the condition of full permutation symmetry [10].

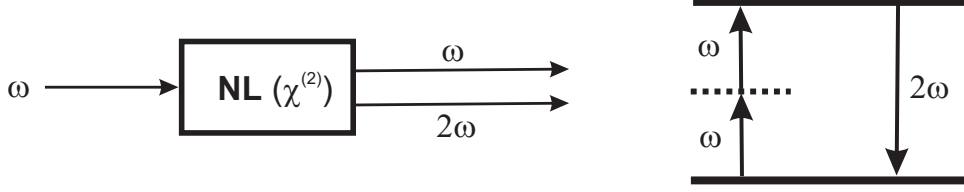


Figure 2.1: Geometry of second harmonic generation process (left) and energy-level diagram describing this process (right).

### 2.2.6 Third order susceptibility

Third-order or cubic polarization reveals itself in media with a center of symmetry. In this case the number of nonlinear optical processes is larger. In isotropic, optical nonactive media, nonlinear influence of electromagnetic waves shows scarcely in allowance of third order polarization, which is given by

$$\vec{P}_3(t) = \chi^{(3)} \vec{E}^3(t), \quad (2.29)$$

induced by an applied field that consists of three frequency components  $\omega_1, \omega_2, \omega_3$ :

$$\vec{E}(t) = \vec{E}_1^3 e^{-i\omega_1 t} + \vec{E}_2^3 e^{-i\omega_2 t} + \vec{E}_3^3 e^{-i\omega_3 t} + c.c., \quad (2.30)$$

Polarization in Eq. (2.29) contains 44 different frequency components:

$$\begin{aligned} &\omega_1, \omega_2, \omega_3, 3\omega_1, 3\omega_2, 3\omega_3, (\omega_1 + \omega_2 + \omega_3), (\omega_1 + \omega_2 - \omega_3), (\omega_1 + \omega_3 - \omega_2), \\ &(\omega_2 + \omega_3 - \omega_1), (2\omega_1 \pm \omega_2), (2\omega_1 \pm \omega_3), (2\omega_2 \pm \omega_1), (2\omega_2 \pm \omega_3), \\ &(2\omega_3 \pm \omega_1), (2\omega_3 \pm \omega_2), \end{aligned} \quad (2.31)$$

and the negative of each.

In general third order nonlinear optical susceptibility ( $\chi^{(3)}$ ) is considered to be a complex quantity:

$$\chi^{(3)} = \chi^{(3)'} + i\chi^{(3)''}, \quad (2.32)$$

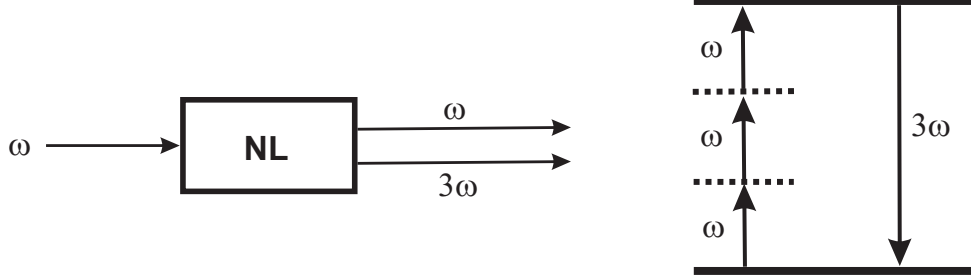


Figure 2.2: Third harmonic generation process (left) and energy level diagram (right).

where the real part ( $\chi^{(3)'}$ ) of third order nonlinear optical susceptibility is related to the nonlinear refractive index ( $n_2$ ) changes by equation:

$$\chi^{(3)'} = \frac{cn_0^2}{12\pi^2}n_2, \quad (2.33)$$

and imaginary part ( $\chi^{(3)''}$ ) is related to the two-photon absorption coefficient ( $\beta$ ) by following relation:

$$\chi^{(3)''} = \frac{n_0^2\lambda}{48\pi^3}\beta. \quad (2.34)$$

### 2.2.7 Microscopic polarization

For device applications the parameters of importance are the components of the macroscopic polarizabilities of the medium, as given in Eq. (2.27), however the microscopic point of view is also very important and very often can give some ideas about observed behaviours. At the molecular level macroscopic polarization can be developed in the dipolar approximation into a power series of external electric field strengths:

$$\vec{P} = N(\alpha_{ij}^h \vec{E}_{loc} + \beta_{ijk}^h \vec{E}_{loc}^2 + \gamma_{ijkl}^h \vec{E}_{loc}^3 + \dots), \quad (2.35)$$

where  $\alpha^h$ ,  $\beta^h$ ,  $\gamma^h$  are the linear polarizability, the first hyperpolarizability, and the second hyperpolarizability, respectively [73].

In the approximation of Lorentz-Lorentz local field model the  $\vec{E}_{loc}$  can be expressed as follows:

$$\vec{E}_{loc} = F\vec{E}, \quad (2.36)$$

where  $F$  is the local field correction factor:

$$F = \frac{n_0^2 + 2}{3}, \quad (2.37)$$

where  $n_0$  is the refractive index of material [74].

Now, the second order hyperpolarizability can be expressed as follows:

$$\gamma^h = \frac{\chi^{(3)}}{F^4 N} \quad (2.38)$$

In the case when investigated material is in solution form, following relation is needed to determine nonlinearity of solution:

$$\chi_{solution}^{(3)} = F^4 N \gamma^h + \chi_{solvent}^{(3)}. \quad (2.39)$$

When the solvent is non polar, the interaction solvent-molecule can be neglect. In this case the relation between the hyperpolarizability  $\gamma^h$  of molecule and third order nonlinear optical susceptibility of solvent ( $\chi_{solvent}^{(3)}$ ) is expressed as follows:

$$\gamma^h = \frac{\chi_{solution}^{(3)} M}{F^4 N_A C}, \quad (2.40)$$

where  $N_A$  is the Avogadro Number ( $N_A = 6.022 \times 10^{23} \text{ 1/mol}$ ),  $M$  is the molar mass and  $C$  is the concentration.

## 2.3 Quantum chemistry

One of the fundamental assumption of quantum mechanics is that all of the properties of the atomic system can be described in terms of the atomic wavefunction  $\psi(\vec{r}, t)$ , which is the solution to the time-dependent Schrödinger equation

$$i\hbar \frac{\partial \psi}{\partial t} = \hat{H} \psi, \quad (2.41)$$

where  $\hat{H}$  is the Hamiltonian operator:

$$\hat{H} = \hat{H}_0 \hat{V}(t), \quad (2.42)$$

where  $\hat{H}_0$  is a Hamiltonian for a free atom and  $\hat{V}(t)$  is an interaction Hamiltonian which describes the interaction of the atom with the electromagnetic field.

### 2.3.1 Hartree-Fock method

In computational physics and computational chemistry, the Hartree-Fock (HF) method is an approximate method for the determination of the ground-state wavefunction and ground-state energy of a quantum many-body system.

The HF method assumes that the exact, N-body wavefunction of the system can be approximated by a single Slater determinant (in the case where the particles are fermions) or by a single permanent (in the case of bosons) of N spin-orbitals. By invoking the variational principle, one can derive a set of N-coupled equations for the N spin orbitals. Solution of these equations yields is the Hartree-Fock wavefunction and energy of the system, which are approximations of the exact ones.

For molecules, Hartree-Fock is the central starting point for most ab initio quantum chemistry methods.

### 2.3.2 Configuration interaction method

Configuration interaction (CI) is a method for solving the nonrelativistic Schrödinger equation

$$\hat{H}\Psi(\vec{R}, \vec{r}) = \left\{ \sum_A \frac{1}{2M_A} \nabla_A^2 + \sum_i \frac{1}{2} \nabla_i^2 + \sum_{A>B} \frac{Z_A Z_B}{R_{AB}} + \sum_{A_i} \frac{Z_A}{r_{Ai}} + \sum_{i>j} \frac{1}{r_{ij}} \right\} \Psi(\vec{R}, \vec{r}) = E\Psi(\vec{R}, \vec{r}), \quad (2.43)$$

where  $i, j$  denote electrons and  $A, B$  denote nuclei, with  $r_{ij} = |\vec{r}_i - \vec{r}_j|$ ,  $R_{Ai} = |\vec{R}_{Ai} - \vec{r}_i|$ , and  $R_{AB} = |\vec{R}_A - \vec{R}_B|$ . Typical applications of the CI method employ the Born-Oppenheimer approximation, whereby the motions of the electrons are treated as uncoupled from those of the nuclei. Thus the “electronic” Schrödinger equation is solved at discrete sets of fixed nuclear positions.



# Chapter 3

## Experimental Techniques

### Contents

---

<b>3.1</b>	<b>Introduction to the chapter</b>	<b>31</b>
<b>3.2</b>	<b>Degenerate four-wave mixing</b>	<b>32</b>
<b>3.3</b>	<b>Z-scan</b>	<b>33</b>
<b>3.4</b>	<b>Harmonic generation</b>	<b>35</b>
3.4.1	Second harmonic generation	35
3.4.2	Third harmonic generation	36
<b>3.5</b>	<b>Photoinduced diffraction gratings</b>	<b>37</b>
3.5.1	Photoisomerization of azobenzene	38
3.5.2	Degenerate two-wave mixing technique	39
<b>3.6</b>	<b>Other techniques</b>	<b>40</b>
3.6.1	Spin coating	40
3.6.2	Atomic force microscope	41

---

### 3.1 Introduction to the chapter

In this chapter we present the experimental techniques of investigation used in this work. These techniques are enable to determine third order nonlinear optical susceptibility (Degenerate four-wave mixing, third harmonic generation, z-scan) and second order nonlinear

optical susceptibility (second harmonic generation). The second part of this chapter contains the degenerate two-wave mixing method using to surface relief grating formation. At the end some other useful experiments are described.

## 3.2 Degenerate four-wave mixing

For characterization the nonlinear optical properties of studied molecules, we have used the degenerate four-wave mixing (DFWM) technique. It is sensitive method to determine the absolute value of third order nonlinear optical susceptibility, which is a complex value in the general case ( $\chi^{(3)} = \chi^{(3)'} + i\chi^{(3)''}$ ). The real part ( $\chi^{(3)'}$ ) of  $\chi^{(3)}$  tensor describe the refractive index changes while the imaginary parts ( $\chi^{(3)''}$ ) describe two photon absorption coefficient ( $\beta$ ).

As a source of excitation we used a Q-switched Nd:YAG laser (Quantel Model YG472) working at 532 nm with 30 ps pulse duration and a repetition frequency of 1 Hz. The geometry of the DFWM experimental setup is schematically presented in Fig. 3.1. First beam splitter (**BS1**) divides the laser beam into two beams. One part of the beam is sent to a photodiode, whose response is used to synchronizing the detection system. The half wavelength plate ( $\lambda/2$ ) and the polarizer (**P**) allow for smooth regulation of the laser beam intensity. The second beam splitter (**BS2**) reflects about 6% of intensity (third beam,  $\langle 3 \rangle$ ). The non-reflected part of the beam goes to the third beam splitter (**BS3**), which divides it into two pump beams  $\langle 1 \rangle$  and  $\langle 2 \rangle$  of the same intensity. These two, high intensity beams, are sent to the studied sample, in a counter propagation configuration and their intensities satisfy the relation  $I_1(z = 0) = I_2(z = l)$ . The third input wave is a weak probe beam ( $I_3 = 10^{-2}I_1$ ) which makes an angle of  $12^\circ$  with respect to the collinear pump beams. Optical delays (**RO1**, **RO2**, **RO3**) are used in order to match temporarily the three interacting beams. The half wavelength plates, located in optical paths of beams  $\langle 1 \rangle$  and  $\langle 2 \rangle$  as well as the polarizer **P** located before the beam splitter **BS5** allow to set up and control the polarizations of the incident beams. The signal wave  $\langle 4 \rangle$  is emitted in the opposite direction to the probe beam. Its polarization is rotated by 90 degrees by the half wave plate and consequently reflected by polarization depending beam splitter **BS5** [75].



but only decrease of the transmission due to the nonlinear absorption in the sample.

In our Z-scan measurements we used a modification of the Z-scan technique, called the optical nonlinear imaging. In that case we use a CCD camera in order to record the beam images when the sample is moved through the focal point.

Figure 3.2 shows the experimental setup. The excitation is provided by a linearly polarized mode locked Nd:YAG laser (Continuum Leopard D-10) at 1064 nm or 532 nm (pulse duration of 16 ps; 10 Hz). The Gaussian laser beam is focused using lens **L1** with focal distance  $f_1 = 20$  mm. The waist radius at the focal plane is  $w_0 = 30 \mu\text{m}$ , corresponding to a Rayleigh length of 2.7 mm (at 1064 nm). At 532 nm, we choose a beam waist radius at the entry of the setup in order to obtain a beam waist at the focused beam approximately the same as the one corresponding to the infrared wavelength ( $w_0 = 26 \mu\text{m}$ ). The measurements were performed using a  $4f$  system [81, 80] with  $5.1 \text{ GW}/\text{cm}^2$  incident peak intensity on the sample.

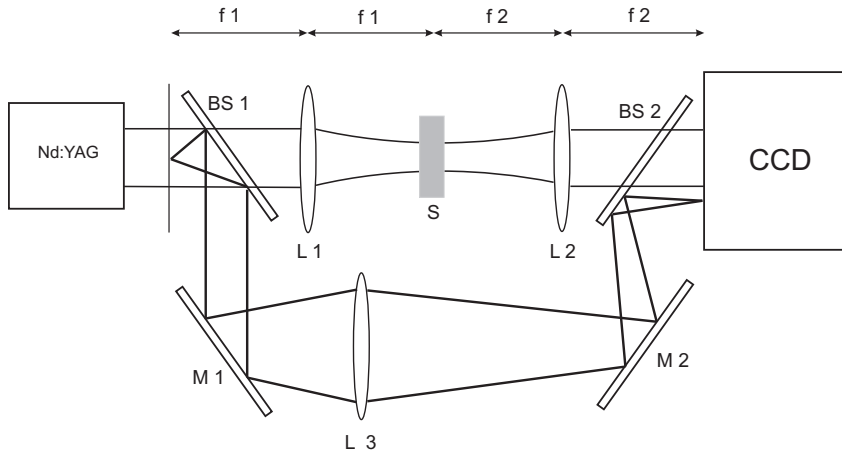


Figure 3.2: Z-scan experimental setup: **S** - sample, **BS** - beam splitter, **L** - lens, **M** - mirror.

As a detector a CCD camera was used in order to record the beam images when the sample is moved through the focal point. The image receiver is a  $1000 \times 1018$  pixels cooled camera ( $-30^\circ\text{C}$ ) operating with a fixed gain. It is placed at a distance equal to  $f_2 = 20$  mm from lens **L2**. From the luminous intensity of these images it is possible to calculate the real part of nonlinear index of refraction  $n_2$  and to plot the Z-scan curves.

A reference beam incident onto a small area of the camera allows the monitoring of the energy fluctuation of the laser. The sample is moved in the focus region along the

beam propagation direction ( $Z$  axis). Negative values of  $Z$  correspond to locations of the sample between the focusing lens and its focal plane. Open and closed Z-scan normalized transmittance were numerically processed from the acquired images by integrating over all the pixels in the first case and over a circular numerical filter in the second one (giving a linear aperture transmittance  $S$  equal to 0.2). Lens **L2** contribute to produce the Fourier transform of the field at the exit surface of the sample, which is physically similar to the far field diffraction obtained with the original Z-scan method.

## 3.4 Harmonic generation

### 3.4.1 Second harmonic generation

The second harmonic generation (SHG) is a coherent process where nonlinear medium generates, through nonlinear polarization,  $2\omega$  frequency wave when is illuminated by  $\omega$  frequency wave. This process concern only non-centrosymmetric materials (without centre symmetry). During this experiment the changes of the SHG intensity versus the incidence angle are measured. When the incidence angle is varied, the length of the optical pathway within nonlinear material is varied as well. When the thickness of the material ( $l$ ) is higher than the coherence length ( $L_c$ ), the waves contract and interfere to each other. The intensity of the second harmonic signal describe a series of maxima and minima called “Maker fringes” [82]. Few years after Maker, Jerphagnon and Kurtz gave theoretical description of the fringes [83].

The Maker fringes characterize the change in the interaction length when this is subjected to a rotational movement. The interaction length ( $L$ ) is given by the following relation:

$$L = \frac{l}{\cos \theta_i} \quad \text{with} \quad \theta_i = \arcsin \left( \frac{\sin \theta_j}{n_0} \right), \quad (3.1)$$

where  $l$  is the thickness of the medium and  $n_0$  is the refractive index.

The second harmonic generation intensity enveloped by Maker fringes is given by:

$$I_M(\theta) = \left( \frac{1}{(n^{(2\omega)})^2 - n^{(\omega)})^2} \right)^2 (d_{eff}(\theta))^2 (I^{(\omega)})^2 (t^{(\omega)}(\theta))^4 (T^{(2\omega)}(\theta)), \quad (3.2)$$

where  $d_{eff}(\theta)$  is the projection of the effective nonlinear coefficient on the electric field of the fundamental wave.  $t^{(\omega)}(\theta)$ ,  $T^{(2\omega)}(\theta)$  are the transmission coefficients at the frequencies

$\omega$  and  $2\omega$ , respectively,  $I^{(\omega)}$  is the intensity of incident beam,  $n^{(\omega)}$  and  $n^{(2\omega)}$  are the refractive indices of fundamental and second harmonic wave, respectively.

The experimental setup of SHG is presented on Fig. 3.3. The detailed description will be provided in third harmonic generation section.

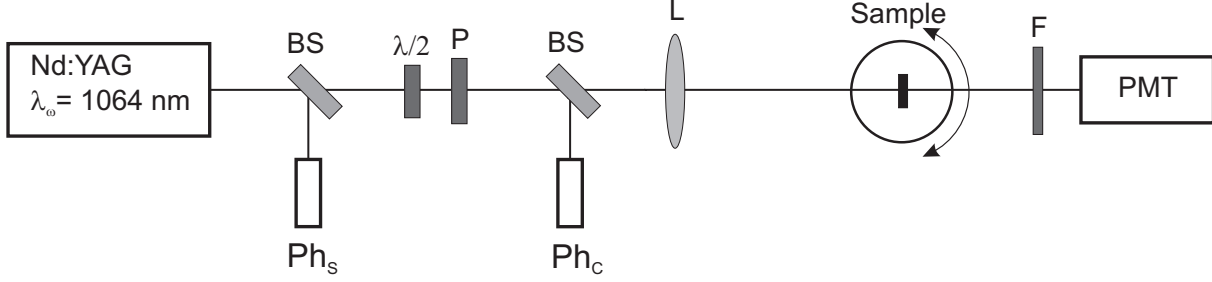


Figure 3.3: Schematic representation of the experimental setup for SHG (and THG) measurements: **BS** - beam splitter,  $\lambda/2$  - half wave plate, **P** - polarizer, **L** - convergent lens (250 mm), **F** - selective filter, **Ph<sub>s</sub>** - synchronization photodiode, **Ph<sub>c</sub>** - control photodiode and **PMT**- photomultiplier tube.

### 3.4.2 Third harmonic generation

Third harmonic generation (THG) technique enables in generating  $3\omega$  frequency wave by illuminated material by  $\omega$  frequency wavelength. This propagation of optical harmonic waves in isotropic nonlinear media was described by Bloembergen and Pershan [84]. Kajzar and Messier [85] described the theoretical bases for third harmonic generation technique (in liquid) and later for thin films [86]. Parallel to Kajzar and Messier other theoretical descriptions have been done i.e. by Reintjes [87] or Kubodera and Kobayashi [88].

The third harmonic generation intensity from thin films (deposited on substrates) is given by [86]:

$$I^{(3\omega)}(\theta) = \frac{64\pi^4}{c^2} \left| \frac{\chi^{(3)}}{\Delta\epsilon} \right|_f^2 \left| e^{i(\varphi_s^{(\omega)} + \varphi_f^{(3\omega)})} [T_1(1 - e^{-i\Delta\varphi_s}) + \rho T_2 e^{-i\Theta}(e^{-i\Delta\varphi_f} - 1)] \right|^2 (I^\omega)^3, \quad (3.3)$$

where  $\Delta\epsilon$  is the dielectric constant dispersion of the medium:

$$(\Delta\epsilon)_{s,f} = \epsilon_{s,f}^{(3\omega)} - \epsilon_{s,f}^{(\omega)} \quad (3.4)$$

with  $\epsilon = n^2$ . The subscripts  $s$  and  $f$  refer to the substrate and thin film, respectively. The phases appearing in Eq. (3.3) are given by:

$$\varphi_{s,f}^{(\omega,3\omega)} = \frac{6\pi l}{\lambda} n_{s,f}^{(\omega,3\omega)} \cos \theta_{s,f}^{(\omega,3\omega)} \quad (3.5)$$

for waves with the frequency  $\omega$  or  $3\omega$  in medium  $s$  (substrate) or  $f$  (film), respectively.  $\theta_{s,f}^{(\omega,3\omega)}$  are the propagation angles in the given medium, for  $\omega$  or  $3\omega$  frequencies.  $l$  is the medium thickness,  $T_1$  and  $T_2$  are the factors arising from transmission and boundary conditions [89]

$$\rho = \frac{\left(\frac{\chi}{\Delta\epsilon}\right)_f^{(3)}}{\left(\frac{\chi}{\Delta\epsilon}\right)_s^{(3)}} \quad (3.6)$$

$\varphi$  is the phase of the thin film susceptibility (or difference with that of substrate if not zero),  $I^{(\omega)}$  is the fundamental beam intensity and the phase mismatches  $\Delta\varphi$  are given by:

$$(\Delta\varphi)_{s,f} = \varphi_{s,f}^{(\omega)} - \varphi_{s,f}^{(3\omega)}, \quad (3.7)$$

where  $\varphi_{s,f}^{(\omega,3\omega)}$  is given by Eq. (3.5).

The third harmonic generation measurements were performed using a Q-switched Nd:YAG laser operating at 1064 nm fundamental wavelength with 16 ps pulse duration and 10 Hz repetition rate. The studied films, deposited on glass substrates, were mounted on a rotation stage. The harmonic intensities were collected as function of the incidence angle, when rotating thin film around the axis perpendicular to the beam propagation direction and coinciding with it. The used experimental setup is similar to this of SHG (cf. Fig. 3.3). The difference is only in the selective filter FL355 (for THG) instead of FL532 (for SHG). The first beam splitter (**Phs**) is used to take off a weak part of the beam for synchronization of detection. The second one (**Phc**) allows to correct the fundamental beam fluctuations. The half wave plate ( $\lambda/2$ ) and the polarizer P control the intensity of incident beam.

### 3.5 Photoinduced diffraction gratings

Polymers containing azo-benzene dyes either as side groups or physically dispersed, can interact with polarized light. This interaction due to reorientation of the side groups,

results in reversible birefringence and dichroism. The trans azobenzene derivatives are stable in an elongated molecular form. In contrast, the cis azobenzenes are photoinduced isomers, taking a bent form, usually revert back to the trans form by thermal or light stimulation [90, 91].

### 3.5.1 Photoisomerization of azobenzene

Photoinduced isomerisation was studied by many researchers [92, 93, 94, 95, 96, 97, 98, 99, 100, 101, 102, 103, 104] and several mechanisms of surface relief grating formation were proposed [90]. Polymers containing the azo groups are able to generate surface relief gratings by irradiation [90, 96]. This phenomenon enables applications like holographic data storage, optical switching, optical data storage, etc [105].

Azobenzene is composed from two phenyl rings linked by an N=N double bond. The term azobenzene or simply azo is often used to refer to a wide class of molecules that share the core azobenzene structure, with different chemical functional groups extending from the phenyl rings. They strongly absorbed light and were used as dyes in a variety of industries. Photoisomerization is the one of the famous properties of azobenzene. The two isomers (cis and trans) can be switched with particular wavelengths of light: ultraviolet or blue light, which corresponds to the energy gap of the  $\pi$ - $\pi^*$  transition, for trans-cis conversion, and blue light, which is equivalent to that of the  $n$ - $\pi^*$  transition, for cis-trans isomerization. The cis- state is less stable than the trans one and with elapsing time cis-azobenzene thermally relax to the trans via cis-trans isomerization [92, 93, 94, 95, 96, 97, 99, 100, 101].

The time dependence of the photoinduced orientation in azobenzene polymers was explained by Dumont et al. [105] and Sekkat et al. [106] within theoretical models taking into account the population decays and growths of both the trans and cis metastable states. In some matrices of bulk polymers, after blocking the light inducing orientation, the reorientation of the azobenzene molecules can be frozen below the glass transition temperature. This is possible due to the restriction of movement of trans molecules by a free volume of the polymer. The reversible photoisomerization process can also lead to the mass transport in polymers with the azobenzene groups attached covalently to the polymer main chain resulting in formation of surface relief grating [96]. The mass redistribution induced by interference pattern by low power laser illumination takes place well below the glass transition temperature of polymers. Several mechanisms were proposed in order to explain the origin of surface relief gratings formation. They include thermal gradient

mechanisms [107], asymmetric diffusion based on the creation of a concentration gradient [101, 108], isomerization pressure [98, 109], mechanisms based on electromagnetic forces - mean field theory [99, 100], permittivity gradient theory [110], and gradient electric force [102]. However, till now this behaviour is still under investigations [111, 112, 113].

### 3.5.2 Degenerate two-wave mixing technique

Degenerate two-wave mixing (DTWM) is the simplification of DFWM technique which allow to obtain information about ability of material to use in optical holography. In this technique two pump laser beams interact with themselves causing deformation of the surface (in a huge simplicity) called “surface relief grating” (SRG). The changes occur not only on the surface but also in the volume and/or the interaction of two beams causes changes of phase and refractive index as well.

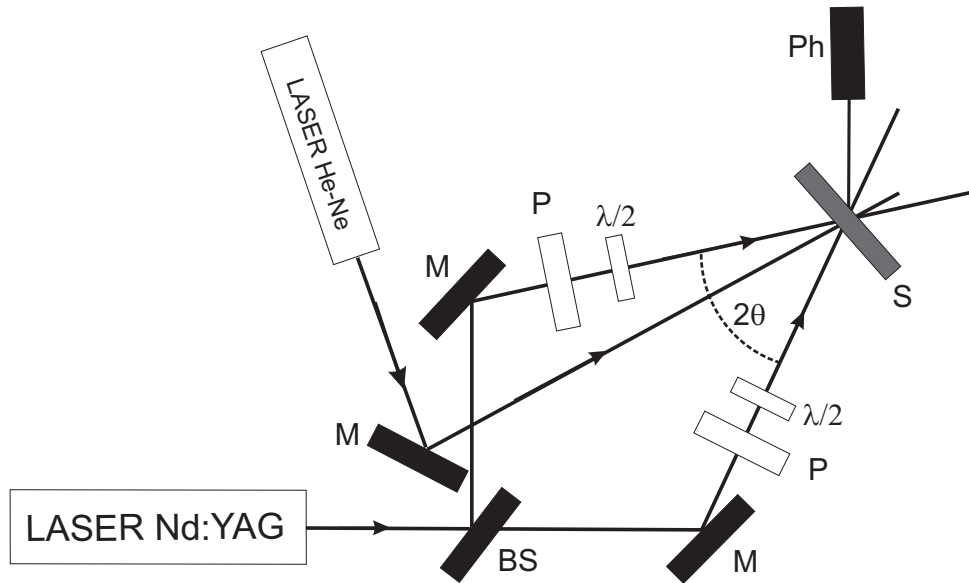


Figure 3.4: Schematic setup for diffracting grating formation experiment, **M** - mirror, **BS** - beam splitter, **P** - polarizer,  $\lambda/2$  - half wave plate, **S** - sample, **Ph** - photodiode.

The experimental setup used for creation and study of the diffraction gratings is shown in Fig. 3.4 [43]. The diffraction gratings were recorded by two interfering 16 ps laser beams with wavelength of 532 nm obtained from pulsed Nd:YAG laser (Continuum Leopard D-10) working at 10 Hz repetition rate and having pulse energy with 1.3 mJ. The gratings

formation was monitored by cw He-Ne laser (30 mW operating at 632.8 nm by measuring the intensity of the first-order diffracted beam in the transmission mode. The polarizations of writing beams were controlled by the systems: polarizer (**P**) - half wave plate ( $\lambda/2$ ), placed on the pathway of beams before the sample. The signal intensity of the first order of diffraction was measured with a photodiode (Centronic Series OSI 5) and this signal was fed to the digital oscilloscope (Tektronix TDS 3054). The sample (**S**) was mounted on a stage perpendicular to the writing beams' bisectrix.

## 3.6 Other techniques

### 3.6.1 Spin coating

This technique consists in depositing a small amount of material solution on the surface of a substrate which is rotated. Usually the acceleration as well as rotation speed can be controllable and/or programmable. Two distinct rotations are used: first one serving for a good spreading out of the solution whereas the second serves to evacuate the solvent. The rotation speeds used are of about a few hundreds rpm and depend on the desired thickness, solution adherence to the substrate and its viscosity.

The initial stage involves delivering a quantity of solution to the surface of the substrate. The film thickness depends on the solution viscosity and on the rotation speed. On the other hand the solution viscosity depends on temperature, solution concentration, on polymer used, its molar mass, and its dispersity as well as on the kind of solvents used. The thickness of film ( $l$ ) increases proportionally to the square of polymer concentration ( $C$ ):

$$l(C) = aC^2 + bC, \quad (3.8)$$

where  $a$  and  $b$  are the proportionality coefficients, for a given polymer and substrate, depending on the rotation speed and solution viscosity. The spinning technique is very frequently used in thin film fabrication for optical applications and often it leads to a partial orientation of polymer chains, with usually the polymer chains preferably oriented parallel to the substrate plane and randomly distributed within.

### **3.6.2 Atomic force microscope**

The atomic force microscope (AFM) is a very high-resolution type of scanning probe microscope, with demonstrated resolution of fractions of a nanometre. The precursor to the AFM, the scanning tunneling microscope, was developed by Gerd Binnig and Heinrich Rohrer in the early 80s. Six years after Binnig, Quate and Gerber invented the first AFM [114]. The AFM is one of the foremost tools for imaging, measuring and manipulating matter at the nanoscale. The term “microscope” in the name is actually a misnomer because it implies looking, while in fact the information is gathered by mechanical probe while is scanned the surface. Piezoelectric elements that facilitate tiny but accurate and precise movements on (electronic) command enable the very precise scanning.



# Chapter 4

## Results - catenanes and rotaxanes

### Contents

---

<b>4.1</b>	<b>Introduction to the chapter</b>	<b>43</b>
<b>4.2</b>	<b>Spectral characterization</b>	<b>44</b>
<b>4.3</b>	<b>Degenerate four-wave mixing</b>	<b>45</b>
4.3.1	Nonlinear transmission	45
4.3.2	Phase conjugation measurements	46
4.3.3	Time resolved measurements	52
<b>4.4</b>	<b>Z-scan</b>	<b>54</b>
<b>4.5</b>	<b>Second harmonic generation</b>	<b>56</b>
<b>4.6</b>	<b>Third harmonic generation</b>	<b>58</b>
<b>4.7</b>	<b>Quantum chemical calculations</b>	<b>59</b>
4.7.1	Dipole moment and HOMO-LUMO bandgap	60
4.7.2	First and second order hyperpolarizability	61

---

### 4.1 Introduction to the chapter

In this chapter the experimental results for catenanes and rotaxanes are described. Absorption is the characterization of material which can help to predict and explain the experimental results and observed phenomena; that is why the part of spectral characterization opens this chapter. The catenanes and rotaxanes were measured using the

techniques described in chapter 3. The theoretical calculations were done as well in order to confirm obtained results.

## 4.2 Spectral characterization

The absorption spectra of solutions in a quartz cuvette were measured using PERKIN ELMER UV/VIS/NIR Lambda 19 spectrometer. The measurements were performed in the spectral region 250-1100 nm at room temperature. The optical absorption spectrum for the *rotaxane* solutions in chloroform ( $\text{CHCl}_3$ ) is shown in Fig. 4.1. To observe the UV part of absorption spectrum we have diluted strongly the solution (0.05 g/L). Its absorption spectrum is shown in Fig. 4.1 by blue line. The molecule is transparent in whole visible. A peak of absorption at around 270 nm is seen due to the absorption by phenyl rings. The decrease of absorption below 400 nm wavelength is due to the absorption coming from glass of used liquid cell (1 mm cuvette). Similar behaviour was observed for *catenane* and *fumrot* [50].

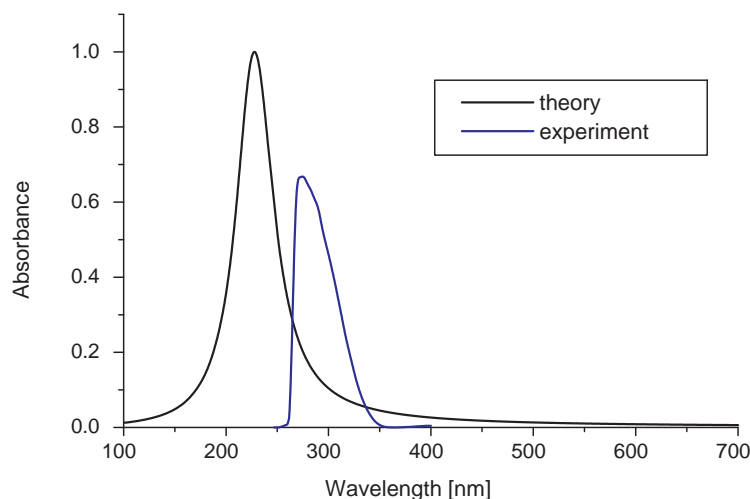


Figure 4.1: Theoretical (black) and experimental (blue) absorption spectra for *rotaxane* dissolved in chloroform (0.05 g/L).

In Fig. 4.1 the calculated spectrum for *rotaxane* is also presented. The theoretically calculated absorption spectral position is blue shifted in comparison to the experimental

spectrum about 30 nm, which is the correct tendency. The reason of disagreement between the theoretical and experimental results of absorption spectra could be due to a quantum chemical calculation without taking into account the interaction between molecule and solvent polarity [87].

The electronic spectra were calculated by the configuration interaction method with the maximum excitation energy up to 8 eV. Local perturbations were considered only within a framework of the isolated molecule. The influence of the intermolecular electron vibration interactions is not taken into account. Therefore deviations from the experimental data will give information concerning the observed intramolecular and intermolecular interactions.

The intensity of absorption was expressed by the formula (4.1):

$$\epsilon_{x,y,z} = \omega \sum_{j=1}^N |\mu_j^{(x,y,z)}|^2 \exp\left(-\left(\frac{E - E_j}{H}\right)^2\right), \quad (4.1)$$

where  $j$  is the number of transition from ground state,  $E_j$  is the transition energy,  $\mu_j(x, y, z)$  is the transition dipole component and  $H$  is the spectral line broadening width.

Figure 4.2 presents the theoretically calculated absorption spectra. These spectra show that all compounds absorb in the region 200 – 450 nm. We can observe that investigated molecules exhibit no measurable absorption at 532 nm what is very important in order to avoid resonance effect in degenerate four-wave mixing experiment.

Due to strong solvent effect theoretically calculated spectral positions of absorption are blue shifted in comparison to the experimental ones (for all studied compounds).

## 4.3 Degenerate four-wave mixing

### 4.3.1 Nonlinear transmission

The knowledge of two photon absorption coefficient ( $\beta$ ) is very important in degenerate four-wave mixing technique as it is related to the imaginary part of the third order nonlinear optical susceptibility. Due to that fact, the nonlinear transmission measurements were performed in solution of studied compounds using Nd:YAG laser operating at 532 nm with 30 ps pulses duration and 1 Hz repetition rate. The intensity transmitted through the sample was measured (by the photodetector) as function of incident intensity. For all studied compounds a linear dependence of transmission as a function of incident beam was observed what implicate the absence of two photon absorption. The linear absorption

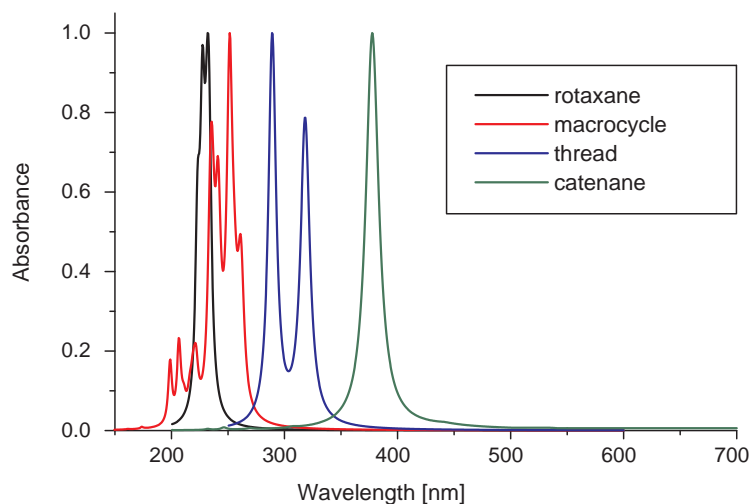


Figure 4.2: Theoretically calculated absorption spectra for *rotaxane*, *macrocycle*, *thread* and *catenane* (peaks counted from the left side) molecules.

coefficients are equal almost zero too.

### 4.3.2 Phase conjugation measurements

The phase conjugation measurements were made at 532 nm using a Q-switched mode locked Quantel Nd:YAG laser of 30 ps pulse duration. The measurements were done as a function of the incident beams polarization (beams  $\langle 1 \rangle$ ,  $\langle 2 \rangle$  and  $\langle 3 \rangle$ ) and the interacting beam intensities. All measurements were made in solution using a cuvette of 1 mm thick. In order to calibrate DFWM measurements, carbon disulfide ( $\text{CS}_2$ ) was used as a reference material.

The experimental results for  $\text{CS}_2$ , solvents: chloroform ( $\text{CHCl}_3$ ) and dimethylsulfoxide (DMSO), and for the solutions of *rotaxane* (5 g/L and 10 g/L; in  $\text{CHCl}_3$ ), *catenane* (10 g/L in DMSO), *thread* (100 g/L in  $\text{CHCl}_3$ ), and *fumrot* (5 g/L in DMSO) are shown in Fig. 4.3 and Fig. 4.4. In these figures  $I_4$  represents the intensity of fourth wave (signal) and  $I_1$  represents the intensity of the pumping beam. For third order nonlinear optical effects the dependence between these two intensities should be a cubic one:

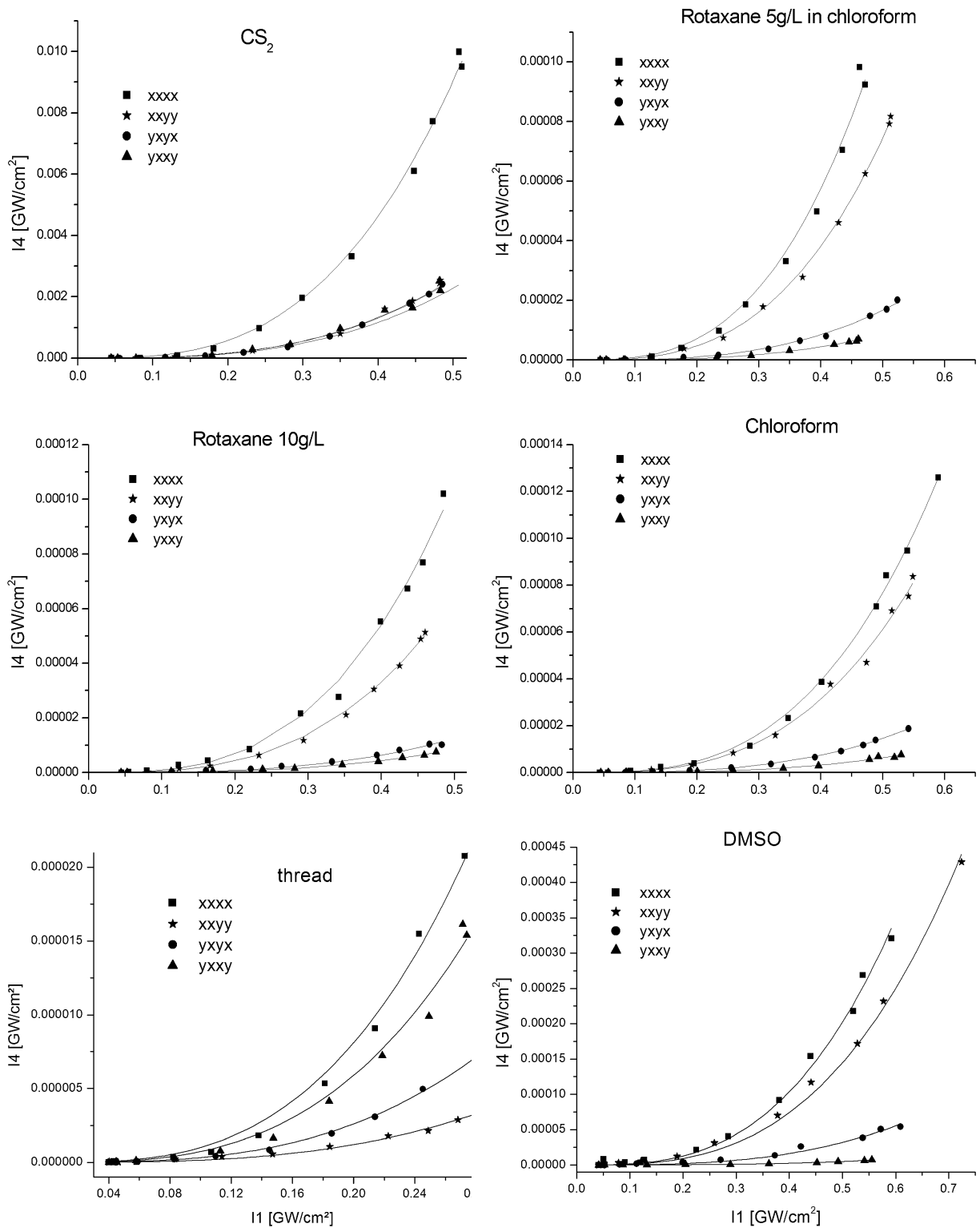


Figure 4.3: DFWM results for  $CS_2$ , *rotaxane* (5 g/L and 10 g/L),  $CHCl_3$ , *thread* and DMSO.

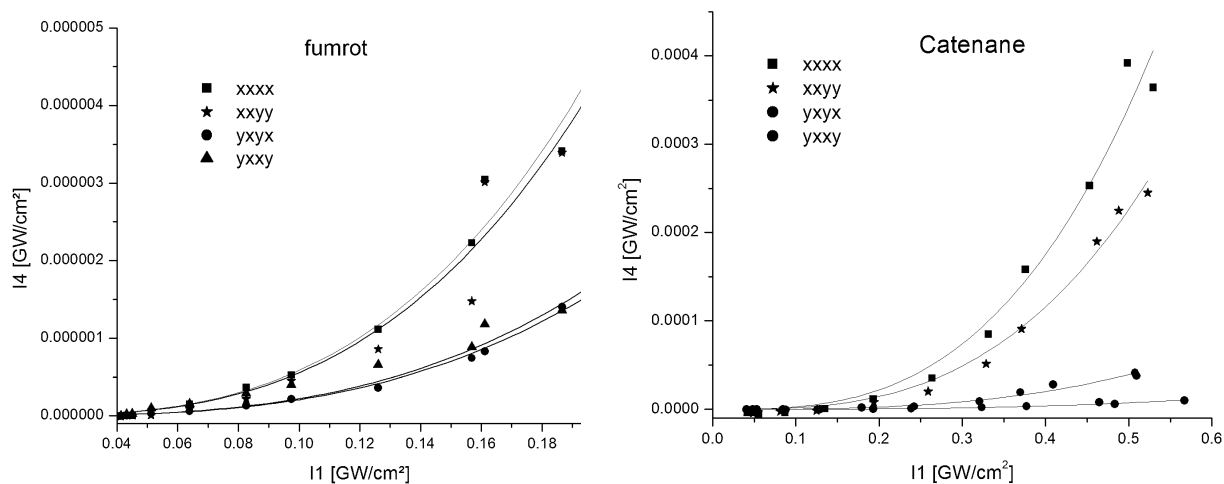


Figure 4.4: DFWM results for *fumrot* and *catenane*.

$$I_4 = aI_1^3 \quad (4.2)$$

The data for pure CS<sub>2</sub> show quite different dependence of the signal intensity on the interacting beams polarization configuration comparing to other obtained results. In CS<sub>2</sub> the signal intensities for *xxyy*, *yxyx*, *yxyx* are almost the same being less than half of that for the parallel polarizations (*xxxx*). For CHCl<sub>3</sub>, DMSO, *catenane*, *rotaxane*, *thread* and *fumrot* solutions the signals for different interacting beams polarization configurations are quite different. One observes, similarly as for CS<sub>2</sub>, the largest signal for the *xxxx* polarization configuration, but for other intensities are quite different, with the largest one for *xxyy* and the smallest for *yxyx*. It is not the case for *thread* where the maximum intensity is for *xxxx* polarization configuration and then for *yxyx*, *yxyx*, *xxyy*, respectively. For an isotropic solution and 1-D molecules the NLO susceptibility  $\chi_{xxyy}^{(3)}$  should be equal to  $\chi_{xxxx}^{(3)}/3$ , what is not in this case. This relation is no more valid for other molecules as it is in the case e.g. of CS<sub>2</sub> [115, 116]. We suppose that exist the rotational contributions to  $\chi^{(3)}$  susceptibility of catenanes and rotaxanes coming either from conjugated  $\pi$  electrons in macrocycle or from their rotational mobility in molecules. At the same time we can suppose that there is no or much weaker rotational contribution in the case of *thread* itself. The increase of signal intensity is seen in Fig. 4.5, where the phase conjugate signals from solutions are compared with those of solvents. It shows important solute contribution, as the solute concentrations are small (5 g/L and 10 g/L for *rotaxane* and 10 g/L for *catenane*). However the low solubility of these molecules

did not allow us to get the full concentration dependence. Indeed in the case of *rotaxane*, we do not see a significant difference for the studied concentrations 5 g/L and 10 g/L (cf. Fig. 4.5).

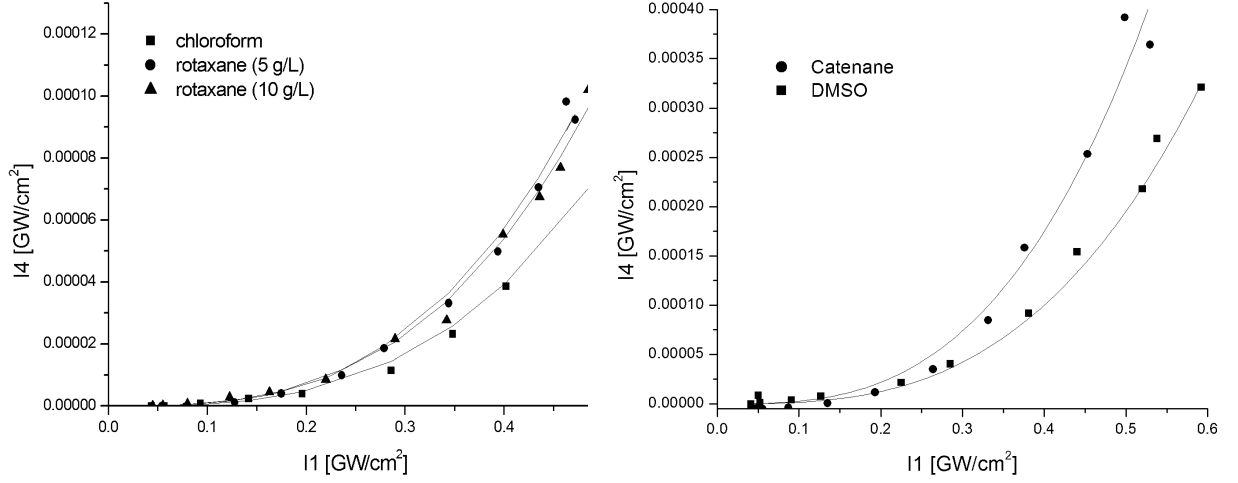


Figure 4.5: Comparison of DFWM results for investigated molecules and their solvents.

The obtained third order nonlinear optical susceptibility of  $\text{CS}_2$  was in the same order as the value published by Derkowska *et al.* [117] ( $\chi^{(3)} = 1.39 \times 10^{-12}$  esu). The effective  $\chi_{eff}^{(3)}$  susceptibility of the studied solution is given by [118]:

$$\chi_{eff}^{(3)} = \left( \frac{n}{n_{ref}} \right)^2 \left( \frac{l_{ref}}{l} \right) \left( \frac{a}{a_{ref}} \right)^{\frac{1}{2}} \chi_{ref}^{(3)}, \quad (4.3)$$

where the subscript *ref* refers to reference;  $n$ ,  $n_{ref}$  are the refractive indices for the sample and the reference, respectively;  $l$  and  $l_{ref}$  are the thicknesses of the studied sample and the reference, respectively, and  $a$  and  $a_{ref}$  are the coefficients calculated from the experimental data using (Eq. 4.2).

Equation (4.3) is valid when the nonlinear medium is perfectly transparent. When the medium absorbs the light, it reads:

$$\chi_{eff}^{(3)} = \left( \frac{n}{n_{ref}} \right)^2 \left( \frac{l_{ref}}{l} \right) \left( \frac{a}{a_{ref}} \right)^{\frac{1}{2}} \frac{\alpha l}{e^{-\frac{\alpha l}{2}} (1 - e^{-\alpha l})} \chi_{ref}^{(3)} \quad (4.4)$$

where  $\alpha$  is the coefficient of absorption.

This method of determining the third order nonlinear susceptibility gives similar results comparing to model proposed by Sahraoui *et al.* [119].

According to the measurement of transmission at 532 nm and the UV-VIS spectra the obtained absorption coefficients are almost equal zero. Consequently we can estimate  $\chi^{(3)}$  values using Eq. (4.4). The results are shown in Table 4.1. It is clearly shown that the obtained results are one order of magnitude less than that ones for reference material ( $\text{CS}_2$ ) or for example for Phthalocyanines [120, 75, 121] but comparable as the values for other new optoelectronic materials (oxazolone containing polymers, cf. [122])

Molecule	$\chi_{xxxx}^{(3)exp} \times 10^{13}$ [esu]	$\chi_{xxyy}^{(3)exp} \times 10^{13}$ [esu]	$\chi_{yyxx}^{(3)exp} \times 10^{13}$ [esu]	$\chi_{yxyx}^{(3)exp} \times 10^{13}$ [esu]
<i>catenane</i>	1.03	0.82	0.74	0.96
<i>thread</i>	1.64	0.63	0.92	1.40
<i>rotaxane</i>	3.47	3.22	0.91	1.25
<i>fumrot</i>	1.24	1.21	0.76	0.75

Table 4.1: Third order susceptibility values for studied molecules.

We notice that the following relationships are verified:

$$\chi_{xxxx}^{(3)exp} \approx 1.8\chi_{yxyx}^{(3)exp} \approx 1.2\chi_{yyxx}^{(3)exp} \approx 2.6\chi_{xxyy}^{(3)exp} \quad (4.5)$$

for *catenane*,

$$\chi_{xxxx}^{(3)exp} \approx 1.6\chi_{yxyx}^{(3)exp} \approx 1.7\chi_{yyxx}^{(3)exp} \approx 1.0\chi_{xxyy}^{(3)exp} \quad (4.6)$$

for *thread*,

$$\chi_{xxxx}^{(3)exp} \approx 12.5\chi_{yxyx}^{(3)exp} \approx 2.9\chi_{yyxx}^{(3)exp} \approx 5.9\chi_{xxyy}^{(3)exp} \quad (4.7)$$

for *rotaxane*,

$$\chi_{xxxx}^{(3)exp} \approx 1.4\chi_{yxyx}^{(3)exp} \approx 1.1\chi_{yyxx}^{(3)exp} \approx 1.3\chi_{xxyy}^{(3)exp} \quad (4.8)$$

for *fumrot*.

Taking advantage of different spatial symmetries involved in the  $\chi^{(3)}$  tensor, we can distinguish different physical mechanisms contributing to third order susceptibility. Since

we have used a laser generating pulses in picosecond regime (30 ps), we can neglect thermal and electrostrictif effects because they are very slow. Two essential local effects contribute to the nonlinearities in isotropic materials subjected to such laser pulses: electronic cloud deformations and nucleolus reorientation (translation, rotations and vibrations of molecule). In consequence one can consider  $\chi^{(3)}$  as being composed of two contributions corresponding to these mechanisms:

$$\chi_{ijkl}^{(3)} = \chi_{ijkl}^{(3)el} + \chi_{ijkl}^{(3)nu}. \quad (4.9)$$

We can show that for isotropic materials, the electronic and nuclear (rotational) contributions of tensorial components satisfy the following relations:

$$\chi_{xxxx}^{(3)el} = 3\chi_{xxyy}^{(3)el} = 3\chi_{yyxx}^{(3)el} = 3\chi_{yxyx}^{(3)el}, \quad (4.10)$$

$$\chi_{xxxx}^{(3)nu} = 8\chi_{xxyy}^{(3)nu} = 8\chi_{yyxx}^{(3)nu} = \frac{4}{3}\chi_{yxyx}^{(3)nu}. \quad (4.11)$$

Experimental results described by formulas (4.5)-(4.8) and (4.10)-(4.11) allow us to deduce the following relationships:

$$\chi_{xxxx}^{(3)el} = 0.78\chi_{xxxx}^{(3)exp}, \quad \chi_{xxxx}^{(3)nu} = 0.22\chi_{xxxx}^{(3)exp} \quad (4.12)$$

for *catenane*,

$$\chi_{xxxx}^{(3)el} = 0.24\chi_{xxxx}^{(3)exp}, \quad \chi_{xxxx}^{(3)nu} = 0.76\chi_{xxxx}^{(3)exp} \quad (4.13)$$

for *thread*,

$$\chi_{xxxx}^{(3)el} = 1.83\chi_{xxxx}^{(3)exp}, \quad \chi_{xxxx}^{(3)nu} = 0.83\chi_{xxxx}^{(3)exp} \quad (4.14)$$

for *rotaxane*,

$$\chi_{xxxx}^{(3)el} = 1.59\chi_{xxxx}^{(3)exp}, \quad \chi_{xxxx}^{(3)nu} = 0.59\chi_{xxxx}^{(3)exp} \quad (4.15)$$

for *fumrot*.

From these results we can conclude that in the cases of *rotaxane*, *fumrot* and *catenane* the electronic contribution is larger than nuclear contribution. On the other hand in the cases of *thread* the nuclear contribution is more important than electronic one. These results are in contradictory with the suppositions and preliminary results

[123]. We suppose that it is due to low concentration of studied solutions from one side and the high contribution coming from solvent from other side. However some theoretical simulations confirm these results.

### 4.3.3 Time resolved measurements

To reveal the transient response and relaxation of the DFWM processes, we used time resolved measurements. This is possible by moving the optic delay line (**RO2**, cf Fig. 3.1). The results are presented in Fig 4.6.

The time resolved profile of the  $I_4$  signal is quite symmetric for all cases, which means that the relaxation of this signal is very fast. The dynamics of the third order response may contain two components: fast instantaneous response which is due to the electronic third order polarizability and slow response which is due to the dephasing of resonant or nonresonant processes in the material. However comparing results for *fumrot* (cf. Fig. 4.6 - *fumrot*) with results for DMSO (cf. Fig. 4.6 - DMSO) we can see some oscillations in the case of *fumrot*. These oscillations are caused rather by unstable intensity of laser than by electrostrictive effects (which was the first our idea).

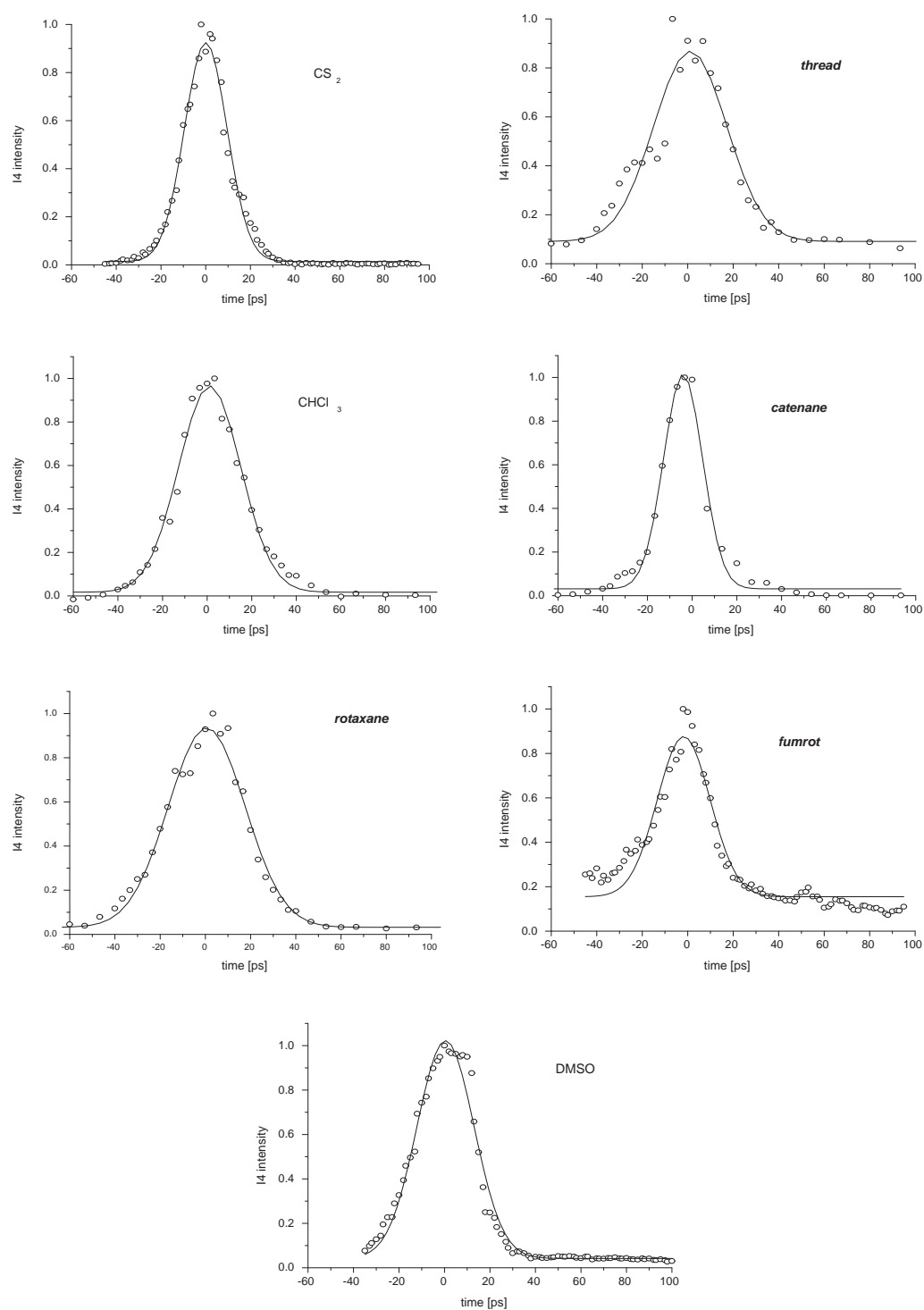


Figure 4.6: Time resolved measurements for CS<sub>2</sub>, *thread*, CHCl<sub>3</sub>, *catenane*, *rotaxane*, *fumrot* and DMSO.

## 4.4 Z-scan

Using the nonlinear optical imaging technique we determined the nonlinear index of refraction ( $n_2$ ) at 532 nm and 1064 nm for the solvent ( $\text{CHCl}_3$ ) and the solutions of 5 g/L and 10 g/L *rotaxane* in chloroform ( $n_2 = \Delta n/I$ , where  $\Delta n$  is the light induced change of refractive index ( $\Delta n = n(I) - n(I = 0)$  where  $I$  is the pump intensity).  $\text{CS}_2$  was used as reference material. All measurements were done in solutions using 1 mm quartz cuvettes. This experiment was set to work at 532 nm and 1064 nm applying a pulsed mode locked Nd:YAG laser with pulse duration 16 ps and frequency 10 Hz. Figures 4.7 and 4.8 present the experimental curves obtained for  $\text{CHCl}_3$  and 10 g/L *rotaxane* solution in  $\text{CHCl}_3$  measured at 5.1  $\text{GW}/\text{cm}^2$ , at 1064 nm. The all optical switching use the light induced refractive index variation, given by

$$n = n_0 + n_2 I, \quad (4.16)$$

where  $n_0$  and  $n_2$  are the linear and nonlinear refractive indices, respectively and  $I$  is the light intensity. The nonlinear index of refraction ( $n_2$ ) is related to the third order nonlinear susceptibility ( $\chi^{(3)}$ ) by following relation:

$$n_2 = \frac{12\pi^2 \chi^{(3)}}{cn_0^2}, \quad (4.17)$$

where  $c$  is the speed of light.

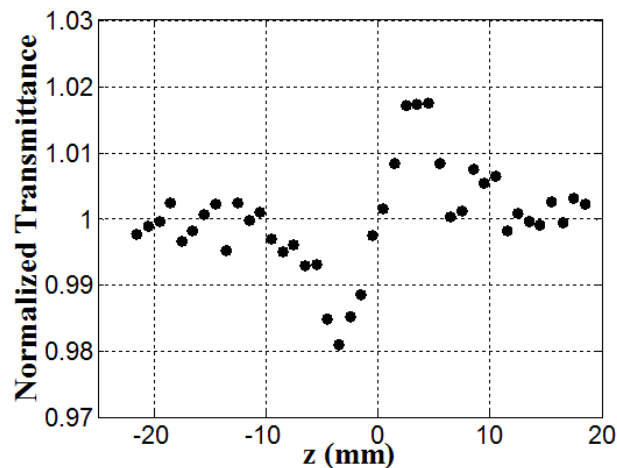


Figure 4.7: Z-scan pattern for chloroform (1064 nm).

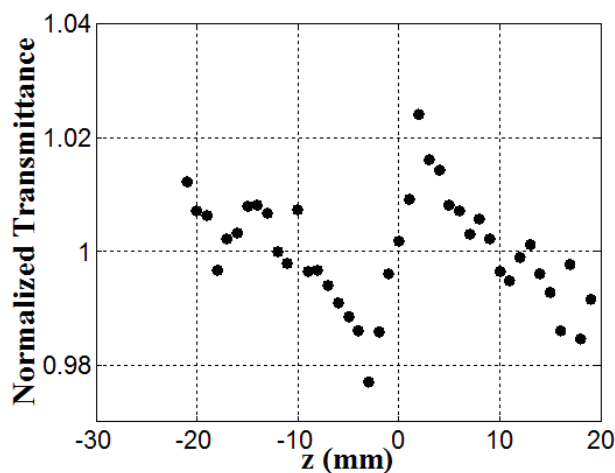


Figure 4.8: Z-scan pattern for a solution of 10 g/L of *rotaxane* in chloroform (1064 nm).

Similar curves were recorded for other solutions and the mean values of  $n_2$  obtained for 532 nm and 1064 nm radiation are summarized in Table 4.2. The profiles are characteristic for positive nonlinear refractive index. As during the DFWM measurements (nonlinear transmission measurements) nonlinear absorption was not observed for all samples, which implies that the two photon absorption coefficients are below the detection limit ( $\beta < 0.1$  cm/GW). The magnitude of  $n_2$  is obtained by comparison with the value for CS<sub>2</sub> ( $3 \times 10^{-18}$  m<sup>2</sup>/W) [124].

In the case of z-scan measurement in rotaxane solution we observed appearance of some flocks due to the high energy necessary for experiment (this energy favouring the aggregation of molecules). A possible explanation of such process is the observed dispersion of experimental points, seen in the case of *rotaxane* solution. All these facts could explain why we have not obtained the expected results, especially at 532 nm. Further measurements will be necessary in order to clarify this entire phenomenon.

Sample	$n_2 \times 10^{18}$ [m <sup>2</sup> /W] at 523 nm	$n_2 \times 10^{18}$ [m <sup>2</sup> /W] at 1064 nm	$\chi^{(3)} \times 10^{23}$ [m <sup>2</sup> /W] at 1064 nm
CS <sub>2</sub>	3.10	3.18	25.34
CHCl <sub>3</sub>	0.35	0.33	3.03
DMSO	-	0.21	1.67
<i>rotaxane</i> in CHCl <sub>3</sub> (5 g/L)	0.48	0.43	3.19
<i>rotaxane</i> in CHCl <sub>3</sub> (10 g/L)	0.54	0.66	-
<i>catenane</i> in DMSO (10 g/L)	-	0.22	1.75
<i>thread</i> in CHCl <sub>3</sub> (100 g/L)	-	0.34	2.71
<i>fumrot</i> in DMSO (5 g/L)	-	0.22	1.75

Table 4.2: Z-scan results.

## 4.5 Second harmonic generation

Thin films of *fumrot* with different thicknesses (150 nm and 200 nm) were prepared to perform harmonic generations. We tried to investigate second harmonic generation by measuring the intensity of the signal when the sample was illuminated by 1064 nm laser light. Unfortunately during this testing there was no response or signal was not measurable. The investigated catenanes and rotaxanes are presumably the centrosymmetric, however it was showed that the vacuum deposited thin films of benzylic amide [2] catenane exhibit second harmonic generation ability [50]. The obtained values, measured in standard SHG experimental setup at 1064 nm with 13 ns pulses and 10 Hz operation rate, are given in Table 4.3. The catenane thin films were rotated along the axis perpendicular to the propagation direction. Two fundamental-harmonic polarization configuration

( $p$ - $p$  and  $s$ - $p$ ) were applied. The nonzero diagonal ( $\chi_{zzz}^{(2)}$ ) and off diagonal ( $\chi_{xxz}^{(2)}$ ) tensor components were determined. The experiment and data were calibrated with an  $\alpha$ -quartz crystal plate ( $\chi_{111}^{(2)} = 0.6$  pm/V [50]).

Thickness [nm]	$\chi_{xxz}^{(2)}$ [pm/V]	$\chi_{zzz}^{(2)}$ [pm/V]
754	$0.0086 \pm 0.001$	$0.034 \pm 0.004$
354	$0.0050 \pm 0.0005$	$0.016 \pm 0.002$
106	$0.0008 \pm 0.00001$	$0.024 \pm 0.002$

Table 4.3: SHG results for *catenane* molecules.  $\chi_{zzz}^{(2)}$  - diagonal,  $\chi_{xxz}^{(2)}$  - off diagonal components of quadratic nonlinear susceptibility [50].

Second harmonic generation signal was also observed for the thin films of *fumrot*, but with earlier corona poling process. The large value of diagonal components of the second order nonlinear susceptibility was obtained ( $\chi_{zzz}^{(2)}$  up to 6.8 pm/V at 1064 nm) [50].

## 4.6 Third harmonic generation

The third harmonic generation intensities were calibrated with THG measurements on a high purity silica slab performed under the same conditions. Figure 4.9 displays the measured THG intensities for the glass plate alone and glass plate with *fumrot* thin films. The third NLO susceptibility of *fumrot* was found to be  $\chi^{(3)} = 4.10 \times 10^{-13}$  esu. As it was expected this value can be well interpreted in terms of bond additivity model, showing no enhancement in ultra fast  $\chi^{(3)}$  susceptibility owing to the peculiar structure and mobility of these molecules.

Molecule	wavelength [nm]	$\chi^{(3)} \times 10^{12}$ [esu]	Reference
<i>fumrot</i>	1907	1.809	[125, 126]
mono nitro <i>fumrot</i>	1907	1.834	[125, 126]
di nitro <i>fumrot</i>	1907	1.990	[125, 126]
<i>norot</i>	1064	0.64	[37]
<i>fumrot</i>	1907	0.49	[37]
<i>norot</i>	1064	0.41	[37]
<i>fumrot</i>	1907	0.42	[37]
<i>catenane</i>	1064	0.29	[50]
<i>fumrot</i>	1064	0.377	[50]
<i>norot</i>	1064	0.579	[50]
<i>catenane</i>	1064	0.29	[50]
<i>fumrot</i>	1907	0.417	[50]
<i>norot</i>	1907	0.686	[50]
<i>fumrot</i>	1907	0.41	this work

Table 4.4: The third order nonlinear optical susceptibility results, for catenanes and rotaxanes, determined by THG technique.

The obtained value show good agreement with these ones obtained and published before. However when we compare the third harmonic generation results obtained for

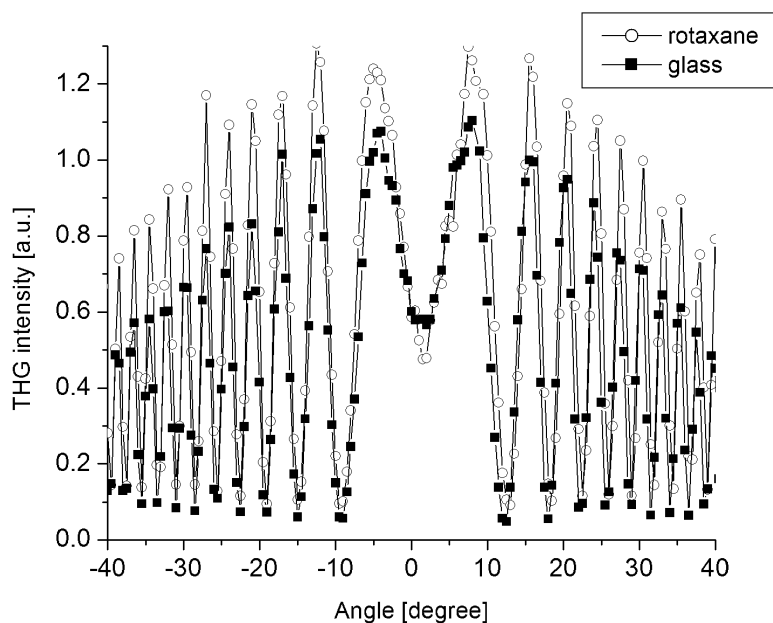


Figure 4.9: Third harmonic generation maker fringes for the glass substrate and 150 nm thick *fumrot* thin film deposited on glass substrate.

*fumrot* with the results obtained for the Phthalocyanines, we see that the values for *fumrot* are one or two orders of magnitude less than for Phthalocyanines [127].

## 4.7 Quantum chemical calculations

All quantum chemical calculations were performed with semi-empirical Parameterized Model number 3 (PM3) method within a framework of the restricted Hartree-Fock approach. The convergence limit up to  $10^{-6}$  eV after 500 iterations was achieved [128, 129]. The calculations mixes all single determinant wavefunctions that can be obtained from the ground state by exciting electrons from a subset of the occupied orbital to a subset of the unoccupied orbital. The subsets are specified as a fixed number, or by an energy criterion associated with the energy difference between the occupied orbital and the unoccupied orbital.

### 4.7.1 Dipole moment and HOMO-LUMO bandgap

Introduction of different molecules causes the substantial changes of both absorption spectra as well as nonlinear optical coefficients. The knowledge about the UV-VIS spectra is necessary to have an idea about the further modifications of materials. The quantum chemical calculations give important information concerning the origin of the observed spectra and information for desirable changes of the chemical content using appropriate substituent. Moreover, some information about nonlinear optical properties of the investigated molecules may be crucial.

Special attention will be devoted to the delocalization of  $\pi$  electrons in different chemical bonds on the output of third order optical properties and a spectral shift of UV absorption.

Assuming a two-level model [130] (only terms involving the ground and the first excited state of the molecule are considered) the first order hyperpolarizability ( $\beta^h$ ) can be calculated quite easily. This model works fairly well for many organic compounds for which difference between the ground and higher excited states is usually much larger than the photon energy (cf. Table 4.5). For many molecules with strong nonlinearities along a single charge transfer (donor - acceptor groups) it is often assumed that one component  $\beta_{xxx}^h$  of the hyperpolarizability tensor along this axis is adequate to describe the nonlinearity in first approximation. Introducing the dispersion free first order hyperpolarizability  $\beta_0^h$  extrapolated to infinite optical wavelengths far away from the electronic resonance was obtained for optical frequency - doubling [11]:

$$\beta_{ijk}^h = 12\pi^2 K \sum_{g=1}^m \frac{E_g^2 |\mu_i^{(g)}| |\mu_j^{(g)}| |M_k^{(g)} - M_k^{(0)}|}{(E_g^2 - 4(\hbar\omega)^2 + H^2)(E_g^2 - (\hbar\omega)^2 + H^2)}, \quad (4.18)$$

where  $|\mu_i^{(g)}|$ ,  $|\mu_j^{(g)}|$  are the transition dipole moments between the highest occupied molecular orbital (HOMO) and the excited state,  $|M_k^{(g)} - M_k^{(0)}|$  is the difference between the excited (configuration interaction (CI) level) state dipole moment and ground state one,  $E_g$  is the transition energy from the ground to excited state,  $\hbar\omega$  is the energy of a incident laser photon,  $H$  determines the line shape broadening,  $m$  is a number of excited state. Indices  $i, j, k, l = x, y, z$  are defined as laboratory Cartesian Coordinate system where  $x$  - axis corresponds to the longest axes of the molecule.

The values of the second order hyperpolarizability may be expressed in terms of the different energy levels from  $g$  to  $m$ , of the molecule:

$$\gamma_{ijkl} = K \sum_{g=1}^m \frac{|\mu_i^{(g)}| |\mu_j^{(g)}| |M_k^{(g)} - M_k^{(0)}| |M_l^{(g)} - M_l^{(0)}|}{(E_g^2 - (2\hbar\omega)^2 + H^2)}. \quad (4.19)$$

Only  $\gamma_{xxxx}$  was calculated, because the maximal output of nonlinear signal was observed usually for the diagonal tensor component, where the  $x$  direction corresponds to polarization direction of the photo inducing beam. The calculated values of the nonlinear optical hyperpolarizabilities are presented in the Table 4.6.

Figure 4.10 presents the calculated molecular orbital wavefunctions corresponding to the HOMO (Highest Occupied Molecular Orbital) and LUMO (Lowest Unoccupied Molecular Orbital) orbitals. The presented contours show how the change of the chemical bonds may change the total molecular charge density contributions. A very significant parameter is a difference between the ground and excited dipole moments. From Fig. 4.10 it is clearly seen that electronic contributions play dominant role in the observed nonlinear optical susceptibilities. This asymmetry in the ground and excited states topology plays an essential role in the observed nonlinear optical properties. A higher charge delocalization is observed for *rotaxane* and *catenane*, where charge jump over from one part of molecule (macrocycle, thread) to the other, what causes large asymmetries in the molecule, and the large change of dipolar moment in basic and excited states. More homogeneous spatial charge density distributions can be observed for the *thread* and *macrocycle*. This is connected with the centrosymmetric character of these molecules, what essentially compensates the gradients of the charge density.

The calculated HOMO and LUMO gaps as well as total dipole moments, which play a key role in the NLO properties, are presented in the Table 4.5. It can be seen that for the *thread* and *macrocycle* the HOMO - LUMO energy splitting gap is larger than for the *rotaxane* and *catenane*. The “combination” of *thread* and *macrocycle* into *rotaxane* decreases energy gap comparing to the *thread* and *macrocycle* alone (cf. Table 4.5) leading to the increase of NLO coefficients. The value of state dipole moments for *catenane* is the highest one and the HOMO - LUMO the lower than for the remaining ones as a consequence the nonlinear optical properties should be higher for this molecule.

### 4.7.2 First and second order hyperpolarizability

The molecular first order hyperpolarizability is the parameter that will have the strongest influence on the electro-optic coefficients. It depends on the shape and size of the molecule and the nature of its donor and acceptor substituents. It also depends strongly on the

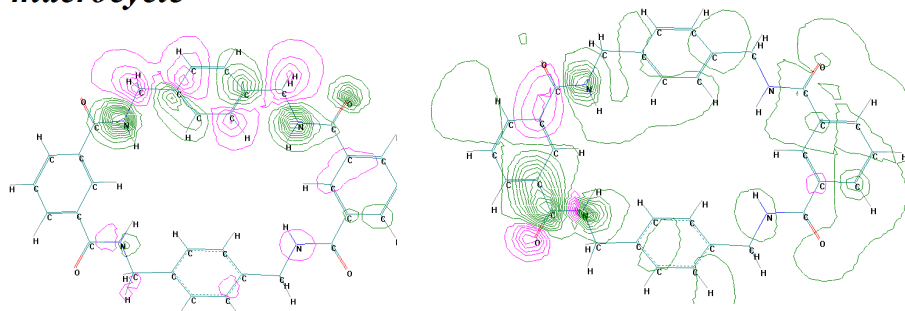
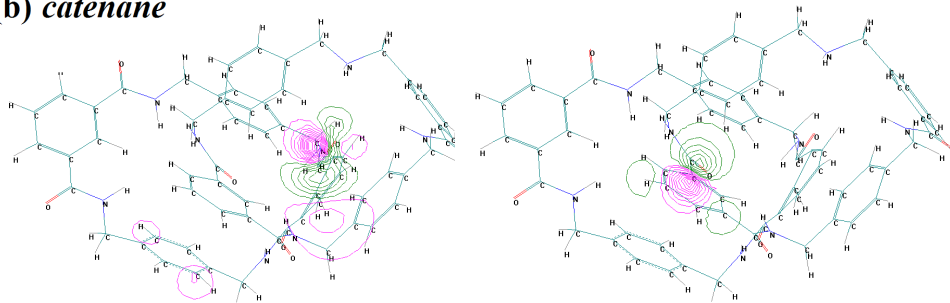
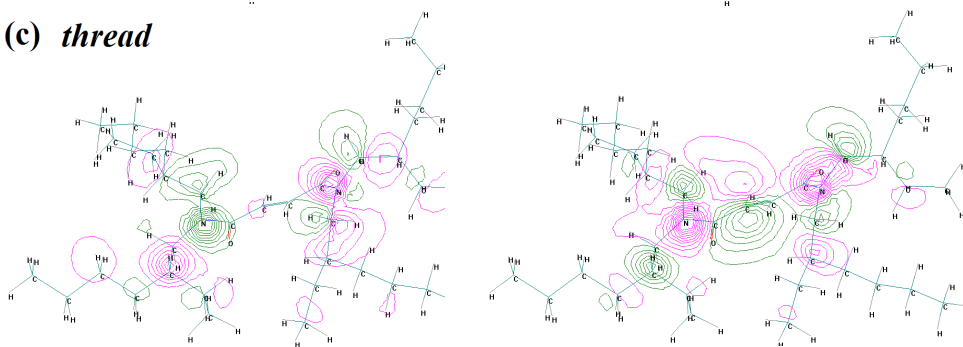
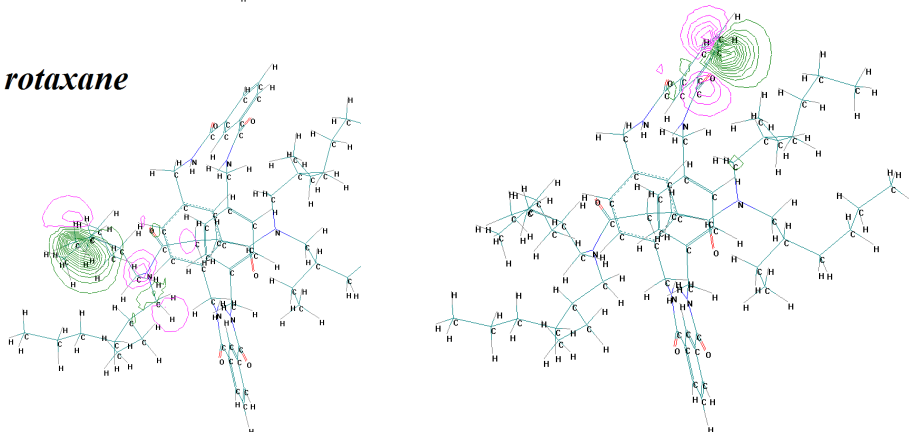
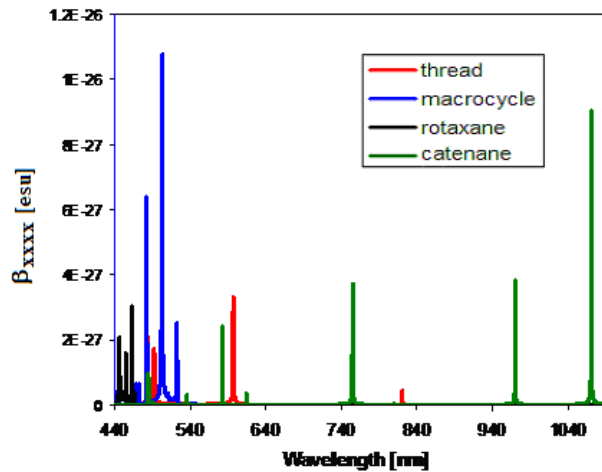
**(a) macrocycle****(b) catenane****(c) thread****(d) rotaxane**

Figure 4.10: Electrostatic potential distributions HOMO (left) and LUMO (right) for (a) *macrocycle*, (b) *catenane*, (c) *thread* and (d) *rotaxane*.

Molecules	Total dipole moment [D]	HOMO [eV]	LUMO [eV]	Energy gap [eV]
<i>thread</i>	5.11	-8.9693	-1.1979	7.7714
<i>macrocycle</i>	2.54	-9.6332	-0.7808	8.8524
<i>rotaxane</i>	1.56	-8.3375	-0.9621	7.3754
<i>catenane</i>	6.27	-7.6536	-1.1912	6.4624

Table 4.5: Principal parameters of the investigated molecules.

Figure 4.11: Dispersion of the molecular first order hyperpolarizabilities  $\beta_{xxx}^h$  for investigated molecules.

frequency of the optical fields and shows resonance enhancement near the charge transfer transition. Figure 4.11 displays the dispersion of  $\beta_{xxx}$  of the studied molecules. The more one of the wavelengths of the interacting beams approach the wavelength of maximum absorption, the more resonance effects come into play. When characterizing nonlinear optical molecules, we can eliminate this effect by introducing the hyperpolarizability  $\beta_0^h$  at zero frequency [11] (cf. Eq. (4.18)). The shift of the frequency to the red leads to an increase of  $\beta_{xxx}^h$  at given frequency  $\omega < \omega_{eg}$  ( $\omega_{eg}$  is the resonance frequency,  $\omega_{eg} = 2\pi c/\lambda_{eg}$ )

what is connected with the influence of the dipole transition moment and the change of the dipole moment between ground and excited state. We can see that the maximal first order hyperpolarizabilities for **thread**, **macrocycle** and **rotaxane** are located in the range of 440 – 600 nm ( $\lambda_{eg} = 200 - 300$  nm; cf. Fig. 4.2). For **catenane** the maximum of the mentioned above coefficient corresponds to wavelength over 1000 nm ( $\lambda_{eg} = 380$  nm).

Molecules	$\gamma^h \times 10^{-33}$ [esu] (exp. DFWM, $\lambda = 532$ nm)	$\gamma^h \times 10^{-35}$ [esu] (theory $\lambda = 532$ nm)	$\beta_{xxx}^h \times 10^{-30}$ [esu] (theory $\lambda = 1064$ nm)
<b>thread</b>	0.6	0.76	1.39
<b>macrocycle</b>	-	-	5.86
<b>rotaxane</b>	1.6	1.07	7.56
<b>catenane</b>	7.9	6.25	80.10
CS <sub>2</sub>	$33.6 \times 10^{-3}$	-	-

Table 4.6: Calculated and measured values of first and second order hyperpolarizabilities.

The calculated values of  $\beta_{xxx}^h$  are shown in the Table 4.6. The first order hyperpolarizability for **catenane** is one order of magnitude larger than that for the other molecules (**thread**, **macrocycle** and **rotaxane**). This enhancement is due to the intramolecular donor-acceptor charge transfer, and can be characterized with good accuracy as consequence from the two level system created by the ground state and the first excited state. The **rotaxane** and **catenane** created from **thread** and **macrocycle** or two **macrocycles**, respectively should have large first order hyperpolarizability because the increasing the number of molecules cause summation of their effects, thus enhancing the asymmetric distortion of the conjugated system. Additionally, the electronic properties of this type of molecule exhibit an unusual attribute, the intramolecular [131] charge transfer between thread and macrocycle or between two macrocycles what we can observe in Fig. 4.10. The obtained values of  $\beta_{xxx}^h$  for **thread**, **macrocycle** and **rotaxane** are comparable with the values obtained for nitroanilines (cf. Ref. [130]), and organometallic complexes (cf. Ref. [132]).

The second order hyperpolarizability ( $\gamma^h$ ) is the sum of the electronic contribution and the contribution coming from the orientation of the permanent dipole momentum

---

in the electric field. Taking into consideration the different mechanism of formation of nonlinearity in experiment and introduced in calculations, we can compare only the trend of changes of nonlinear coefficient collected in Table 4.6. We have good agreement between the theoretical calculations and experimental data of the second order hyperpolarizability for all compounds. The reason of some disagreement could be simply attributed to the possible errors in quantum-chemical methods, but we cannot rule out a strong influence of the solvent effect. We can see that creating one molecule on the basis of *thread* and *macrocycle* or two *macrocycles* leads to a substantial increase of nonlinear optical coefficients for *rotaxane* and *catenane* what outcome from theoretical calculation and experimental data.



# Chapter 5

## Results - DNA

### Contents

---

<b>5.1</b>	<b>Introduction to the chapter . . . . .</b>	<b>67</b>
<b>5.2</b>	<b>Spectral characterization . . . . .</b>	<b>67</b>
<b>5.3</b>	<b>Second harmonic generation . . . . .</b>	<b>71</b>
<b>5.4</b>	<b>Third harmonic generation . . . . .</b>	<b>72</b>
<b>5.5</b>	<b>Degenerate two-wave mixing . . . . .</b>	<b>74</b>

---

### 5.1 Introduction to the chapter

In this chapter we present the results of preparation and study of nonlinear optical properties of functionalized DNA with active nonlinear optical molecule - disperse red 1. The nonlinear optical properties were studied using harmonic generation techniques. These studies allowed us to obtain information on the electronic contributions to cubic susceptibilities in these supramolecular structures and the influence of adding active nonlinear optical molecules to the complex of DNA-CTMA. Also some NLO properties were explored in the degenerate two-wave mixing technique providing for information about optical holographic properties. Interesting results were obtained.

### 5.2 Spectral characterization

The absorption spectra for functionalized DNA were measured in the same manner as in the case of catenanes and rotaxanes molecules. Figure 5.1 shows absorption spectra of

DNA-CTMA and DNA-CTMA-DR1 (5% DR1 concentration) and DR1 in solutions.

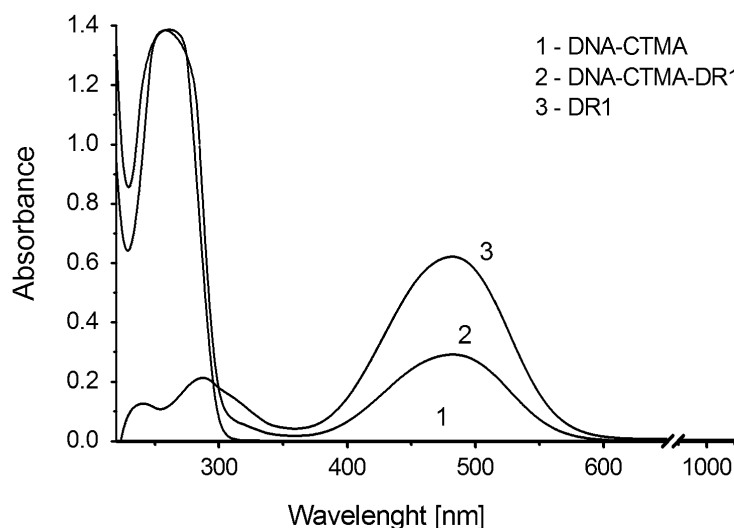


Figure 5.1: The absorbance spectra of DNA-CTMA (curve 1), DNA-CTMA-DR1 (5%) (curve 2) and DR1 (curve 3) in solutions.

DR1 is well known 1D charge transfer molecule, with electron donating ( $\text{CH}_3$ ) and electron accepting ( $\text{NO}_2$ ) end groups, separated by a  $\pi$  electron transmitter, composed of two phenyl rings and  $-\text{N}=\text{N}-$  segment (cf. Fig. 1.15). Due to the strong  $\pi$  electron conjugation DR1 is used not only for second order NLO effects, but is also interesting for third order effects. The UV absorption of nucleobases at around 260 nm is clearly seen in the first two absorption spectra (curves 1 and 2 in Fig. 5.1). This strong absorption band corresponds to the  $\pi - \pi^*$  transition of electrons of  $\text{C}=\text{C}$  bond of DNA bases. The second absorption band at around 490 nm in DNA-CTMA-DR1 (curve 2) is similar to that of pure DR1 (spectrum 3) showing very similar solvent influence.

Figure 5.2 shows absorption spectra of thin films of pure DNA-CTMA (1) and doped DNA-CTMA-DR1 (5%) (2), DNA-CTMA-DR1 (10%) (3) and DNA-CTMA-DR1 (15%) (4), respectively. The observed optical densities scale well with the solute concentration when corrected for thin film thicknesses. UV absorption bands of DNA are not seen because of substrate (glass) absorption.

Disperse red 1 purchased from Aldrich, was purified by a double recrystallization from an absolute methanol solution. The hexadecyltrimethylammonium chloride (CTMA),

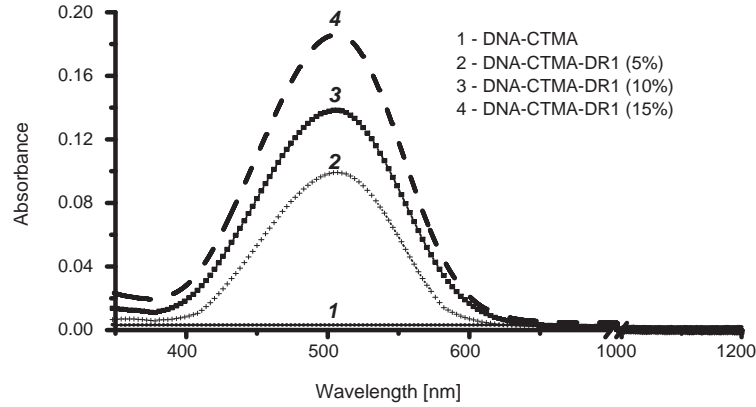


Figure 5.2: The absorbance spectra of DNA-CTMA (curve 1) and DNA-CTMA-DR1 (5%) (curve 2), DNA-CTMA-DR1 (10%) (curve 3), DNA-CTMA-DR1 (15%) (curve 4) thin films.

poly(9-vinylcarbazole), poly(methylmethacrylate) and organic solvents used in this study were also purchased from Aldrich and used as supplied, without any further purification. The high molecular weight ( $M_w > 10^6$  Daltons) of DNA rendered inhomogeneous film thickness due to high solution viscosity. In order to reduce the viscosity of the DNA-based solutions an ultrasonic procedure was used in 18 M $\Omega$  cm deionized water which reduced the molecular weight of the DNA [133].

After sonication, aqueous solution of DNA- Na<sup>+</sup> was added drop-wise to one litre of aqueous CTMA solution and stirred at room temperature for 6 hours. The DNA-CTMA complex precipitate was collected by vacuum filtration through a 0.4  $\mu$ m nylon filter, washed with deionized water (18 M $\Omega$  cm) and then dried in a vacuum oven at 35°C.

The DNA-CTMA complex was then dissolved in butanol and functionalized with DR1 (30% in weight). For comparison, DR1 was also added to PMMA (cf. Fig. 5.3(a)) and PVK (cf. Fig. 5.3(b)) in trichloroethane, with the same concentration of DR1 chromophore (30%). The resulting solutions of DNA-CTMA-DR1, PMMA-DR1 and PVK-DR1 were then filtered with a 0.4  $\mu$ m pore size nylon syringe filter.

All thin films were prepared at room temperature under an ambient pressure by spin coating process on BK7 glass slides with a Delta 10 Microtec spin coater, with the speed between 1000 rpm and 2500 rpm. The thicknesses of the films were measured with Dektak

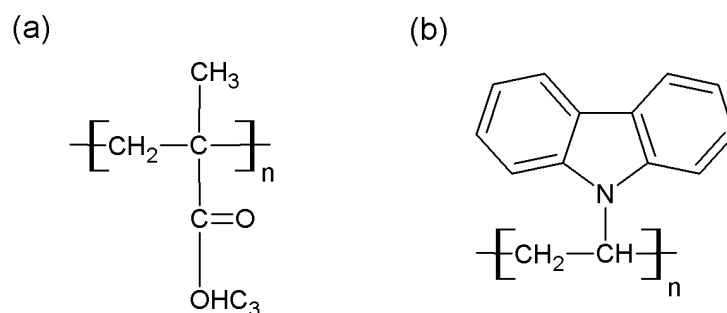


Figure 5.3: Chemical structures of PMMA (a) and PVK (b) matrices.

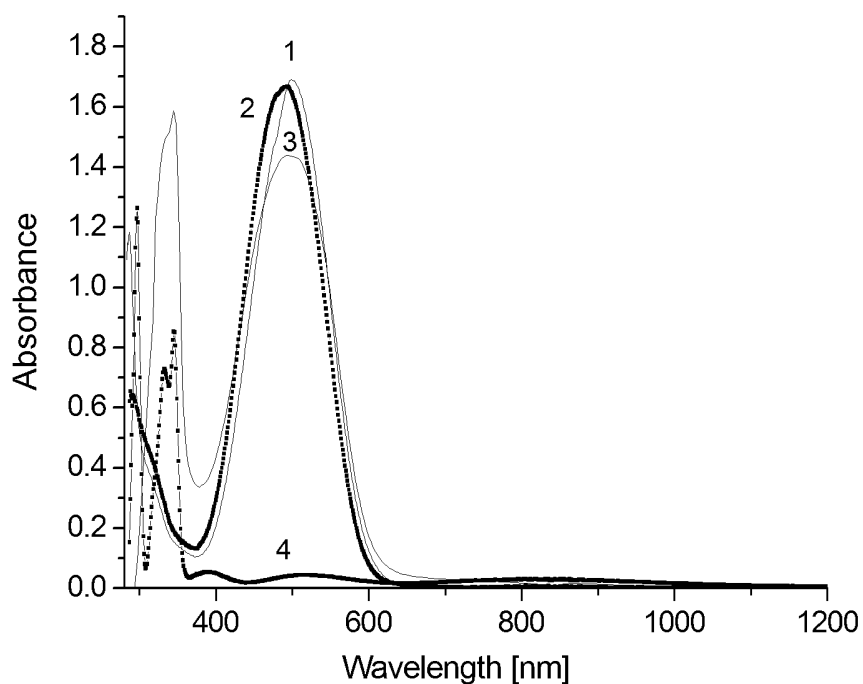


Figure 5.4: The absorbance spectra of thin films of DNA-CTMA-DR1 (1), PMMA-DR1 (2), PVK-DR1 (3) and PVK alone (4).

6.0 M Stylus profiler and were about  $1.37\ \mu\text{m}$  (DNA-CTMA-DR1),  $1.4\ \mu\text{m}$  (PMMA-DR1) and  $1.2\ \mu\text{m}$  (PVK-DR1). After deposition, the thin films were baked at  $70^\circ\text{C}$  for 60 min to remove any remaining solvent. In this process the good homogeneity was obtained (for

all cases). The absorption spectra of the studied thin films are presented in Fig. 5.4.

### 5.3 Second harmonic generation

Second harmonic generation is a nonlinear optical process in which a nonlinear material generates photons with twice energy when illuminated. Using the Ti:Sapphire laser (750 nm) with pulses of 70 fs, we obtained images of the second harmonic generated by the DNA-CTMA-DR1 samples (cf. Fig. 5.5). The measurements were done in the Center for Microscopy-Microanalysis and Information Processing at the University “Politehnica” of Bucharest in Romania.

The white areas (cf. Fig 5.5) show the second harmonic generation signal. Not for all samples and not for all areas the shg signal has been observed. However we think that it is necessary to investigate more carefully this phenomenon.

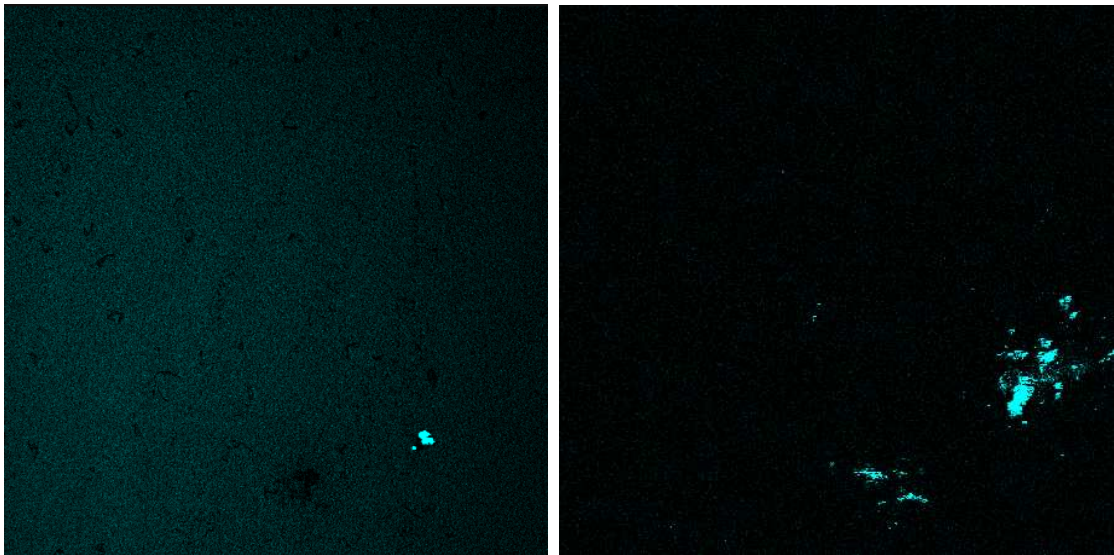


Figure 5.5: Transmission image that reveals second harmonic generation (white area). The DNA-CTMA-DR1 thin film deposited on the glass substrate were investigated.

## 5.4 Third harmonic generation

Third harmonic generation measurements were performed (in Commissariat à l'Energie Atomique (CEA), Saclay, France) to determine the electronic part of third order nonlinear susceptibility. The samples were illuminated with 1064 nm Nd:YAG laser beam (13 ns, 10 Hz) and the generated signal was measured by the photomultiplier. Due to isotropic samples, vertical ( $s$ ) polarization was used. The thin films of DNA complexes were kept in a vacuum chamber during the measurements in order to avoid the air contributions [85]. As a reference material and for calibration high purity silica slab ( $\text{SiO}_2$ ) was used.

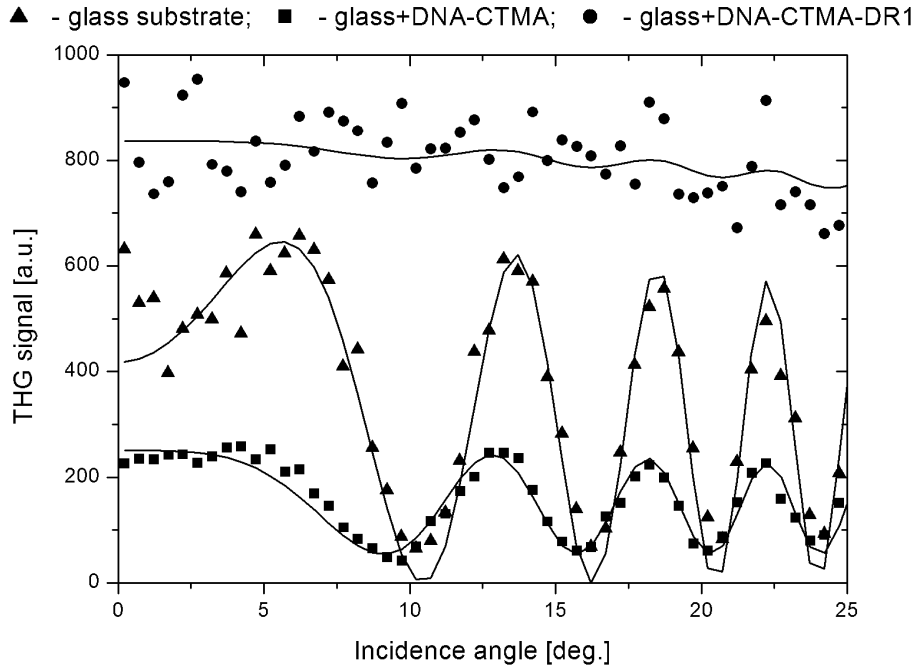


Figure 5.6: Measured (shapes) and calculated (solid lines) THG intensities for glass substrate, DNA-CTMA and DNA-CTMA-DR1 thin films.

Figure 5.6 displays typical plots of THG intensities versus incident angle (measured values - shapes, fitted - continuous lines) coming from the glass plate alone, glass plate with DNA-CTMA and glass plate with DNA-CTMA-DR1 thin films. Due to the interference of the free and bound waves in the glass slab in the case of glass substrate alone the Maker fringes are observed. Such behaviour is normal for the case when the coherence length for

material ( $5.62 \mu\text{m}$ ) is much smaller than the glass slab thickness ( $1040 \mu\text{m}$ ). We can see a monotonically varying, with incidence angle, contribution from thin films of DNA-CTMA and DNA-CTMA-DR1 to that of substrate (cf. Fig. 5.6). In all cases these contributions are decreasing with the increasing incidence angle due to the envelope function (less light coupled into thin film when increasing the incidence angle). This is due to the fact that the thin film thickness is smaller than the coherence length ( $7.4 \mu\text{m}$  for DNA-CTMA and DNA-CTMA-DR1 [54]). It is also seen that in the case of DR1 doped films the thin film contribution is much more important than in the case of undoped film.

In order to get an accurate value for the thin films third order nonlinear susceptibility ( $\chi^{(3)}$ ) the THG intensities were square fitted to the Eq. (3.3). The results of the fit are shown (solid lines in Fig. 5.6). A good agreement between the calculated and measured third harmonic generated intensities is observed. For the fitting procedure, the values of the refractive indices for DNA-CTMA, those were reported by Grote, et. al. [54], were used. For DNA-CTMA-DR1 the same refractive indices were used as for DNA-CTMA. Indeed, for the relatively small concentration of DR1, significant change of the refractive index is not expected for the doped film. Also, in the case of THG in thin films, the harmonic intensities do not depend on the difference of refractive indices. A correction for the absorption at the harmonic wavelength in the DNA-CTMA-DR1 film was applied by introducing a complex index of refraction in the calculations.

Sample	thickness [ $\mu\text{m}$ ]	refractive index [esu]	$\chi^{(3)} \times 10^{14}$ [esu]
DNA-CTMA	0.367	1.488	$11.5 \pm 0.1$
DNA-CTMA-DR1 (5%)	3.484	1.488	$155.0 \pm 16$
DNA-CTMA-DR1 (10%)	4.060	1.488	$69 \pm 7$
DNA-CTMA-DR1 (15%)	3.484	1.488	$85 \pm 9$
glass	1041	1.507	$2.1 \pm 0.2$
SiO <sub>2</sub>	1010	1.450	$1.43 \pm 0.14$

Table 5.1: The third harmonic generation results for studied samples.

The values obtained from measurements are listed in Table 5.1. For the silica calibra-

tion the value determined by Gubler and Bosshard [134] ( $\chi^{(3)} = (1.43 \pm 0.14) \times 10^{-14}$  esu) was used. In the case of DNA-CTMA films the value of THG susceptibility about one order of magnitude larger than for  $\text{SiO}_2$  was observed. This difference may be well accounted for by the presence of highly polarizable conjugated  $\pi$  electrons in DNA. For the doped DNA-CTMA complex with only 5% of DR1, THG susceptibility was two orders of magnitude larger than for fused silica. This increase is due to nonlinear response of the doping chromophore DR1 (two photon resonance for the 532 nm wavelength is expected). The  $\chi^{(3)}$  values are much higher than for other dopants (i.e. CoPc [135]). Indeed, the double of the fundamental photon energy  $2\omega$  matches well the transition energy to the first excited singlet state. For the DNA-CTMA the response originates from DNA, as CTMA molecules do not contain conjugated  $\pi$  electrons, known to be at the origin of large nonlinear response in organic compounds.

## 5.5 Degenerate two-wave mixing

The search of new materials for applications in optics, optoelectronics and particularly in optical data storage, based on simple holographic effect, is subject of interest of many researchers [90, 91, 136, 98, 104, 103, 102, 100]. It is well known that materials which exhibit birefringence and dichroism can be used in applications including optical data storage and optical information processing. However, the process of photoinduced modification/organization of the material's surface can not easily be explained. There are only a few models which try to describe this behaviour [90], however, in the case of DNA, these models are not sufficient because of DNA's complex structure.

The molecules containing photoisomerizable  $-\text{C}=\text{C}-$  or  $-\text{N}=\text{N}-$  segments exhibit reversible trans-cis photoisomerization and thermal relaxation and show ability to form surface relief grating. The best known representative of an azobenzene derivative, with reversible photoisomerization, is DR1 (with  $-\text{N}=\text{N}-$  bonds, cf. Fig. 1.15). These molecules can be oriented during polarized irradiation with absorbed light on the basis of angular hole burning model [137]. We used DR1 as the guest in a guest-host system. For comparison we used different polymeric matrices as hosts: DNA-CTMA, polymethylmethacrylate (PMMA; cf. Fig. 5.3(a)) and poly(9-vinylcarbazol) (PVK; cf. Fig. 5.3(b)).

The grating formation experiment was done using degenerate two-wave mixing experimental setup described in chapter 3. With the *ss* polarization configuration setup, we compared the dynamics of the photoinduced inscription of the diffraction gratings for the

three guest-host systems: DNA-CTMA-DR1, PMMA-DR1 and PVK-DR1 (cf. Fig. 5.7). We worked within the Bragg light scattering regime and only one order of diffraction was observed [138]. The 532 nm light absorption in the sample caused a trans-cis isomerization process of DR1 [91]. As already mentioned, the speed of the build up of diffraction grating in the sample as function of time was monitored by measuring the intensity of the first order of diffraction (further called “the signal”) beam. The grating was read up by a cw He-Ne laser (polarized vertically).

For all studied samples, doped with the same amount of DR1, the dynamics of the diffraction signal, which is directly related to the grating formation, exhibits very fast growth rate, after exposition to the laser light. However the shortest time of writing is in the case of thin films based on DNA-CTMA-DR1 compared to the other studied matrices (cf. Fig. 5.7).

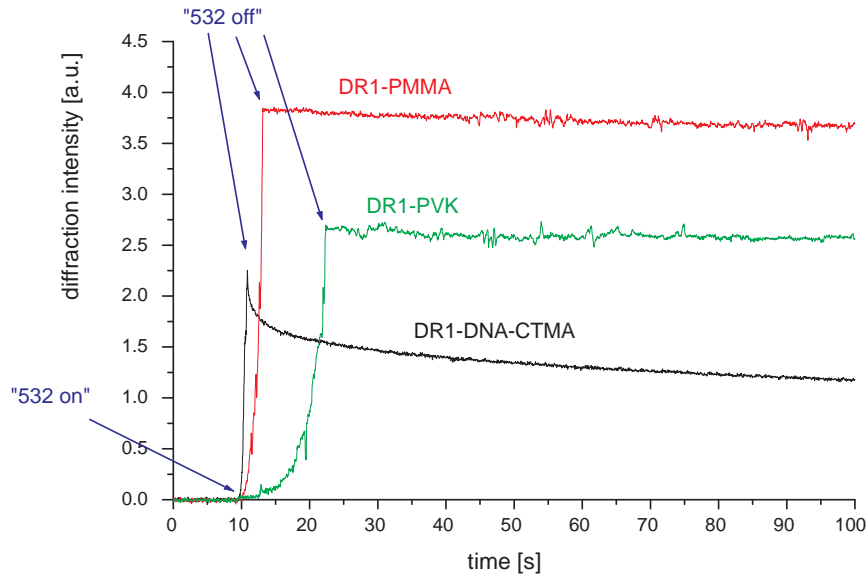


Figure 5.7: Example of the dynamics of the gratings inscribed in the PMMA-DR1, PVK-DR1 and DMA-CTMA-DR1 materials using 16 ps pulses of 532 nm laser light with a 10 Hz repetition rate. Monitoring was done using a He-Ne laser light scattering.

Also the decay process depends on the matrix. For PMMA-DR1 and PVK-DR1 the gratings appeared to be fairly stable. For DNA-CTMA-DR1 we observed not negligible

relaxation of the grating. After switching on the 532 nm inscription beams, we noticed continuation of the grating growth (cf. Fig. 5.8).

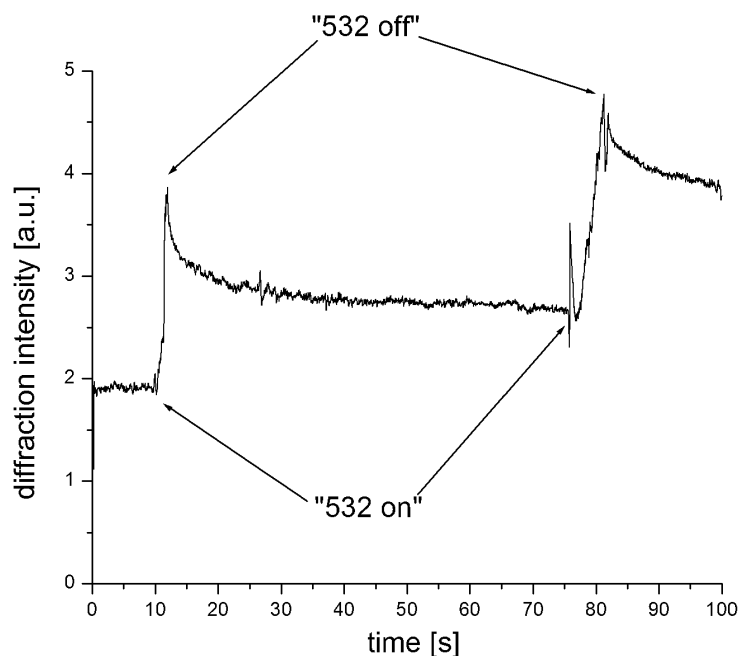


Figure 5.8: The dynamics of diffracting grating formation with two times started and two times stopped of writing process. The “532 on” means switching on the inscription laser light, while the “532 off” - the cutting off it during the permanent presence of the probe cw He-Ne laser beam.

We notice that for DNA-CTMA-DR1, each pulse of the laser was able to create a well readable grating (see inset to Fig. 5.9). In the case of PMMA-DR1 and PVK-DR1 or in the case for other holographic materials (i.e. for organometallic complexes, see Ref. [113]) we did not observe any relaxation after the inscribing pulses, whereas in the case of DNA-CTMA-DR1, visible relaxation had occurred (as is in the case for azo carbazole compounds, see Ref. [112]), but nevertheless did not affect the fastest speed of grating formation. This could be due the fact that for the DNA-CTMA-DR1 we have larger charge transfer determining the induced dipole moments playing principal role for the optically poled systems [139, 140].

We have also checked the influence of the polarization configuration of writing beams (configuration *ss*, *pp* (cf. Fig. 5.9) and *sp*) on the kinetics of grating formation. In the case of PMMA-DR1 and PVK-DR1 the build up of a signal was the fastest when light was

polarized parallel ( $ss$  or  $pp$ ), whereas for light polarized perpendicularly ( $sp$ ) the build up of signal was slower. However, in the case of DNA-CTMA-DR1 for  $sp$  polarization we did not observe any light diffraction. In the latter mentioned material the  $ss$  and  $pp$  polarizations resulted in almost the same speed of grating creation, however the decay time is faster when the grating is written with  $pp$  beams (cf. Fig. 5.9).

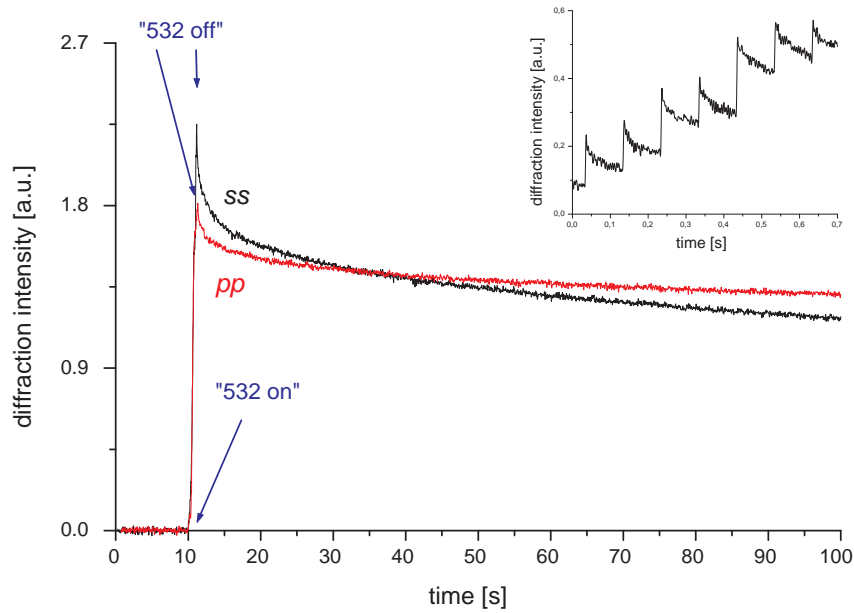


Figure 5.9: Dynamics of the build up and decay of the grating process in DNA-CTMA-DR1 for two polarizations of writing beams:  $ss$  - upper curve,  $pp$  - lower curve and details after each pulse of writing beams - inset.

Our samples were free to deform (thin films on the glass substrate) and surface relief gratings (SRGs) could be formed. We observed them after inscription process using atomic force microscope (Autoprobe CP Research Veeco). The scan was done in the contact mode.

Figure 5.10 shows the AFM pictures of two dimensional views of the surface relief gratings obtained on spin coated thin films of PMMA-DR1, PVK-DR1 and DNA-CTMA-DR1 and the cross-sections' profiles for these results. For the case of PMMA-DR1 we obtained a typical result of the relief pattern with a regular sinusoidal shape up to 200 nm

depth (about 125 nm for PVK-DR1 and 70 – 160 nm for DNA-CTMA-DR1).

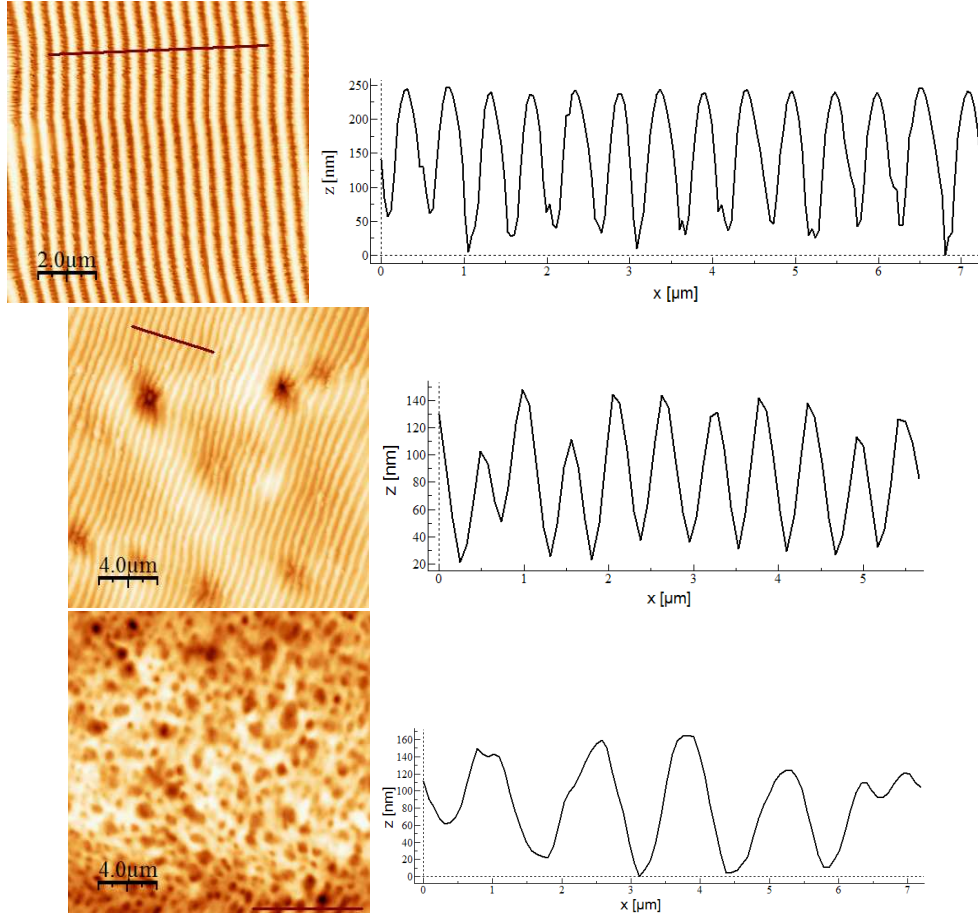


Figure 5.10: AFM two-dimensional views of surface topography (left) and cross-section plots (right) for PMMA-DR1 (a), PVK-DR1 (b) and DNA-CTMA-DR1 (c) after degenerate two-wave mixing experiment.

The grating period  $\Lambda$ , measured by AFM was about  $0.52 \mu\text{m}$ , and was consistent with the theoretically calculated one using Eq. (5.1)

$$\Lambda = \frac{\lambda}{2 \sin \theta}, \quad (5.1)$$

where  $\lambda$  is the wavelength of the writing beams and  $(2\theta)$  is the angle between the two writing beams [141]. The AFM pictures (cf. Fig. 5.10) of the obtained gratings show that: PMMA-DR1 system forms regular SRGs as usually observed, the SRG for PVK-DR1 is less regular in shape than for PMMA-DR1, and no SRG is observed in thin films of DNA-

CTMA-DR1. However, we did observe different topographies as compared to the surfaces before irradiation (height of irregular structure is in the range about 70 – 160 nm). We propose two explanations for this behaviour. Firstly, no SRG is created in the case of DNA-CTMA matrix; or secondly, SRG relaxes immediately (cf. Fig. 5.9) and, therefore, we have a permanent refractive index and/or absorption coefficient change in the material bulk only (the signal of the first order of diffraction even after few weeks was observed).

This last explanation is close to be true when we observe images from confocal scanning laser microscope which scanned our sample (DNA-CTMA-DR1) through its volume. One of the taken resulting images is shown on Fig. 5.11. It is clearly seen that we have some circular order of molecules (not visible on the surface). Further investigations are needed to understand and explain this phenomenon.

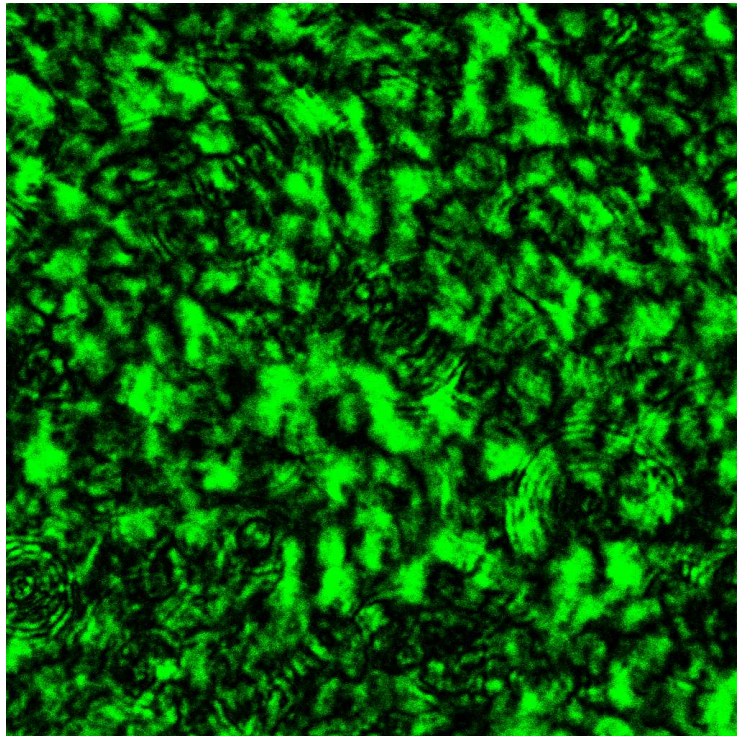


Figure 5.11: Image of DNA-CTMA-DR1 sample measured by confocal scanning laser microscope. Picture was taken during cross section sample's scanning.



# Chapter 6

## Conclusions and perspectives

### Contents

---

<b>6.1</b>	<b>Conclusions</b>	<b>81</b>
<b>6.2</b>	<b>Perspectives</b>	<b>83</b>
6.2.1	New family of rotaxanes	83
6.2.2	DNA holography	83

---

### 6.1 Conclusions

Catenanes and rotaxanes are the molecules which deserve for interest in the nonlinear optics due to their unique architecture and nonlinear properties.

We conclude, that we have an important rotational contribution to  $\chi^{(3)}$  susceptibility of *thread* coming either from rotational mobility in molecule. However, we did not observe significant rotational contribution in the case of *rotaxane*, *fumrot* and *catenane*, as we expected. We suppose that the obtained results are due to very low concentration of solutions. Unfortunately tested molecules are insoluble at higher concentration in most common organic solvents. So, we were not able to test solutions at higher concentration. In order to get better insights in  $\chi^{(3)}$  contributions further experiments are needed. However the obtained results are original and important for nonlinear optical applications. In order to reach this goal we have started to design more soluble new compounds based on TTF-base molecules.

From calculations is clearly seen that *catenane* is the best candidate from among studied molecules. The maximally value of second order hyperpolarizability  $\gamma_{xxxx}^h$  was

obtained for mentioned compound equal  $6.25 \times 10^{-35}$  esu, what is connected with the difference between ground and excited dipole moments.

The obtained values of calculated second order nonlinear hyperpolarizabilities are comparable with the nonlinear coefficients obtained for molecules in Ref. [130]. We can expect that for these molecules the inter- and intra- molecular electron vibration interactions plays a key role in the observed nonlinearities what was not taken into account in suggested theoretical calculations.

The functionalization of rotaxane molecules grow up their physical properties, while in the case of DNA modification is necessary to use this “molecule of life” for nonlinear optical applications.

DNA complexes with CTMA surfactant were doped with a DR1, NLO molecules in order to get NLO properties of otherwise inactive DNA matrix. The compounds can be processed into good optical quality thin films by solution spinning technique. The spectral characteristics of DNA-CTMA-DR1 complexes are very similar to that of pure DR1 solution in butanol and in thin films. The NLO properties of thin films were characterized by third harmonic generation technique which gives the fast, electronic third order nonlinear susceptibility.

The THG measurements give almost one order of magnitude higher value of  $\chi^{(3)}$  susceptibility for pure DNA-CTMA thin film than for the commonly used reference material ( $\text{SiO}_2$ ). This increase is apparently due to the presence of conjugated  $\pi$  electrons in nucleobases. A significantly increase of  $\chi^{(3)}$  susceptibility is observed for DNA-CTMA-DR1 system. The largest, relative increase (with respect to the number of doping molecules) is observed at 5% doping level. In the case of studied system we observe a decrease of NLO susceptibility for higher dopant concentration (10% and 15%), although still significantly larger than for undoped systems. We suppose that it could be caused by interaction with matrix (DC Stark effect) or by large local field factor.

It is possible to write diffraction gratings in thin films of DNA-CTMA-DR1 with ps laser pulses and with a fast write up time, faster than in the two other matrices: PVK and PMMA. No surface relief gratings formation was observed in this material, contrary to the case when the matrix was PMMA or PVK. The explanation of this behaviour is not simple and need further deep investigations. Our preliminary results suggest to change the polarization of writing beams for circular due to circular tendency observed in the DNA-CTMA-DR1 structure.

---

## 6.2 Perspectives

### 6.2.1 New family of rotaxanes

Due to problems with solubility it is necessary to synthesize new more soluble molecules. We propose the rotaxanes of redox-active metallo-rings incorporating the TTF unit (discrete cyclic nanostructures). The synthesis will use a metal-mediated self-assembly strategy ( $M = \text{Pd}, \text{Pt}, \text{Re} \dots$ ), using a wide range of TTF-based precursors. The solid-state organization of such multi-TTF systems, using the well-established coordinating properties of the pyridyl group for transition metals, associated with the generation of the different stable oxidation states of the TTF units by electrocrystallization techniques, should lead to very exciting electroconductive and magnetic coupling properties from these multidimensional systems.

### 6.2.2 DNA holography

It was effectively shown that DNA-CTMA complex is very good matrix for optical applications. We want to continue investigate the optical properties of these compounds, especially of its application of holography. Described results show promising behaviours and deserve for future investigations. For better understanding the inscription of diffracting grating future investigations (with more configurations than only linear polarizations) are necessary. Also the decisive experiment is needed to know if the surface relief grating is created or it is other type of grating. Finally we plan to do a hologram as a final work of this adventure with DNA holography. However the experimental physics is so beautiful that new ideas appearing suddenly and sometimes with such idea starts a new adventure.



# Bibliography

- [1] C. Collier, E. Wong, M. Belohradsky, F. Raymo, J. Stoddart, P. Kuekes, R. Williams, J. Heath, Electronically configurable molecular-based logic gates, *Science* 285 (1999) 391–394.
- [2] C. Collier, G. Mattersteig, E. Wong, Y. Luo, K. Beverly, J. Sampaio, F. Raymo, J. Stoddart, J. Heath, A [2]catenane-based solid state electronically reconfigurable switch, *Science* 289 (2000) 1172–1175.
- [3] A. Pease, J. Jeppesen, J. Stoddart, Y. Luo, C. Collier, J. Heath, Switching devices based on interlocked molecules, *Accounts of Chemical Research* 34 (2001) 433–444.
- [4] P. Franken, A. Hill, C. Peters, G. Weinreich, Generation of optical harmonics, *Physical Review Letters* 7 (1961) 118–120.
- [5] M. Goppert-Mayer, Two-quantum processes, *Annalen der Physik* 9 (1931) 273–294.
- [6] N. Bloembergen, *Nonlinear Optics*, Benjamin, New York, 1965.
- [7] Y. Shen, *The Principles of Nonlinear Optics*, Wiley, New York, 1984.
- [8] M. Levenson, S. Kano, *Introduction to nonlinear laser spectroscopy*, Academic Press, 1988.
- [9] P. Prasad, D. Williams, *Introduction to nonlinear optical effects in molecules and polymers*, Wiley-Interscience, 1991.
- [10] R. Boyd, *Nonlinear Optics*, Academic Press, San Diego, 2003.
- [11] C. Bosshard, K. Sutter, P. Pretre, J. Hulliger, M. Florsheimer, P. Kaatz, P. Gunter, *Organic nonlinear optical materials*, Gordon and Breach, Basel, 1995.
- [12] S. Kielich, *Molekularna optyka nieliniowa*, PWN, Warszawa, 1977.

- 
- [13] T. Gase, D. Grando, P. Chollet, F. Kajzar, A. Lorin, D. Tedard, D. Leigh, Thin films of benzylic amide [2]catenane as a novel versatile photonic material, *Photonics Science News* 3 (1998) 16–21.
- [14] T. Gase, D. Grando, P. Chollet, F. Kajzar, A. Murphy, D. Leigh, Linear and unanticipated second-order nonlinear optical properties of benzylic amide [2]catenane thin films: Evidence of partial rotation of the interlocked molecular rings in the solid state, *Advanced Materials* 11 (1999) 1303–1306.
- [15] D. Grando, T. Gase, F. Kajzar, M. Fanti, F. Zerbetto, A. Murphy, D. Leigh, Non-linear optical properties of benzylic amide [2] catenanes: a novel versatile photonic material, *Molecular Crystals and Liquid Crystals* 353 (2000) 545–559.
- [16] A. Lane, D. Leigh, A. Murphy, Peptide-based molecular shuttles, *Journal of American Chemical Society* 119 (1997) 11092–11093.
- [17] H. Yu, Y. Luo, K. Beverly, J. F. Stoddart, H.-R. Tseng, J. Heath, The molecule-electrode interface in single-molecule transistors, *Angewandte Chemie International Edition English* 42 (2003) 5706–5711.
- [18] P.-L. Anelli, N. Spencer, J. Stoddart, A molecular shuttle, *Journal of American Chemical Society* 113 (1991) 5131–5133.
- [19] R. Bissell, E. Cordova, A. Kaifer, J. Stoddart, A chemically and electrochemically switchable molecular shuttle, *Nature* 369 (1994) 133–137.
- [20] J.-P. Collin, P. Gavina, J. Sauvage, Electrochemically induced molecular motions in coppercomplexed threaded systems: From the unstoppered compound to the semi-rotaxane and the fully blocked rotaxane, *New Journal of Chemistry* 21 (1996) 525–528.
- [21] H. Murakami, A. Kawabuchi, K. Kotoo, M. Kunitake, N. Nakashima, A light-driven molecular shuttle based on a rotaxane, *Journal of American Chemical Society* 119 (1997) 7605–7606.
- [22] T. Kelly, M. Bowyer, K. Bhaskar, D. Bebbington, A. Garcia, F. Lang, M. Kim, M. Jette, A molecular brake, *Journal of American Chemical Society* 116 (1994) 3657–3658.

- 
- [23] T. Kelly, I. Tellitu, J. Sestelo, In search of molecular ratchets, *Angewandte Chemie International Edition English* 36 (1997) 1866–1868.
- [24] A. Davis, Tilting at windmills? the second law survives, *Angewandte Chemie International Edition English* 37 (1998) 909–910.
- [25] T. Bedard, J. Moore, Design and synthesis of a “molecular turnstile”, *Journal of American Chemical Society* 117 (1995) 10662–10671.
- [26] R. Hernandez, H.-R. Tseng, J. Wong, J. Stoddart, J. Zink, An operational supramolecular nanovalve, *Journal of American Chemical Society* 126 (2004) 3370–3371.
- [27] A. Braunschweig, B. Northrop, J. Stoddart, Structural control at the organic-solid interface, *Journal of Material Chemistry* 16 (2005) 32–44.
- [28] J. Berna, D. Leigh, M. Lubomska, S. Mendoza, E. Perez, P. Rudolf, G. Teobaldi, F. Zerbetto, Macroscopic transport by synthetic molecular machines, *Nature Materials* 4 (2005) 704–710.
- [29] J.-P. Collin, C. Dietrich-Buchecker, P. Gavin, A. Jimenez-Molero, J.-P. Sauvage, Shuttles and muscles: Linear molecular machines based on transition metals, *Accounts of Chemical Research* 34 (2001) 477–487.
- [30] H. Frisch, E. Wasserman, Chemical topology, *Journal of American Chemical Society* 83 (1961) 3789–3795.
- [31] I. Harrison, S. Harrison, The synthesis of a stable complex of a macrocycle and threaded chain, *Journal of American Chemical Society* 89 (1967) 5723–5724.
- [32] G. Schill, H. Zollenkopf, Rotaxane, *Nachr. Chem. Tech.* 15 (1967) 149.
- [33] D. Leigh, A. Murphy, J. Smart, A. Slawin, Optical and low frequency electric field testing of the mobility of mobile part in catenanes and rotaxanes, *Angewandte Chemie International Edition English* 36 (1997) 728–732.
- [34] D. Leigh, A. Murphy, J. Smart, M. Deleuze, F. Zerbetto, Controlling the frequency of macrocyclic ring rotation in benzylic amide [2]catenanes, *Journal of American Chemical Society* 120 (1998) 6458–6467.

- 
- [35] V. Balzani, M. Gomez-Lopez, F. Stoddart, Molecular machines, *Accounts of Chemical Research* 31 (1998) 405–414.
- [36] D. Stewart, D. Ohlberg, P. Beck, Y. Chen, R. Williams, J. Jeppesen, K. Nielsen, J. Stoddart, Molecule-independent electrical switching in pt/organic monolayer/ti devices, *Nano Letters* 4 (2004) 133–136.
- [37] V. Bermudez, P. Chollet, F. Gatti, F. Kajzar, D. Leigh, A. Lorin, S. Zhang, Linear and nonlinear optical properties of rotaxanes: novel versatile photonic materials, in: M. Eich, M. G. Kuzyk, C. M. Lawson, R. A. Norwood (Eds.), *Linear, Nonlinear and Power-Limiting Organics*, Vol. 4106, 2000, pp. 318–328.
- [38] C. Joachim, J. Gimzewski, A. Aviram, Electronics using hybrid-molecular and mono-molecular devices, *Nature* 408 (2000) 541–548.
- [39] D. Leigh, Molecules in motion: Towards hydrogen bond-assembled molecular machines, in: F. Charra, V. Agranovich, F. Kajzar (Eds.), *Organic Nanophotonics*, 2003, pp. 47–56.
- [40] K. Nowicka, P. Chollet, F. Kajzar, G. Bottari, F. Gatti, D. Leigh, A. Miniewicz, Optical and low frequency electric field testing of the mobility of mobile parts in catenanes and rotaxanes, *Nonlinear Optics and Quantum Optics* 32 (2004) 175–186.
- [41] I. Arfaoui, V. Bermudez, G. Bottari, C. D. Nadai, J. Jalkanen, F. Kajzar, D. Leigh, M. Lubomska, S. Mendoza, J. Niziol, P. Rudolf, F. Zerbetto, Surface enhanced second harmonic generation from macrocycle, catenane and rotaxane thin films: Experiments and theory, *Journal of Physical Chemistry B* 110 (2006) 7648–7652.
- [42] I. Rau, F. Kajzar, Catenanes and rotaxanes - new classes of molecules with mobile parts for applications in photonics, *Revista De Chimie* 58 (2007) 861–865.
- [43] R. Czaplicki, O. Krupka, Z. Essaidi, A. El-Ghayoury, F. Kajzar, J. Grote, B. Sahraoui, Grating inscription in picosecond regime in thin films of functionalized dna, *Optics Express* 15 (2007) 15268–15273, highlighted in *Nature Photonics*, 2 (2007) 6.
- [44] D. Amabilino, J. Stoddart, Interlocked and intertwined structures and superstructures, *Chemical Review* 95 (1995) 2725–2828.

- 
- [45] F. Arico, J. Badjic, S. Cantrill, A. Flood, K.-F. Leung, Y. Liu, J. Stoddart, Templated synthesis of interlocked molecules, *Topics in Current Chemistry* 249 (2005) 203–259.
- [46] A. Johnston, D. Leigh, R. Pritchard, M. Deegan, Facile synthesis and solid-state structure of a benzylic amide [2]catenane, *Angewandte Chemie International Edition English* 34 (1995) 1209–1212.
- [47] A. Johnston, D. Leigh, L. Nezhat, J. Smart, M. Deegan, structurally diverse and dynamically versatile benzylic amide [2]catenanes assembled directly from commercially available precursors, *Angewandte Chemie International Edition English* 34 (1995) 1212–1216.
- [48] A. Johnston, D. Leigh, A. Murphy, J. Smart, M. Deegan, structurally diverse and dynamically versatile benzylic amide [2]catenanes assembled directly from commercially available precursors, *Journal of American Chemical Society* 118 (1996) 10662–10663.
- [49] F. Gatti, D. Leigh, S. Nepogodiev, A. Slawin, S. Teat, J. Wong, Structurally diverse and dynamically stiff, and sticky in the right places: The dramatic influence of pre-organizing guest binding sites on the hydrogen bond-directed assembly of rotaxanes, *Journal of American Chemical Society* 123 (2001) 5983–5989.
- [50] J. Niziol, K. Nowicka, F. Kajzar, *Non-Linear optical properties of matter*, Springer, Dordrecht, 2006, Ch. Linear and nonlinear optical properties of selected rotaxanes and catenanes, pp. 609–643.
- [51] J. Watson, F. Crick, A structure for deoxyribose nucleic acid, *Nature* 171 (1953) 737–738.
- [52] K. Tanaka, Y. Okahata, A dna-lipid complex in organic media and formation of an aligned cast film, *Journal of American Chemical Society* 118 (1996) 10679–10683.
- [53] J. Grote, J. Hagen, J. Zetts, R. Nelson, D. Diggs, M. Stone, P. Yaney, E. Heckman, C. Zhang, W. Steier, A.-Y. Jen, L. Dalton, N. Ogata, M. Curley, S. Clarson, F. Hopkins, Investigation of polymers and marine-derived dna in optoelectronics, *Journal of Physical Chemistry B* 108 (2004) 8584–8591.

- 
- [54] J. Grote, D. Diggs, R. Nelson, J. Zetts, F. Hopkins, N. Ogata, J. Hagen, E. Heckman, P. Yaney, M. Stone, L. Dalton, Dna photonics [deoxyribonucleic acid], *Molecular Crystals and Liquid Crystals* 426 (2005) 3–17.
- [55] P. Gupta, P. Markowicz, K. Baba, J. O'Reilly, M. Samoc, P. Prasad, J. Grote, Dna-normocer based biocomposite for fabrication of photonic structures, *Applied Physics Letters* 88 (2006) 213109(1–3).
- [56] A. Steckl, Dna - a new material for photonics?, *Nature Photonics* 1 (2007) 3–5.
- [57] A. Miniewicz, A. Kochalska, J. Mysliwiec, A. Samoc, M. Samoc, J. Grote, Deoxyribonucleic acid-based photochromic material for fast dynamic holography, *Applied Physics Letters* 91 (2007) 041118(1–3).
- [58] B. Derkowska, K. Jaworowicz, O. Krupka, M. Karpierz, M. Wojdyla, W. Bala, J. Grote, F. Kajzar, B. Sahraoui, Influence of different peripheral substituents on the nonlinear optical properties of cobalt phthalocyanine core, *Journal of Applied Physics* 101 (2007) 083112(1–8).
- [59] J. Mysliwiec, A. Miniewicz, I. Rau, O. Krupka, B. Sahraoui, F. Kajzar, J. Grote, Biopolymer-based material for optical phase conjugation, *Journal of Optoelectronics and Advanced Materials* 10 (2008) 2146–2150.
- [60] L. Wang, J. Yoshida, N. Ogata, S. Sasaki, T. Kamiyama, Self-assembled supramolecular films derived from marine deoxyribonucleic acid (dna) - cationic surfactant complexes: large-scale preparation and optical and thermal properties, *Chemistry of Materials* 13 (2001) 1273–1281.
- [61] H.-A. Wagenknecht, Vom mechanismus zur anwendung ladungstransfer durch die dna, *Chemie in unserer Zeit* 5 (2002) 318–330.
- [62] L. Tang, Z. Sun, J. Guo, Z. Wang, Study on the interaction of anticancer drug mitoxantrone with dna by fluorescence and raman spectroscopies, *Chinese Optics Letters* 4 (2006) 101–104.
- [63] A. Samoc, A. Miniewicz, M. Samoc, J. Grote, Refractive-index anisotropy and optical dispersion in films of deoxyribonucleic acid, *Journal of Applied Polymer Science* 105 (2007) 236–245.

- 
- [64] L. Hansen, L. Jensen, J. Jacobsen, Bis-intercalation of a homodimeric thiazole orange dye in dna in symmetrical pyrimidine-pyrimidine-purine-purine oligonucleotides, *Nucleic Acids Research* 24 (1996) 859–867.
- [65] S. Asayama, A. Maruyama, C.-S. Cho, T. Akaike, Design of comb-type polyamine copolymers for a novel ph-sensitive dna carrier, *Bioconjugate Chemistry* 8 (1997) 833–838.
- [66] H.-W. Fink, H. Schmid, E. Ermantraut, T. Schulz, Electron holography of individual dna molecules, *Journal of Optical Society of America A* 14 (1997) 2168–2172.
- [67] X. Dou, T. Takama, Y. Yamaguchi, K. Hirai, H. Yamamoto, S. Doi, Y. Ozaki, Quantitative analysis of double-stranded dna amplified by a polymerase chain reaction employing surface-enhanced raman spectroscopy, *Applied Optics* 37 (1998) 759–763.
- [68] E. Heckman, J. Grote, F. Hopkins, P. Yaney, Performance of an electro-optic waveguide modulator fabricated using a deoxyribonucleic-acid-based biopolymer, *Applied Physics Letters* 89 (2006) 181116(1–3).
- [69] J. Petykiewicz, *Wave optics*, PWN, Warszawa, 1992.
- [70] J. Reintjes, *Nonlinear optical parametric progresses in liquid and gases*, Academic Press, 1984.
- [71] D. Chemla, J. Zyss (Eds.), *Nonlinear optical properties of organic molecules and crystals*, Academic Press, 1987.
- [72] P. Yeh, *Introduction to photorefractive nonlinear optics*, Wiley-Interscience, 1993.
- [73] F. Kajzar, J. Swalen (Eds.), *Organic Thin Films for Waveguiding Nonlinear Optics*, Gordon and Breach, 1996.
- [74] M. Kuzyk, C. Dirk (Eds.), *Characterization Techniques and Tabulations for Organic Nonlinear Optical Materials*, Marcel Dekker, Inc., New York, 1998.
- [75] B. Derkowska, M. Wojdyla, R. Czaplicki, Z. Sofiani, W. Bala, B. Sahraoui, Influence of the central metal atom on the nonlinear optical properties of MPcs solutions and thin films, *Optics Communications* 274 (2007) 206–212.
- [76] M. Sheik-Bahae, A. Said, E. V. Stryland, High-sensitivity, single-beam  $n_2$  measurements, *Optics Letters* 14 (1989) 955–957.

- 
- [77] M. Sheik-Bahae, J. Wang, R. DeSalvo, D. Hagan, E. V. Stryland, Measurement of nondegenerate nonlinearities using a two-color z scan, *Optics Letters* 17 (1992) 258–260.
- [78] T. Xia, D. Hagan, M. Sheik-Bahae, E. V. Stryland, Eclipsing z-scan measurement of  $\lambda/10^4$  wave-front distortion, *Optics Letters* 19 (1994) 317–319.
- [79] K. Tseng, K. Wong, G. Wong, Femtosecond time-resolved z-scan investigations of optical nonlinearities in ZnSe, *Optics Letters* 21 (1996) 180–182.
- [80] G. Boudebs, S. Cherukulappurath, Nonlinear refraction measurements in presence of nonlinear absorption using phase object in a 4f system, *Optics Communications* 250 (2005) 416–420.
- [81] G. Boudebs, S. Cherukulappurath, Nonlinear optical measurements using a 4f coherent imaging system with phase objects, *Physical Review A* 69 (2004) 053813(1–6).
- [82] P. Maker, R. Terhune, M. Nisenoff, C. Savage, Effects of dispersion and focusing on the production of optical harmonics, *Physical Review Letters* 8 (1962) 21–22.
- [83] J. Jerphagnon, S. Kurtz, Maker fringes: a detailed comparison of theory and experiment for isotropic and uniaxial crystals, *Journal of Applied Physics* 41 (1970) 1667–1681.
- [84] N. Bloembergen, P. Pershan, Light waves at the boundary of nonlinear media, *Physical Review* 128 (1962) 606–622.
- [85] F. Kajzar, J. Messier, Third-harmonic generation in liquids, *Physical Review A* 32 (1985) 2352–2363.
- [86] F. Kajzar, J. Messier, C. Rosilio, Nonlinear optical properties of thin films of polysilane, *Journal of Applied Physics* 60 (1986) 3040–3044.
- [87] C. Reichardt, *Solvents and solvent effects in organic chemistry*, VCH Verlagsgesellschaft mbH, D-6940 Weinheim, Germany, 1988.
- [88] K. Kubodera, H. Kobayashi, Determination of third-order nonlinear optical susceptibilities for organic materials by third-harmonic generation, *Molecular Crystal and Liquid Crystal* 182 (1990) 103–113.

- 
- [89] F. Kajzar, *Characterization Techniques and Tabulations for Organic Nonlinear Optical Materials*, Marcel Dekker, Inc., New York, 1998, Ch. Third Harmonic Generation, pp. 767–839.
- [90] G. Yager, C. Barrett, All-optical patterning of azo polymer films, *Current Opinion in Solid State and Materials Science* 5 (2001) 487–494.
- [91] C. Cojocariu, P. Rochon, Light-induced motions in azobenzene containing polymers, *Pure and Applied Chemistry* 76 (2004) 1479–1497.
- [92] T. Todorov, L. Nikolova, N. Tomova, Polarization holography. 2: Polarization holography gratings in photoanisotropic materials with and without intrinsic birefringence, *Applied Optics* 23 (1984) 4588–4591.
- [93] L. Nikolova, P. Markovskiy, N. Tomova, V. Dragostinova, N. Mateva, Optically-controlled photo-induced birefringence in photo-anisotropic materials, *Journal of Modern Optics* 35 (1988) 1789–1799.
- [94] P. Ramanujam, S. Hvilsted, I. Zebger, H. Siesler, On the explanation of the biphotonic processes in polyesters containing azobenzene moieties in the side chain, *Macromolecular Rapid Communications* 16 (1995) 455–461.
- [95] P. Rochon, E. Batalla, A. Natansohn, Optically induced surface gratings on azoaromatic polymer films, *Applied Physics Letters* 66 (1995) 136–138.
- [96] D. Kim, S. Tripathy, L. Li, J. Kumar, Laser-induced holographic surface relief gratings on nonlinear optical polymer films, *Applied Physics Letters* 66 (1995) 1166–1168.
- [97] G. Malliaras, V. Krasnikov, H. Bolink, G. Hadziioannou, Transient behavior of photorefractive gratings in a polymer, *Applied Physics Letters* 67 (1995) 455–457.
- [98] C. Barrett, A. Natansohn, P. Rochon, Mechanism of optically inscribed high-efficiency diffraction gratings in azo polymer films, *Journal of Physical Chemistry* 100 (1996) 8836–8842.
- [99] T. Pedersen, P. Johansen, N. Holme, P. Ramanujam, S. Hvilsted, Mean-field theory of photoinduced formation of surface reliefs in side-chain azobenzene polymers, *Physical Review Letters* 80 (1998) 89–92.

- 
- [100] I. Naydenovay, T. Petrova, N. Tomova, V. Dragostinova, L. Nikolova, T. Todorov, Polarization holographic gratings with surface relief in amorphous azobenzene containing methacrylic copolymers, *Journal of Optics A: Pure and Applied Optics* 7 (1998) 723–731.
- [101] P. Lefin, C. Fiorini, J.-M. Nunzi, Anisotropy of the photo-induced translation diffusion of azobenzene dyes in polymer matrices, *Journal of Optics A: Pure and Applied Optics* 7 (1998) 71–82.
- [102] J. Kumar, L. Li, X. Jiang, D. Kim, T. Lee, S. Tripathy, Unusual polarization dependent optical erasure of surface relief gratings on azobenzene polymer films, *Applied Physics Letters* 72 (1998) 2096–2099.
- [103] R. Loucif-Saibi, K. Nakatani, J. Delaire, M. Dumont, Z. Sekkat, Photoisomerization and second harmonic generation in disperse red one-doped and -functionalized poly(methyl methacrylate) films, *Chemistry of Materials* 5 (1993) 229–236.
- [104] D. Sek, E. Schab-Balcerzak, M. Solyga, A. Miniewicz, Polarisation-sensitive holographic recording in polyimide-containing azo-dye, *Synthetic Metals* 127 (2002) 89–93.
- [105] Z. Sekkat, W. Knoll (Eds.), *Photorefractive organic thin films*, Academic Press, San Diego, 2002.
- [106] M. Dumont, Z. Sekkat, R. Loucif-Saibi, K. Nakatani, J. Delaire, Photoisomerization, photo-induced orientation and orientational relaxation of azo dyes in polymeric films, *Nonlinear Optics* 5 (1993) 395–406.
- [107] S. Bian, J. Williams, D. Kim, L. Li, S. Balasubramanian, J. Kumar, S. Tripathy, Photoinduced surface deformations on azobenzene polymer films, *Journal of Applied Physics* 86 (1999) 4498–4508.
- [108] P. Lefin, C. Fiorini, J.-M. Nunzi, Anisotropy of the photoinduced translation diffusion of azo dyes, *Optical Materials* 9 (1998) 323–328.
- [109] C. Barrett, P. Rochon, A. Natansohn, Model of laser-driven mass transport in thin films of dye-functionalized polymers, *Journal of Chemical Physics* 109 (1998) 1505–1516.

- 
- [110] A. Leopold, J. Wolff, O. Baldus, M. Huber, T. Bieringer, S. Zilker, Thermally induced surface relief gratings in azobenzene polymers, *Journal of Chemical Physics* 113 (2000) 833–837.
- [111] G. Pawlik, W. Kordas, A. Mitus, B. Sahraoui, R. Czaplicki, F. Kajzar, Model kinetics of surface relief gratings formation in organic thin films: Experimental and monte carlo studies, in: J. Grote, F. Kajzar, M. Lindgren (Eds.), *Optical Materials in Defence Systems Technology IV*, 2007, p. 674007.
- [112] R. Czaplicki, S. Dabos-Seignon, I. Rau, O. Krupka, J. Niziol, M. Bednarz, J. Pieliowski, A. Meghea, M. Bakasse, B. Sahraoui, Photoinduced gratings in functionalized azo-carbazole compounds in picosecond regime, *Molecular Crystals and Liquid Crystals* 485 (2008) 288–300.
- [113] J. Luc, K. Bouchouit, R. Czaplicki, J.-L. Fillaut, B. Sahraoui, Study of surface relief gratings on azo organometallic films in picosecond regime, *Optics Express* 16 (2008) 15633–15639.
- [114] G. Binning, C. Quate, C. Gerber, Atomic force microscope, *Physical Review Letters* 56 (1986) 930–933.
- [115] R. Hellwarth, Third order optical susceptibilities of liquids and solids, *Progress in Quantum Electronics* 5 (1979) 1–68.
- [116] W. Sun, C. Byeon, M. Mckerns, C. Lawson, S. Dong, D. Wang, G. Gray, Characterization of the third - order nonlinearity of  $[(\text{CH}_3 - \text{TXP})\text{Cd}]\text{Cl}$ , in: C. Lawson (Ed.), *Power - Limiting Materials and Devices*, 1999, pp. 107–116.
- [117] B. Derkowska, J. Mulatier, I. Fuks, B. Sahraoui, X. N. Phu, C. Andraud, Third-order optical nonlinearities in new octupolar molecules and their dipolar subunits, *Journal of the Optical Society of America B* 18 (2001) 610–616.
- [118] W. Sun, C. Byeon, M. Mckerns, C. Lawson, J. Dunn, M. Hariharasarma, G. Gray, Enhancement of the third-order susceptibility of *cis-mo(co)*<sub>4</sub>(*pph*<sub>3</sub>)<sub>2</sub> solution by oxygen in different solvents, in: C. Lawson (Ed.), *Nonlinear Optical Liquids for Power Limiting and Imaging*, 1998, pp. 108–115.
- [119] B. Sahraoui, G. Rivoire, Degenerate four-wave mixing in absorbing isotropic media, *Optics Communications* 138 (1997) 109–112.

- 
- [120] B. Derkowska, M. Wojdyla, Z. Sofiani, R. Czaplicki, M. Addou, W. Bala, B. Sahraoui, Third-order nonlinear optical properties of cupc: influence of thickness and concentration, in: T. Yeates, K. Belfield, F. Kajzar (Eds.), *Nonlinear Optical Transmission and Multiphoton Processes in Organics IV*, 2007, p. 63300F.
- [121] B. Derkowska, M. Wojdyla, W. Bala, K. Jaworowicz, M. Karpierz, R. Czaplicki, B. Sahraoui, Dependence of the third order nonlinear optical susceptibility on concentration and peripheral substituent of metallophthalocyanines, *Molecular Crystals and Liquid Crystals* 485 (2008) 965–973.
- [122] V. Smokal, R. Czaplicki, B. Derkowska, O. Krupka, A. Kolendo, B. Sahraoui, Synthesis and study of nonlinear optical properties of oxazolone containing polymers, *Synthetic Metals* 157 (2007) 708–712.
- [123] I. Rau, R. Czaplicki, A. Humeau, J. Luc, B. Sahraoui, G. Boudebs, F. Kajzar, D. Leigh, J. Berna-Canovas, Linear and nonlinear optical properties of selected rotaxane molecule, *Proceeding SPIE* 6343 (2006) 63433C(1–9).
- [124] M. Sheik-Bahae, A. Said, T. Wei, D. Hagan, E. van Stryland, Sensitive measurements of optical nonlinearities using a single beam, *IEEE Journal of Quantum Electronic* 26 (1990) 760–769.
- [125] V. Bermudez, T. Gase, F. Kajzar, N. Capron, F. Zerbetto, F. Gatti, D. Leigh, S. Zhang, Rotaxanes - novel photonic molecules, *Optical Materials* 21 (2002) 39–44.
- [126] V. Bermudez, P. Chollet, F. Kajzar, A. Lorin, G. Bottari, F. Gatti, D. Leigh, Light induced changes in no2-substitued rotaxanes: Switching behavior in a mechanically interlocked architecture, *Molecular Crystals and Liquid Crystals* 374 (2002) 343–356.
- [127] M. Wojdyla, W. Bala, B. Derkowska, Z. Lukasiak, R. Czaplicki, Z. Sofiani, S. Dabos-Seinon, B. Sahraoui, Photoluminescence and third harmonic generation in znpc thin films, *Nonlinear Optics and Quantum Optics* 35 (2006) 103–119.
- [128] M. Dewar, E. Zorbish, E. Healy, J. Stewart, Development and use of quantum mechanical molecular models. 76. am1: a new general purpose quantum mechanical molecular model, *Journal of American Chemical Society* 107 (1985) 3902–3909.

- 
- [129] M. Dewar, K. Dieter, Evaluation of am1 calculated proton affinities and deprotonation enthalpies, *Journal of American Chemical Society* 108 (1986) 8075–8086.
- [130] J. Oudar, D. Chemla, Hyperpolarizabilities of the nitroanilines and their relations to the excited state dipole moment, *Journal of Chemical Physics* 66 (1977) 2664.
- [131] G. Kelly, F. Darviche, N. Robertson, T. Gelbrich, M. Hursthouse, D. Thomas, I. Butler, Directly-linked intramolecular donor-acceptor compounds of ferrocene and tetracyanoanthraquinodimethane, *Inorganic Chemistry Communications* 8 (2005) 874–877.
- [132] M. Casalboni, F. Sarcinelli, R. Pizzoferrato, R. D’Amato, A. Furlani, M. Russo, Second-harmonic generation and absorption spectra of platinum organometallic complexes incorporated in pmma films, *Chemical Physics Letters* 319 (1999) 107–112.
- [133] Z. Sekkat, D. Morichere, M. Dumont, R. Louicif-Saibi, J. Delaire, Photoisomerization of azobenzene derivatives in polymeric thin films, *Journal of Applied Physics* 71 (1992) 1543–1545.
- [134] U. Gubler, C. Bosshard, Optical third-harmonic generation of fused silica in gas atmosphere: Absolute value of the third-order nonlinear optical susceptibility  $\chi^{(3)}$ , *Physical Review B* 61 (2000) 10702–10710.
- [135] O. Krupka, B. Derkowska, R. Czaplicki, I. Rau, A. El-Ghayoury, B. Sahraoui, J. Grote, F. Kajzar, Preparation and study of nonlinear optical properties of functionalized dna thin films, in: J. Grote, F. Kajzar, N. Kim (Eds.), *Organic Photonic Materials and Devices IX*, 2007, p. 64700E.
- [136] R. Birabassov, N. Landraud, T. Galstyan, A. Ritcey, C. Bazuin, T. Rahem, Thick dye-doped poly(methyl methacrylate) films for real-time holography, *Applied Optics* 37 (1998) 8264–8269.
- [137] M. Dumont, A. Osman, On spontaneous and photoinduced orientational mobility of dye molecules in polymers, *Chemical Physics* 245 (1999) 347–462.
- [138] M. Moharam, T. Gaylord, R. Magnusson, Criteria for raman-nath regime diffraction by phase gratings, *Optics Communications* 32 (1980) 19–23.

- [139] A. Migalska-Zalas, Z. Sofiani, B. Sahraoui, I. Kityk, V. Yuvshenko, J.-L. Fillaut, J. Perruchon, T. Muller,  $\chi^{(2)}$  grating in ru derivative chromophores incorporated within the pmma polymer matrices, *Journal of Chemical Physics B* 108 (2004) 14942–14947.
- [140] I. Kityk, M. Makowska-Janusik, E. Gondek, L. Krzeminska, A. Danel, K. Plucinski, S. Benet, B. Sahraoui, Optical poling of oligoether acrylate photopolymers doped by stilbene-benzoate derivative chromophores, *Journal of Physics: Condensed Matter* 16 (2004) 231–239.
- [141] H. Taunaumang, M. Solyga, M. Tija, A. Miniewicz, On the efficient mixed amplitude and phase grating recording in vacuum deposited disperse red 1, *Thin Solid Films* 461 (2004) 316–324.

# A

## Systems of units

There are several different systems of units that are used in nonlinear optics, however the most often used are: - SI (MKS - Meter Kilogram Second) - and Gaussian (CGS-Centimetr Gram Second) [10]. In this appendix we show how to convert physical values from one system to another.

In the Gaussian system of units, the polarization  $\vec{P}(t)$  is related to the electric field  $\vec{E}(t)$  by equation

$$\vec{P}(t) = \chi^{(1)}\vec{E}(t) + \chi^{(2)}\vec{E}^2(t) + \chi^{(3)}\vec{E}^3(t) + \dots, \quad (\text{A.1})$$

while in the SI system the same Eq. (A.1) can be expressed as follows:

$$\vec{P}(t) = \epsilon[\chi^{(1)}\vec{E}(t) + \chi^{(2)}\vec{E}^2(t) + \chi^{(3)}\vec{E}^3(t) + \dots], \quad (\text{A.2})$$

where

$$\epsilon = 8.85 \times 10^{-22} \frac{F}{m}, \quad (\text{A.3})$$

denotes the permittivity of free space.

In CGS system all of the fields ( $\vec{E}$ ,  $\vec{P}$ ,  $\vec{D}$ ,  $\vec{B}$ ,  $\vec{H}$  and  $\vec{M}$ ) have the same units, for instance the units of  $\vec{P}$  and  $\vec{E}$  are given by:

$$[\vec{P}] = [\vec{E}] = \frac{\text{statvolt}}{\text{cm}} = \frac{\text{statcoulomb}}{\text{cm}^2} = \left(\frac{\text{erg}}{\text{cm}^3}\right)^{1/2}, \quad (\text{A.4})$$

while in the SI system the units of  $\vec{P}$  and  $\vec{E}$  are as follows:

$$[\vec{P}] = \frac{C}{m^2}, \quad (\text{A.5})$$

$$[\vec{E}] = \frac{V}{m}. \quad (\text{A.6})$$

From Eq. A.1 is clearly seen that the dimensions of susceptibilities are as follows:

$$\chi^{(1)} - \text{dimensionless}, \quad (\text{A.7})$$

$$[\chi^{(2)}] = \left[ \frac{1}{E} \right] = \frac{cm}{\text{statvolt}} = \left( \frac{erg}{cm^3} \right)^{-1/2}, \quad (\text{A.8})$$

$$[\chi^{(3)}] = \left[ \frac{1}{E^2} \right] = \frac{cm^2}{\text{statvolt}^2} = \left( \frac{erg}{cm^3} \right)^{-1}. \quad (\text{A.9})$$

The units of the nonlinear susceptibilities are often not stated explicitly in the CGS system. The value is rather given in electrostatic units (esu). In the SI system the units of susceptibilities are as follows:

$$\chi^{(1)} - \text{dimensionless}, \quad (\text{A.10})$$

$$[\chi^{(2)}] = \left[ \frac{1}{E} \right] = \frac{m}{V}, \quad (\text{A.11})$$

$$[\chi^{(3)}] = \left[ \frac{1}{E^2} \right] = \frac{m^2}{V^2}. \quad (\text{A.12})$$

The conversion between CGS and SI units need some attention. The relations between the susceptibilities are [73]:

$$\chi_{SI}^{(n)} = \frac{4\pi}{(10^{-4}c)^{n-1}} \chi_{CGS}^{(n)}, \quad (\text{A.13})$$

where  $c = 3 \times 10^8$  m/s. Consequently, for second and third order susceptibility the relations are as follows [73, 10]:

$$\chi_{SI}^{(2)} = \frac{4\pi}{3 \times 10^4} \chi_{CGS}^{(2)} = 4.189 \times 10^{-4} \chi_{CGS}^{(2)}, \quad (\text{A.14})$$

$$\chi_{SI}^{(3)} = \frac{4\pi}{(3 \times 10^4)^2} \chi_{CGS}^{(3)} = 1.4 \times 10^{-8} \chi_{CGS}^{(3)}. \quad (\text{A.15})$$

# B

## Notations, symbol and abbreviations

$\alpha$	absorption coefficient
$\alpha^h, \alpha_{ij}^h$	linear polarizability
AFM	atomic force microscope
$\vec{B}$	magnetic induction vector
$\beta$	two photon absorption coefficient
$\beta^h, \beta_{ijk}^h$	first order hyperpolarizability; second order nonlinear polarizability
BDMA	cetylbenzyltrimethylammonium
BK7	borosilicate glass
<b>BS</b>	beam splitter
$c$	light speed in vacuum
$C$	concentration
<b><i>catenane</i></b>	benzylic amide [2] catenane
<b>CCD</b>	charge-coupled device
$\text{CHCl}_3$	chloroform
CI	configuration interaction (method)
CP	cetylpyridinium chloride
$\text{CS}_2$	carbon disulfide
CTMA	hexadecyltrimethylammonium chloride
$\vec{D}$	electric displacement vector
<b>D</b>	diaphragm
DFWM	degenerate four-wave mixing
DMSO	dimethyl sulfoxide
DNA	deoxyribonucleic acid

---

DR1	disperse red 1; N-Ethyl-N-(2-hydroxyethyl)-4-(4-nitrophenylazo)aniline
$\vec{E}$	electric field vector
Et <sub>3</sub> N	triethylamine
<b>F</b>	filter
$F$	local field correction factor
<b>FL532, FL355</b>	selective filter
<b><i>fumrot</i></b>	benzylic amide [2] rotaxane; fumaramide [2] rotaxane
$\gamma^h, \gamma_{ijkl}^h$	second order hyperpolarizability; third order nonlinear polarizability
$\chi^{(n)}, \chi_{ijkl}^{(n)}$	n-th order nonlinear susceptibility
$\vec{H}$	magnetic field vector
HCl	hydrogen chloride
HF	Hartree Fock
$I$	intensity
$\vec{j}$	current density vector
$\vec{k}$	wave vector
$\kappa$	extinction coefficient
$l$	thickness of medium
$L_c$	coherence length
<b>L</b>	lens
$\lambda$	wavelength
$\lambda/2$	half wavelength plate
$\vec{M}$	magnetic polarization vector
<b>M</b>	mirror
$M$	molar mass
<b><i>macrocycle</i></b>	benzylic amide macrocycle
$M_w$	molecular weight
MeOH	methanol
$n_2$	nonlinear refractive index ( $n = n_0 + n_2 I$ )
$N_A$	Avogadro constant
NaHCO <sub>3</sub>	sodium bicarbonate
<b>Nd:YAG</b>	Nd:YAG (neodymium-doped yttrium aluminium garnet; Nd : Y <sub>3</sub> Al <sub>5</sub> O <sub>12</sub> )
NIR	near infrared spectrum
NLO	nonlinear optics
NO <sub>2</sub>	nitrogen dioxide

---

OKE	optical Kerr effect
<b>P</b>	polarizer
$\vec{P}$	electric polarization vector
$\vec{P}_L$	linear polarization
$\vec{P}_{NL}$	nonlinear polarization
<b>Phc, Phs</b>	photodiode (control, synchronization)
PMMA	poly(methyl methacrylate); poly(methyl 2-methylpropenoate)
<b>PMT</b>	photomultiplier tube
PVK	polyvinylcarbazole; poly(9-vinylcarbazole)
$R$	reflection
$\rho$	charge density
<b>RO</b>	delay line
<b>S</b>	sample
SHG	second harmonic generation
SiO <sub>2</sub>	silicon dioxide; silica
<i>rotaxane</i>	benzylic amide [2] rotaxane (with aliphatic chains)
$T$	transmission
$\theta$	angle
THG	third harmonic generation
<i>thread</i>	fumaramide thread with aliphatic chains
TTF	tetrathiafulvalene
$\vec{u}$	unit vector
UV	ultraviolet
VIS	visible spectrum



# C

## Publications and communications

### C.1 Publications

1. *Nonlinear optics and surface relief gratings in alkynyl-ruthenium*, B. Sahraoui, J. Luc, A. Meghea, **R. Czaplicki**, J.-L. Fillaut and A. Migalska-Zalas, *Special issue of Journal of Optics A: Pure and Applied Optics, "Optics of Nanocomposite Materials"*, **11**, (2009) 024005 (26pp).
2. *Study of surface relief gratings on azo organometallic films in picosecond regime*, J. Luc, K. Bouchouit, **R. Czaplicki**, J.-L. Fillaut and B. Sahraoui, *Optics Express*, **16**, (2008) 15633-15639.
3. *Dependence of the third order nonlinear optical susceptibility on concentration and peripheral substituent of metallophthalocyanines*, B. Derkowska, M. Wojdyla, W. Bala, K. Jaworowicz, M. Karpierz, **R. Czaplicki** and B. Sahraoui, *Molecular Crystals and Liquid Crystals*, **485**, (2008) 965-973.
4. *New methacrylic oxazolone and thiazolidinone containing polymers for nonlinear optical applications*, V. Smokal, A. Kolendo, O. Krupka, B. Derkowska, **R. Czaplicki** and B. Sahraoui, *Molecular Crystals and Liquid Crystals*, **485**, (2008) 1011-1018.
5. *Photoinduced gratings in functionalized azo-carbazole compounds in picosecond regime*, **R. Czaplicki**, S. Dabos-Seignon, I. Rau, O. Krupka, J. Niziol, M. Bednarz, J. Pielichowski, A. Meghea, M. Bakasse and B. Sahraoui, *Molecular Crystals and Liquid Crystals*, **485**, (2008) 288-300.

6. ***Nonlinear optical properties of thiazolidinone derivatives***, V. Smokal, B. Derkowska, **R. Czaplicki**, O. Krupka, A. Kolendo and B. Sahraoui, *Optical Materials*, In Press, Corrected Proof, (2008).
7. ***The Class of Molecules with Mobile Parts: Catenanes and Rotaxanes for Nonlinear Optical Applications***, **R. Czaplicki**, Z. Essaidi, I. Rau, A. Meghea, F. Kajzar, J. Berna-Canovas, D.A. Leigh and B. Sahraoui, *2007 International Conference on Transparent Optical Networks "Mediterranean Winter" IEEE Cat. No.: CFP0733D-CDR*, ISBN: 978-1-4244-1639-4, (2007).
8. ***Polymers with Benzylidene Fragment for Nonlinear Optical Application***, V. Smokal, B. Derkowska, **R. Czaplicki**, O. Krupka, A. Kolendo and B. Sahraoui, *2007 International Conference on Transparent Optical Networks "Mediterranean Winter" IEEE Cat. No.: CFP0733D-CDR*, ISBN: 978-1-4244-1639-4, (2007).
9. ***Nonlinear optical cubic effects in functionalized DNA***, **R. Czaplicki**, O. Krupka, A. Meghea, J.G. Grote, F. Kajzar and B. Sahraoui, *Digest Journal of Nanomaterials and Biostructures*, **2**, (2007) 277-283.
10. ***Model kinetics of Surface Relief Gratings formation in organic thin films: Experimental and Monte Carlo studies***, G. Pawlik, W. Kordas, A.C. Mitus, B. Sahraoui, **R. Czaplicki** and F. Kajzar, *Proceedings of SPIE - The International Society for Optical Engineering*, **6740**, (2007) 674007.
11. ***Synthesis and study of nonlinear optical properties of oxazolone containing polymers***, V. Smokal, **R. Czaplicki**, B. Derkowska, O. Krupka, A. Kolendo, and B. Sahraoui, *Synthetic Metals*, **157**, (2007) 708-712.
12. ***Grating inscription in picosecond regime in thin films of functionalized DNA***, **R. Czaplicki**, O. Krupka, Z. Essaidi, A. El-Ghayoury, F. Kajzar, J.G. Grote and B. Sahraoui, *Optics Express*, **15**, (2007) 15268-15273. highlighted in *Nature Photonics*, "Holography, DNA Stripes (Research Highlits)", **2**, (2008) 6-7.
13. ***Preparation and study of nonlinear optical properties of functionalized DNA thin films***, O. Krupka, B. Derkowska, **R. Czaplicki**, I. Rau, A. El-Ghayoury, B. Sahraoui, J.G. Grote and F. Kajzar, *Proceedings of SPIE - The International Society for Optical Engineering*, **6470**, (2007) 64700E.

14. ***Influence of the central metal atom on the nonlinear optical properties of MPcs solutions and thin films***, B. Derkowska, M. Wojdyla, **R. Czaplicki**, Z. Sofiani, W. Bala and B. Sahraoui, *Optics Communications*, **274**, (2007) 206-212.
15. ***Third-order nonlinear optical properties of CuPc: influence of thickness and concentration***, B. Derkowska, M. Wojdyla, Z. Sofiani, **R. Czaplicki**, M. Addou, W. Bala and B. Sahraoui, *Proceedings of SPIE - The International Society for Optical Engineering*, **6330**, (2007) 63300F.
16. ***Functionalized Azo-Carbazole Compounds for Nonlinear Optical Application***, **R. Czaplicki**, S. Dabos-Seignon, F. Kajzar, M. Bakasse, J. Niziol, M. Bednarz and B. Sahraoui, *2006 International Conference on Transparent Optical Networks* **2**, art. no. 4013732, (2006) 283-286.
17. ***Linear and nonlinear optical properties of a rotaxane molecule***, I. Rau, **R. Czaplicki**, A. Humeau, J. Luc, B. Sahraoui, G. Boudebs, F. Kajzar, D.A. Leigh and J. Berna-Canovas, *Proceedings of SPIE - The International Society for Optical Engineering*, **6343 II** (2006) 63433C.
18. ***Photoluminescence and Third Harmonic Generation in ZnPc Thin Films***, M. Wojdyla, W. Bala, B. Derkowska, Z. Lukasiak, **R. Czaplicki**, Z. Sofiani, S. Dabos-Seignon and B. Sahraoui, *Nonlinear Optics and Quantum Optics*, **35** (2006) 103-119.

## C.2 Communications

1. ***Nonlinear optical properties of nanomotors for optoelectronic applications (Invited Lecture)***, **R. Czaplicki** and B. Sahraoui, *27-28 October 2008 - Rencontre Nationale: Matière Condensée et Modélisation des Systèmes (MCMS'2008)*, Fes, Marocco
2. ***New class of highly conjugated nanomotors: catenanes and rotaxanes as potential candidates for nonlinear optical applications (Invited Lecture)***, **R. Czaplicki**, Z. Essaidi, F. Kajzar and B. Sahraoui, *8-13 June 2008 - 3rd International Conference Smart Materials Structure Systems (CIMTEC 2008)*, Acireale, Sicily, Italy

3. ***Polymerization ability, nonlinear optical properties of methacrylic monomers and polymers with benzylidene moiety (Poster)***, V. Smokal, O. Krupka, A. Kolendo, B. Derkowska, **R. Czaplicki** and B. Sahraoui, 26-30 May 2008 - 7-th International Conference Electronic Processes in Organic Materials (ICEPOM-7), Lviv, Ukraine
4. ***The Class of Molecules with Mobile Parts: Catenanes and Rotaxanes for Nonlinear Optical Applications***, **R. Czaplicki**, Z. Essaidi, I. Rau, A. Meghea, F. Kajzar, J. Berna-Canovas, D.A. Leigh and B. Sahraoui, 06-08 December 2007 - International Conference on Transparent Optical Networks "Mediterranean Winter" 2007 (ICTON MW'07), Sousse, Tunisia
5. ***Polymers with Benzylidene Fragment for Nonlinear Optical Application (Poster)***, V. Smokal, **R. Czaplicki**, B. Derkowska, O. Krupka, A. Kolendo and B. Sahraoui, 06-08 December 2007 - International Conference on Transparent Optical Networks "Mediterranean Winter" 2007 (ICTON MW'07), Sousse, Tunisia
6. ***Model kinetics of Surface Relief Gratings formation in organic thin films: Experimental and Monte Carlo studies (Invited Lecture)***, G. Pawlik, W. Kordas, A.C. Mitus, B. Sahraoui, **R. Czaplicki** and F. Kajzar, 17-20 September 2007 - SPIE Europe Security + Defence 2007, Florence, Italy
7. ***Rotational contribution to cubic susceptibility of rotaxanes and catenanes in solution***, F. Kajzar, I. Rau, **R. Czaplicki**, A. Humeau, J. Luc, O. Krupka and B. Sahraoui, 17-20 September 2007 - SPIE Europe Security + Defence 2007, Florence, Italy
8. ***Nonlinear Optical Properties of Different Poly(organophosphazanes) as Suitable Materials for Optical Holography (Invited Lecture)***, B. Sahraoui, **R. Czaplicki**, S. Dabos-Seignon, F. Kajzar, E. Blaz, M. Bednarz and J. Niziol, 2-6 September 2007 - The International Conference on Structural Analysis of Advanced Materials (ICSAM), Patras, Greece
9. ***Nonlinear optical properties of lactone and lactame derivatives (Poster)***, V. Smokal, A. Kolendo, **R. Czaplicki**, O. Krupka, B. Derkowska, B. Sahraoui and F. Kajzar, 15-18 July 2007 - 3-rd French - Polish Symposium on Spectroscopy of Modern Materials in Physics, Chemistry and Biology, Clermont-Ferrand, France

10. *Design and synthesis of a new series of alkynyl ruthenium chromophores for nonlinear optical applications (Invited Lecture)*, B. Sahraoui, A. Migalska-Zalas, I. Rau, **R. Czaplicki** and J. Luc, 8-12 July 2007 - IX International Conference on Frontiers of Polymers and Advanced Materials, Cracow, Poland
11. *Dependence of the third order nonlinear optical susceptibility on concentration and perypheral substituent of metallophthalocyanines (MPcs)*, B. Derkowska, M. Wojdyla, W. Bala, K. Jaworowicz, M. Karpierz, **R. Czaplicki** and B. Sahraoui, 8-12 July 2007 - IX International Conference on Frontiers of Polymers and Advanced Materials, Cracow, Poland
12. *New methacrylic oxazalone and thiozolidone containing monomers for nonlinear optical application (Poster)*, V. Smokal, B. Derkowska, **R. Czaplicki**, O. Krupka, B. Sahraoui and A. Kolendo, 8-12 July 2007 - IX International Conference on Frontiers of Polymers and Advanced Materials, Cracow, Poland
13. *Optical holography in picosecond regime on thin films of functionalised DNA (Poster)*, O. Krupka, **R. Czaplicki**, F. Kajzar, A. El-Ghayoury, B. Derkowska, J.G. Grote and B. Sahraoui, 8-12 July 2007 - IX International Conference on Frontiers of Polymers and Advanced Materials, Cracow, Poland
14. *Photoinduced gratings in functionalized azo-carbazole compounds in picosecond regime (Poster)*, **R. Czaplicki**, M. Bednarz, J. Niziol, S. Dabos-Seignon, O. Krupka, M. Bakasse, J. Pielichowski and B. Sahraoui, 8-12 July 2007 - IX International Conference on Frontiers of Polymers and Advanced Materials, Cracow, Poland
15. *Catenanes and rotaxanes as new class of nanomotors for nonlinear optical applications*, **R. Czaplicki**, 28 June 2007 - Journée scientifique "Molécules pour l'Optique Linéaire et Non Linéaire", Rennes, France
16. *Nonlinear Optical Properties Of Functionalized DNA*, O. Krupka, **R. Czaplicki**, B. Sahraoui, F. Kajzar and J. Grote, 17-20 May 2007 - IX International Workshop Nonlinear Optics Applications (NOA), Swinoujscie, Poland

17. ***Molecular nanomotors: catenanes and rotaxanes for nonlinear optical applications***, R. Czaplicki, Z. Essaidi, O. Krupka, G. Boudebs, F. Kajzar, I. Rau, J. Berna-Canovas, D.A. Leigh and B. Sahraoui, 17-20 May 2007 - IX International Workshop Nonlinear Optics Applications (NOA), Swinoujscie, Poland
18. ***Design and synthesis of a new nanocomposites based on alkynyl ruthenium chromophores for nonlinear optical applications***, B. Sahraoui, A. Migalska-Zalas, R. Czaplicki and J. Luc, 22-24 February 2007 - BRAMAT, Brasov, Romania
19. ***Nonlinear optical properties of functionalized DNA thin films***, O. Krupka, R. Czaplicki, A. El-Ghayoury, I. Rau, B. Sahraoui, F. Kajzar and J.G. Grote, 20-25 January 2007 - Photonics West, San Jose, California, USA
20. ***On the importance of rotational contributions to cubic susceptibility in catenanes and rotaxanes (Invited Lecture)***, I. Rau, R. Czaplicki, A. Humeau, B. Sahraoui, G. Boudebs, O. Krupka, D.A. Leigh, J. Berna-Canovas and F. Kajzar, 20-25 January 2007 - Photonics West, San Jose, California, USA
21. ***Third-Order Nonlinear Optical Properties Of Selected Rotaxanes (Invited Lecture)***, I. Rau, R. Czaplicki, A. Hameau, B. Sahraoui, G. Boudebs, O. Krupka, D.A. Leigh, J. Berna-Canovas and F. Kajzar, 25-29 September 2006 - 6-th International Conference Electronic Processes in Organic Materials (ICEPOM-6), Gurzuf, Crimea, Ukraine
22. ***Nonlinear optical properties of selected rotaxanes (Invited Lecture)***, F. Kajzar, R. Czaplicki, O. Krupka, I. Rau, B. Sahraoui, J. Canovas and D. Leigh, 11-14 September 2006 - Optics/Photonics in Security and Defence, Stockholm, Sweden
23. ***Third-order nonlinear optical properties of CuPc: influence of thickness and concentration***, B. Sahraoui, Z. Sofiani, B. Derkowska, M. Wojdyla, R. Czaplicki, P. Rytlewski, M. Addou and W. Bala, 13-17 August 2006 - Optics Photonics, San Diego, California USA
24. ***Functionalized Azo-Carbazole Compounds for Nonlinear Optical Application (Invited Lecture)***, R. Czaplicki, S. Dabos-Seignon, F. Kajzar,

M. Bakasse, J. Niziol, M. Bednarz and B. Sahraoui, *18-22 June 2006 - 8-th International Conference on Transparent Optical Networks ICTON 2006, Nottingham, United Kingdom*

25. ***Non-linear optical studies of functionalized organometallic ruthenium complexes***, J. Luc, **R. Czaplicki**, I.V. Kityk, A. Migalska-Zalas, J-L. Fillaut and B. Sahraoui, *07-10 June 2006 - International Symposium on Molecular Materials based on Coordination and Organometallic Chemistry MOLMAT 2006, Lyon, France*
26. ***Linear and nonlinear optical properties of selected rotaxanes (Invited Lecture)***, I. Rau, **R. Czaplicki**, A. Humeau, J. Luc, B. Sahraoui, G. Boudebs, F. Kajzar, D.A. Leigh and J. Berna-Canovas, *05-08 June 2006 - Photonics North, Quebec City, Canada*
27. ***Photoluminescence and third harmonic generation in ZnPc thin films***, M. Wojdyla, W. Bala, B. Derkowska, Z. Lukasiak, **R. Czaplicki**, Z. Sofiani, S. Dabos-Seinon and B. Sahraoui, *15-20 January 2006 - 3-rd International Conference on Photoresponsive Organics and Polymers, 2-nd France-Korea Bilateral Symposium on Photonic Materials and Devices, Val Thorens, Savoie, France*



## Résumé

La synthèse de caténanes et rotaxanes remonte aux années 60. Aujourd'hui la plupart de ces molécules enchevêtrées, synthétisées comportent jusqu'à 4 éléments et ce nombre continu de croître. Toutefois, ces molécules restent relativement petites, comparées à celles trouvées dans la nature tels que les caténanes présents dans l'ADN. Les caténanes et rotaxanes sont des molécules mécaniquement assemblées, composées de pièces mobiles, liées, ou non (ou plus d'elles), pouvant se mouvoir et/ou se déplacer par rapport aux autres. Cette architecture unique les rend très intéressants et fait d'eux des candidats potentiels pour les machines moléculaires, ainsi que pour des applications dans le domaine de l'optique non linéaire, en particulier dans la photonique, l'optoélectronique et le stockage de données optique.

Dans ce travail, nous exposons les résultats de nos recherches portant sur les propriétés optiques non-linéaires de quelques caténanes et rotaxanes. Ces propriétés non-linéaires ont été abordées par différentes techniques. Les résultats montrent une importante contribution électronique dans la susceptibilité non-linéaire de troisième ordre confirmée par des calculs théoriques au niveau moléculaire.

Nous exposons également les résultats des propriétés optiques non linéaires de l'ADN fonctionnalisé. Ces résultats montrent une recrudescence des non linéarités quand l'ADN modifiée est utilisé. Par ailleurs, on a observé les meilleurs résultats dans des expériences d'holographie quand l'ADN-CTMA est utilisé comme matrice pour le dopage du disperse red 1.

**Mots-clés:** caténanes, rotaxanes, ADN, optique non linéaire, réseaux de surface.

## Abstract

The concept of interlocked molecules is known from sixties and up to now catenanes and rotaxanes of up to 4 components were synthesized and still the number of components increase. These are relatively small molecules when in nature large catenanes are present in DNA molecules. Catenanes and rotaxanes are mechanically interlocked molecules composed of moving parts, held together, where one (or more of them) can move and/or positioning with respect to the other. This unique architecture makes them very interesting as possible candidates for molecular machine-type applications in the field of nonlinear optics particularly in photonics, optoelectronics and optical data storage.

In this work we report the results of our studies of nonlinear optical properties of some selected catenanes and rotaxanes. The nonlinear properties were studied by different techniques. The results show important electronic contribution to the third order nonlinear susceptibility confirmed by theoretical calculations at the molecular level.

Also, we report the results of nonlinear optical properties of functionalized DNA. The results show high enhancement of nonlinearity when the modified DNA was used. At the same time the best results were observed in holography experiments when DNA-CTMA was used as a matrix for doping of disperse red 1.

**Keywords:** catenanes, rotaxanes, DNA, third order nonlinearity, surface relief grating.